UNIVERSITÀ
DEGLI STUDI
DI BRESCIA

DIPARTIMENTO DI INGEGNERIA CIVILE, ARCHITETTURA, TERRITORIO, AMBIENTE E DI MATEMATICA

Corso di Laurea Magistrale
in CIVIL AND ENVIRONMENTAL ENGINEERING

Tesi di Laurea

REVISITING THE DESIGN FLOOD ESTIMATION PRACTICES UNDER THE DYNAMIC UNIT HYDROGRAPH APPROACH

Relatore: Chiar.mo Prof. Roberto Ranzi

Correlatore: Chiar.mo Prof. Andreas Efstratiadis

Laureanda:
Eleni Maria Michailidi

Matricola n. 710774

Anno Accademico 2020/2021

DEDICATION

To Prof. Andreas, third thesis' the charm.

ABSTRACT

REVISITING THE DESIGN FLOOD ESTIMATION PRACTICES UNDER THE DYNAMIC UNIT HYDROGRAPH APPROACH

The unit hydrograph (UH) has been a common tool used to represent the complicated processes of surface runoff routing. Key assumption is that the rainfall – runoff transformation is represented through a unit pulse response function of a linear system. The UH shape is mainly determined by the peak and base time, associated with the basin's response time. However, it is known that the latter is significantly influenced by precipitation and should, thus, be regarded as variable. Consequently, the UH cannot be considered a characteristic basin property, but a dynamic element. In order to employ the concept of the dynamic UH, whose shape is adapted to excess rainfall intensity, an empirical synthetic UH is introduced, with parameters expressed as functions of the time of concentration, combined with the NRCS-CN method. The model's validity is tested against observed events from basins located in Italy, Greece and Cyprus, and regional formulas are provided explaining the variability of the two parameters (base and peak time) across basins with different characteristics. Finally, a proposal for hydrological design for small basins is presented.

ABSTRACT

RIVISITAZIONE DELLE PRATICHE DI STIMA DELLE PIENE DI PROGETTO CON L'APPROCCIO DELL'IDROGRAMMA UNITARIO DINAMICO

L'idrogramma unitario (UH) è uno strumento di comune utilizzo per rappresentare i complicati processi della propagazione del deflusso superficiale. Una delle ipotesi chiave è il fatto che la trasformazione precipitazione-deflusso è rappresentata attraverso una funzione di risposta all'impulso unitario di un sistema lineare. La forma dell'idrogramma unitario è determinata principalmente dal tempo di picco e di base, associati al tempo di risposta del bacino. Tuttavia, è noto che quest'ultimo è significativamente influenzato dalle precipitazioni e dovrebbe essere considerato variabile. Di conseguenza, l'UH non può essere considerato una proprietà caratteristica del bacino, ma un elemento dinamico. Utilizzando il concetto di un UH dinamico, la cui forma è adattata all'intensità di pioggia in eccesso, si introduce un UH sintetico ed empirico, con parametri espressi in funzione del tempo di corrivazione, abbinato con il metodo NRCS-CN per la depurazione della pioggia netta. La validità del modello viene testata rispetto agli eventi osservati nei bacini situati in Italia, Grecia e Cipro e vengono fornite formule regionali che spiegano la variabilità dei due parametri (tempo di picco e di base) tra bacini con caratteristiche diverse. Viene infine presentata una proposta di progettazione idrologica per piccoli bacini.

TABLE OF CONTENTS

LIST OF TABLES

LIST OF FIGURES

Figure Page

1. INTRODUCTION

1.1 General overview

For many decades, the unit hydrograph (UH) theory has been used for representing, in a simple and parsimonious manner, the highly-complicated processes of surface runoff routing. It is assumed that the transformation of rainfall into runoff is represented through a unit pulse response function of a linear system, thus the ordinates of the unit hydrograph for a given duration are proportional to the total runoff. In fact, the UH shape is mainly determined by two time characteristics, i.e. the time to peak and the base time, that are in turn associated with the response time of the river basin (either defined as the lag time or the time of concentration). However, both theoretical proof and empirical evidence imply that the response time of a basin actually exhibits significant variability against rainfall and thus, it should be regarded as a variable rather than a constant property.

A direct consequence of the above is that the UH cannot be considered a characteristic property of the basin as conventionally tackled, but a dynamic element, which also depends on the excess rainfall intensity. Evidently, as rainfall varies during a storm event, the runoff routing process and its mathematical formulation through the UH is also varying. Despite the fairly rich literature regarding the dynamic nature of *tc*, much less has been written on the application of a dynamic UH.

In order to employ the concept of the dynamic unit hydrograph, whose shape is adapted to the excess rainfall intensity, a synthetic UH is introduced, with time parameters expressed as functions of the time of concentration, combined with the well-known NRCS-CN method for the estimation of direct runoff (NRCS, 2004). The validity of this approach is tested against observed flood events from a number of watersheds from Italy, Greece and Cyprus. Based on the outcomes of these analyses, regional formulas are also provided, explaining, with good predictive capacity, the variability of the two time-parameters across basins with different characteristics and under very limited resources. In the end, a hydrological design approach is introduced, as well, ready to be implemented to small mountainous basins.

1.2 Structure of the thesis

This thesis is structured in eight distinct chapters, including the present one. In the second chapter, a comprehensive literature review is presented, regarding the concept of the time of concentration and important aspects on event-based hydrological modelling. In particular, focus is given primarily on the NRCS-CN approach and on the most important SUHs, highlighting their discrepancies, specifically in the case of mountainous Mediterranean basins.

In the third chapter the methodological approach is introduced. First, an improvement on the estimation of the varying time of concentration, as developed by Michailidi *et al.* (2018), is provided. Then, the methodology for adapting the varying time of concentration concept in flood modelling through the development of a dynamic SUH is presented.

In the fourth chapter the application of the proposed methodology is introduced. In particular, the data collection and processing phase description is developed, along with details regarding the calibration framework.

The thesis proceeds with the fifth chapter that includes the results of this analysis. More specifically, the outcomes from the calibration process are presented, along with the regionalisation of the time parameters of the dynamic SUH. The validation of the regionalised parameters is later carried out and a proposal for hydrological design is introduced, ready to be implemented in small basins.

In the final chapters of the thesis the general conclusions, stemming from this research are presented, along with opportunities for further research. Finally, the bibliographical section and the appendices, presenting the results from the implementation of the proposed model, conclude this thesis.

2. LITERATURE REVIEW

2.1 Estimation of the time of concentration

The time of concentration is a common hydrological tool, used for the hydrological design in the Rational method or the Synthetic Unit Hydrograph. There are numerous definitions regarding *tc*, but typically, it is considered as the longest travel time that runoff takes to travel from the hydraulically most distant point in the watershed to the outlet (NRCS, 2004). In the literature there is a plethora of formulas for its estimation, taking into consideration the basin's geomorphological characteristics of the basin. Among these formulas one can distinguish the ones provided by Ventura (1905) and Pasini (1914), developed for Italian rural basins, and associating *tc* with the basin area and the slope of the main stream, with the latter one integrating the length of the main stream to his formula, as well. Similarly, Giandotti (1934) associated *tc* with the basin area, the length of the flow route and the elevation difference between the centroid of the basin and its outlet, calibrating his formula on 12 watersheds with areas ranging between 170 and 70 000 km^2. Viparelli (1961, 1963) expressed the time of concentration in a more physically-based manner, as the maximum distance between the watershed divide and the outlet and the mean flow channel velocity. More recently, Bocchiola *et al.* (2003), focusing entirely on Italian basins, associated the lag time- a time characteristic of the basin's response- with the basins' geomorphological characteristics and the maximum potential saturation of the soil. A comprehensive review of various time of concentration formulas is provided by Michailidi *et al.* (2018) and Gericke and Smithers (2014).

However, it has been widely accepted that *tc* is not a constant parameter, based only on the basin's characteristics but depends highly on the velocity and thus the travel time of the generated runoff, propagating along the river network. In fact, ignoring the reduction of *tc* with the increase of excess rainfall intensity can lead to significant underestimation of flood flows, particularly for extreme flood events (Michailidi *et al.*, 2018).

In the literature, numerous authors have produced empirically- (Askew, 1970; Papadakis and Kazan, 1987), experimentally- (Izzard, 1946; US Army Corps of Engineers', 1954) and theoretically- (Morgali and Linsley, 1965; Aron et al., 1991; Loukas and Quick, 1996) derived formulas that associate the time of concentration (or lag-time) with a characteristic hydrological quantity, such as excess rainfall intensity. With the diffusion of GIS tools during the last three decades more "physically" sounder approaches were introduced that allowed the employment of flow velocity methods at the grid scale, where the velocities, and thus the time of concentration, are estimated cell by cell, for a given runoff depth. However, computational costs and discretization issues can render these methods unattractive for everyday-design practice. Michailidi *et al.* (2018) have proposed a methodology, based on the logic of urban sewer network design, in order to associate the time of concentration, *tc*, with the excess rainfall intensity; the computational procedure has been automatized in a GIS environment, is computationally efficient and deals with the discretization problems. As an alternative, the authors have also introduced a regional formula in case of absence of GIS tools.

2.2 Event-based hydrological modelling

2.2.1 A note on the abstraction ratio

The NRCS-CN method (NRCS, 2004) is one of the most prevailing methods for event-based hydrological design, transforming a design hyetograph (or any rainstorm event) into surface runoff. It expresses the temporal evolution of the hydrological losses during a rainfall event by the following equation:

$$Q = \begin{cases} 0, & P \leq I_a \\ \dfrac{(P - I_a)^2}{P + S - I_a}, & P > I_a \end{cases} \tag{2.1}$$

where P is the cumulated rainfall depth (mm), I_a is the initial abstraction (mm), which consists mainly of interception, infiltration during early parts of the storm and surface depression storage, Q is the runoff depth (mm) or else the runoff volume produced from the effective rainfall, S is the potential maximum retention after the rainfall start (mm). The abstraction can be expressed as $Ia = \Lambda s$ where λ is the abstraction ratio, assuming values from 0 to 1.

Its popularity is due to its simplicity, its parsimony and its establishment by the Soil Conservation Service, a federal agency in the U.S.. Details on the method are published in the National Engineering Handbook Section 4 (USDA, 1985), along with an example of its application in the hourly scale.

The potential maximum retention is estimated through the curve number formula as, $S=254(100/CN-1)$, where the curve number CN is a measure of the basin's runoff capability, depending on land use, hydrogeology and antecedent moisture conditions of the basin and assuming values from 1 to 100.

NRCS suggests the value 0.2 for λ, since 50% of the field values (filtration measurements conducted in small rural basins in the US) were located between 0.095 and 0.38 (NRCS, 2004). However, the latter generalisation has been questioned numerous times in the past mainly due to its inconsistency with observed flood events, which showed a much lower λ value.

Hawkins and Khojeini (2000) after analysing 5501 events from 86 small watersheds in the U.S. have concluded that λ ranges from 0.0001 to 0.2907 with a mean value of 0.0607 and a median of 0.038. They proposed a more appropriate value of $\lambda = 0.05$, that will produce greater runoff. Unfortunately, the regional characteristics (land use, permeability etc.). Similarly, Woodward et al. (2003) conducted a more extensive research (i.e. 28301 events from 307 watersheds) and realized that λ does not only vary greatly between watersheds but also between storms. Over 90% of the values were below 0.2 with the range from 0.0005 to 0.4910 and a median of 0.0476. Mishra et al. (2006) investigated 18 different models for loss abstraction in 84 small watersheds (0.17 to 71.99 ha) and have concluded that the standard curve number method with $\lambda=0.2$ ranked much worse in model performance in respect with the same NRCS-CN model but considering a varying λ parameter. In the latter, the parameter λ ranged from 0.00 to 0.33 with the mean and median equal to 0.13.

Baltas *et al.* (2007) performed a similar research in a small basin (15.18 km^2) with steep slopes (21%) in Attica, Greece, and attempted to qualitatively associate the differences in the abstraction ratio with the prevailing geology and land cover. The results showed that the northern part of the basin, which is the least impervious, responded to λ values between 0.014 and 0.054 with an average value of 0.037. The average value of the entire basin was lower; this difference is attributed to the urban character of the southern part and to the marl formations. On the same note, Shi *et al.* (2009) carried out their study in the Three Gorges area in China, in the Wangjiaqiao watershed (16.7 km^2). This watershed is characterised as steep (average slope 42.4%). The ratio varied from 0.010 to 0.154 with median and mean equal to 0.048 and 0.052, respectively. The suggested value by NRCS overestimated runoff in small events and underestimated it in large ones. Recently, Yuan *et al.* (2014) came to the conclusion that for larger channels and finer soils the abstraction ratio decreases, after studying the events of 10 watersheds located in an experimental semiarid watershed in Arizona (148 km^2) covered mainly by sandy loam. The average of the optimised abstraction ratio for all the catchments was 0.12 within the range of 0.01 to 0.53.

All of the above studies and numerous others reported in the exhaustive review by Verma *et al.* (2017)- proof of the importance of correctly estimating the net rainfall (Grimaldi *et al.*, 2013a, 2013b)- pointed to a mean λ smaller than 0.2. The abstraction ratio varied even within different storms of the same basin.

Logically enough, the abstraction ratio has been often associated with the basin's slope, permeability characteristics, and vegetation state and spatial variability of precipitation, even though an attempt to tabulate its values has yet to be carried out. In fact, Shi and Wang (2020) noted that as the slope increases, the abstraction ratio decreases, due to the decreased infiltration capacity of the terrain, while abstraction values for a highly permeable basin located in the volcanic Jeju island of Korea yielded, in the majority of the events, values greater than 0.2 (Kang and Yoo, 2020). To the same conclusion regarding the dependence of the abstraction value on the catchment imperviousness arrived Krajewski *et al.* (2020), as well, when investigating the variability of the abstraction ratio in urban and agroforest land uses in two small Polish watersheds. Their results highlighted the variation of the abstraction ratio between events and seasons and concluded that for an urban and an agroforested basin, the average λ value was equal to 0.026 and 0.047, accordingly, prompting for the local verification of the ratios in other basins.

This modification in the abstraction ratio from the standard values requires the adjustment of the tabulated CN values provided by the NRCS (2004). To this end, in the recent ASCE-ASABE-NRCS Task Group on Curve Number Hydrology (2017) the following formula has been suggested linking the maximum potential retention, *S*, for a λ equal to 0.2 with the one of a λ equal to 0.05:

$$S_{05} = 1.42 S_{20} \tag{2.2}$$

Therefore, the adjusted CN values are given by the formula:

$$CN_{05} = CN_{20}/(1.42 - 0.0042 CN_{20}) \tag{2.3}$$

The CN can be further adjusted to the different Antecedent Moisture Conditions (AMC) of type I and II by the following formulas:

$$CN_{I} = 4.2 CN_{II}/(10 - 0.058 CN_{II}) \tag{2.4}$$

$$CN_{III} = 23 CN_{II}/(10 + 0.13 CN_{II}) \tag{2.5}$$

Type I corresponds to dry conditions, i.e. with antecedent 5-day precipitation of less than 13 mm (or less than 35 mm, for vegetation cover during a period of development), type II to average conditions, i.e. antecedent precipitation between 13 and 38 mm (or 35 and 53 mm, for the development phase), while type III to wet conditions, i.e. antecedent precipitation greater than 38 mm (or greater than 53 mm, for the development phase).

2.2.2 A look on some unit hydrographs (UH)

In common hydrological flood modelling problems, a design hydrograph is requested in order to dimensionalize a structure. This design hydrograph is the product of the temporal transformation of a design rainfall into discharge at the basin's outlet, through the unit hydrograph (UH). After adopting a UH, for a known effective rainfall in discreet time the hydrograph at the outlet is calculated using the superposition principle. Empirical SUHs' are the ones preferred for common everyday-hydrological studies due to their simplicity and parsimony. They include, among else, the polygonal-formed Snyder hydrograph (Snyder, 1938), the triagonal-formed U.K. Institute of Hydrology hydrograph (Sutcliffe, 1978) and the triagonal-formed SCS hydrograph, whose basic time parameters are the peak time (time in which the SUH reaches its peak) and the base time (time from the beginning until the end of the SUH). In Table 1 a review of the base and peak time of the most common empricial SUHs' is given. A much more extensive study on Unit Hydrographs in general is presented in Singh *et al.* (2014).

As one may notice (Table 1), in the NRCS and the U.K. Institute of Hydrology hydrographs, the base time is only a few multiples of the time of concentration (or the peak time). What happens, however, when the basin filters rainfall slower? Michailidi *et al.* (2013) investigated the NRCS-CN method for loss estimation and the triangular SUH (Sutcliffe, 1978) in two basins in Greece and Cyprus (Sarantapotamos and Peristerona) and observed that it failed to reproduce not only the peak but also the base time and the exponential recession limb, even with calibrated parameters. In particular, the recession limb appeared very linear and the attenuation time was small. The immediate response of the basins also contributed to the small base time, since the base time is only ~2.5 times the time to peak in both the methods (U.K. Institute of Hydrology, NRCS).

These results were in agreement with the comparative study of Nigussie *et al.* (2016) who showed that although the NRCS hydrograph performs best in peak estimation, it fails to approximate the recession limb. The same problem occurred with the rest of the hydrographs; the ones that performed adequately in peak estimation had difficulty reproducing the base time and vice versa. Bhunya *et al.* (2011) have criticised the NRCS hydrograph due to its applicability, given its present form, only in small to midsize basins. In order to deal with the discrepancies of the method, Yannopoulos *et al.* (2006) tested two events in a basin in Thessaly, Greece, by changing the *CN* and the lag time of the hydrograph and modifying, in this way, the hydrograph's features (base time, peak) to improve the simulations, but, due to the meager number of events, a general conclusion could not be drawn.

Table 1. Literature approaches for the definition of base and peak time of the SUH.

Authors	Peak time, t_p (h)	Base time, t_b (h)	Remarks
NRCS (2004)	$\frac{DT}{2}+t_l$	$2.67t_p$	Lag time (time from the centroid of excess rainfall to peak discharge) $t_l=0.6\ t_c$, *DT*: duration of unit excess rainfall (h).

U.K. Institute of Hydrology (Sutcliffe, 1978)	$0.9t_l$	$2.52t_p$	
Snyder (1938)	$C_t(LL_c)^{0.3}$	$3+3(\frac{t_p}{24})$	C_t: coefficient depending on basin characteristics, L (km): length of main stream, L_c (km): distance from watershed outlet to a point on main stream nearest to the center of the watershed area; defined in the fairly mountainous Appalachian Highlands.

2.2.3 The subsurface flow

After observing the temporal evolution of the majority of the historical events of the study basins it became obvious that the flood attenuation of the basins seemed very slow, almost exponential- in most cases multiples of the time of concentration- and very smooth, despite the complex rainfall patterns. This phenomenon can be attributed to subsurface storm flow (or interflow, through flow, hypodermic flow), which is the water draining from the unsaturated zone of the soil and above the groundwater level. Basins with permeable soils, steep slopes and narrow valley bottoms favour this mechanism (Efstratiadis *et al.*, 2014) that can be considered as a predominant runoff mechanism in well-vegetated areas (Hewlett, 1974). In the earlier years it was believed that the main flood mechanism was the Hortonian overland flow; a flow that occurs when rainfall intensity exceeds the top soil's infiltration capacity (Horton, 1931). Subsurface storm flow is a much slower and smooth process than Hortonian surface flow, which happens very quick and whose pattern follows the one of the rainfall.

The first to introduce the importance of subsurface storm flow in the runoff process was Hewlett (1961). Kirkby and Chorley (1967) claimed that it is capable of producing runoff peaks in hydrographs. These rapid rises were explained from Hewlett and Hibbert (1967) as a result of drops of water "bumping" into other drops that are already in the soil, achieving a "snowlballing" effect. Freeze (1972) compared hydrographs resulting from different flood mechanisms (e.g. Hortonian, subsurface, base flow) and was sceptical about the consideration of subsurface storm flow as a significant mechanism in the runoff process, adding that its occurrence is feasible only under specific geomorphological contexts- convex hillshopes feeding steeply incised channels. He added that subsurface flow consists of subsurface storm flow and baseflow, or in other words, saturated flow from the channel bed reaching the channel, as well as percolation from the seepage faces to the banks. Knisel (1973) criticised Freeze (1972) for downplaying the importance of subsurface storm flow in the runoff process, stating that it may influence highly the flood volume. Hewlett (1974) added that subsurface storm flow can be defined as any quantity of water passing the gauging station that has entered through the soil surface and has travelled through that for an undefined amount of time.

Thus, separating storm and base flow- generated by the rainfall that infiltrates to the groundwater and later feeds the stream- is largely subject to the reasearcher's judgement.

2.2.4 Integration of excess rainfall intensity in the Unit Hydrograph theory

As mentioned in the previous chapters, the association of the time of concentration with excess rainfall intensity has been widely accepted. This dependency can have a direct implication on the Unit Hydrographs, since, as it has been previously shown, their parameters are directly associated with the time of concentration. The first (to the author's knowledge) who have explicitly accounted for a variable time magnitude depending on the excess rainfall in a UH was Reed et al. (1975). The authors have considered Nash's linear reservoir model (Nash, 1957), lagging the produced runoff of each time step based on the respective rainfall excess. The model was fitted in a flood event and compared with a linear model, revealing the superiority of the former in producing the peak. Additionally, it was noted by the authors that the application of a variable lag model will enable the establishment of correlations between the model's parameters and physical characteristics of the basin, in order to assist the estimation of the parameters in ungauged basins. On the same note, Caroni et al. (1986) concluded that for an accurate representation of rainfall-runoff transformation, models providing for variable lag-time of the response function should be introduced. For linear time-variant rainfall-runoff models one can refer among else to Mandeville and O'Donnell (1973), Diskin and Boneh (1974).

Rodríguez-Iturbe *et al.* (1982) working on the hypothesis of the geomorphologic IUH (Rodríguez-Iturbe and Valdés, 1979) in a nonlinear framework, developed a geomorphoclimatic IUH that allowed the estimation of the unit impulse response function for a given particular rainfall input, considering the velocity parameter as a function of the effective rainfall intensity and duration. The main parameters of the IUH were the bifurcation ratio, length ratio and area ratio, among else, which could be obtained after some elaborations in a GIS environment. Similarly, Wang et al. (1981) introduced non-linearity into a geomorphologic IUH through the dependence of the mean holding time of a basin with rainfall intensity.

More recently, Cho et al. (2018) implemented a distributed Clark's UH, incorporating spatially and temporally variable flow along with the NRCS-CN method (NRCS, 2004), in the pixel-scale to estimate spatially distributed runoff depths from distributed rainfall fields and to produce separated unit hydrographs, thus obtaining a direct runoff hydrograph. Results demonstrated relatively good fit to observed flow in four watersheds in central USA. On a similar note, Risva (2018) managed to achieve an impressive agreement between observed and simulated events in Nedontas basin (also a study basin in this paper) by introducing an event-based distributed hydrological model. The author employed an improved NRCS-CN scheme with a velocity-based approach in the grid-scale to determine the flood hydrograph, while the time of concentration was assumed as a function of runoff intensity.

To the author's knowledge, the first to introduce an empirical SUH in the context of event-based hydrological modelling, integrating the concept of the varying time of concentration was Michailidi (2018). In fact, the above model is improved for the scopes of this thesis and regional relationships will be provided, as it will be seen in the next chapter.

3. METHODOLOGY

3.1 Improving the estimation of the intensity-based time of concentration

As mentioned in the previous chapter, regional relationships regarding the intensity-based time of concentration in a GIS framework were provided by Michailidi *et al.* (2018). The authors have discretized the study basins in a sufficient number of sub-basins and estimated the runoff travel time in each basin. For the most upstream basin, where a well-defined flow route is absent and shallow flow prevails, the authors estimated the travel time, *t*, as $t=L/(Ks^{0.5})$, where *k* is a roughness coefficient (m s^{-1}) related to soil conditions, *S* is the average slope of the overland flow (m m^{-1}), and L (m) is the length of the overland flow, as measured from the most hydraulically distant point to the beginning of the well-formed main stream.

In this chapter, the proposed relationships are somewhat improved by estimating the overland travel time of the most upstream sub-basin as a function of excess rainfall intensity, based on the following equation (Chow *et al.*, 1988):

$$t = L^{0.6}n^{0.6}/({i_e}^{0.4}S^{0.3}) \tag{3.1}$$

where i_e is the average excess rainfall intensity (m s^{-1}), *L* is the length of the overland flow (m), *n* is the Manning's roughness coefficient and *S* is the slope (m m^{-1}). Manning's roughness coefficient was determined using land cover information. The regional formulas previously developed by Michailidi *et al.* (2018) were updated, using the intensity-based overland travel time of eq. (3.1) for the most upstream sub-basin and newer formulas for the basins were provided (Eq. (3.2)-(3.4)). Since the scope of this thesis regards primarily the integration of the time of concentration in the hydrological design, the results of this analysis are presented briefly here, without focusing with many details on the case studies or the methodology for estimating the varying *tc*. The reader is therefore, redirected to the already published work, mentioned previously.

$$t_0 = 30.0\, nL^{0.164} b^{0.058} J^{-0.358} \tag{3.2}$$

$$\beta = 0.40 - 0.03 A^{0.304}\, L^{0.548} b^{-1.543} \tag{3.3}$$

$$t_c = t_0 i_e^{-\beta} \tag{3.4}$$

It should be noted that the newly developed and improved relationships differ from the older ones mainly at low values of excess rainfall intensities (e.g. < 1-2 mm/hour). Additionally, the β exponent shows less variability and is now closer to the theoretical value of 0.4. The predictive capacity of the new equations is very satisfactory, as can be seen in Figure 3.1.

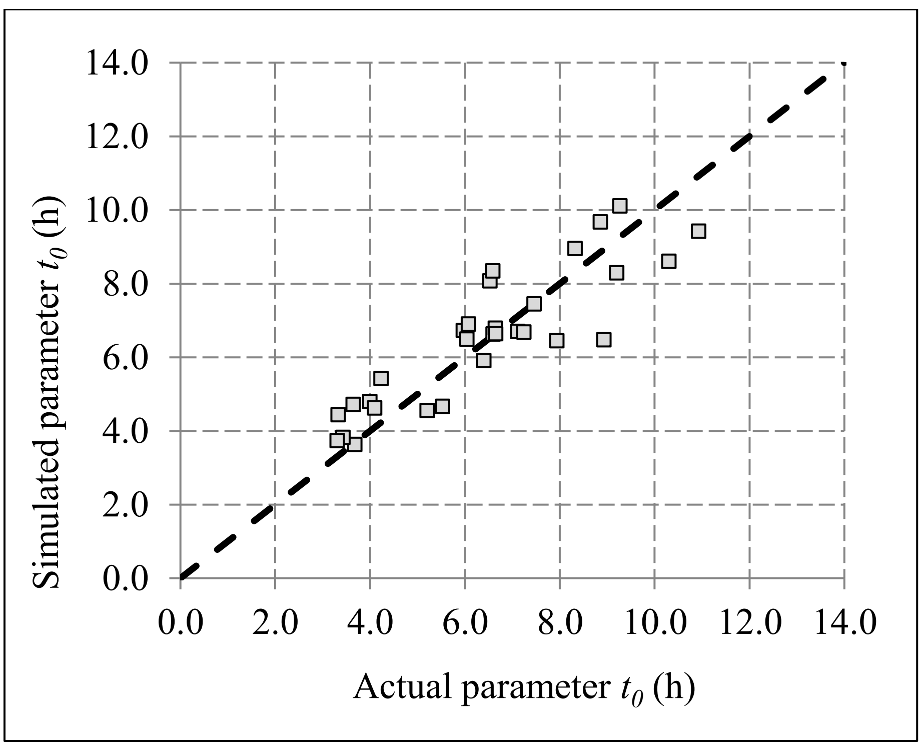

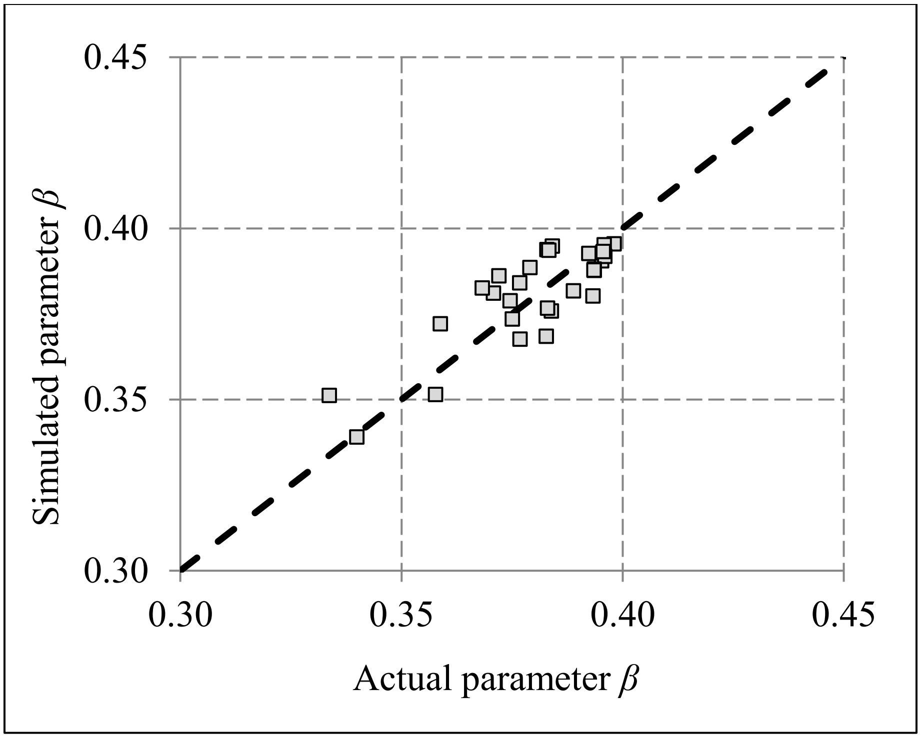

Figure 3.1: Comparison of actual (i.e. estimated through the GIS procedure) and simulated (by the corresponding regional formulas) parameters t_0 (top) and β (bottom).

It should be mentioned that t_0 is also highly correlated with the θ parameter of the reduction curve introduced by Bacchi *et al.* (1992). The reduction curves mirror the local character of the flood event, as they represent, in a synthetic manner, the speed of the growing and recession phase of the flood event at a given section. More specifically, θ is the scale of fluctuation, or else the integral of the autocorrelation function of the discharge process and can be interpreted as a characteristic response time of the basin (Ranzi *et al.*, 2006), measuring a rate of decrease of the autocorrelation function (Franchini and Galeati, 2000). Ranzi *et al.* (2006) provided regional relationships for θ, in particular for impermeable Apennine basins $\theta=12.694L^{0.64}/\Delta z^{0.5}$, where θ is in in h, L is the main stream length (km) and Δz is the difference between mean and outlet elevation (m). Franchini and Galeati (2000) associated θ with the time lag or *tlag*, which is the time from the center of mass of rainfall excess to the center of mass of direct runoff, using the equation $\theta = m\ tlag$, where m can range around the values 1.6-2, depending on the order of the Autoregressive Gaussian process used to describe discharge. Time lag has also been associated with tc with the formula $tc = k\ tlag$, where k can range between 1.4-1.67 (McCuen, 2009). For the study basins presented in the paper of Michailidi *et al.* (2018), the (unit) time lag is calculated setting $k=1.67$, which is the value suggested by NRCS and the tc equations (3.2)-(3.4), considering an excess rainfall intensity of 1 mm/h (or else the *unit time of concentration*) and it is compared with the time lag calculated from the equation of Franchini and Galeati (2000) for $m=2$, which corresponds to a Gaussian process of order 4- thus more appropriate for discharge time series, as they exhibit a high degree of autocorrelation- and the regional relationship for θ of Ranzi *et al.* (2006). As it can be seen from Figure 3.2, the calculated time lags from the two approaches are very near the theoretical line 1:1, which is a further validation of the satisfactory performance of the developed regional relationships for tc.

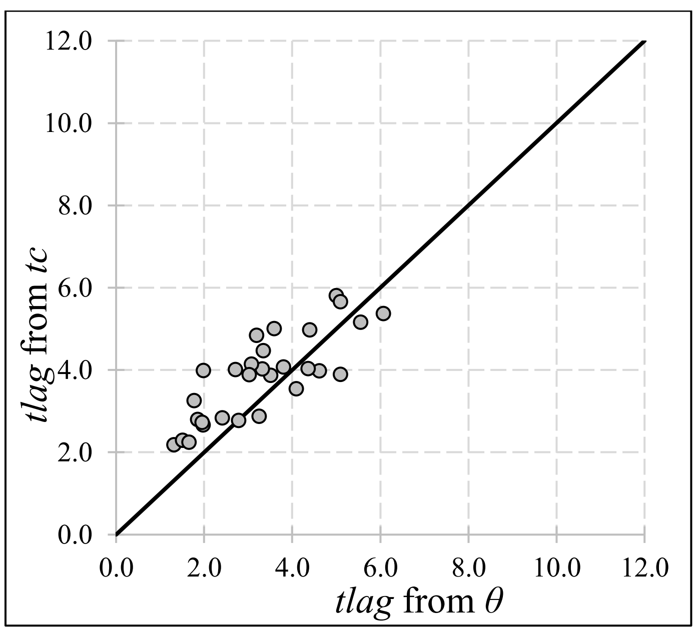

Figure 3.2: Comparison between *tlag*, calculated from the *tc* and from *θ*.

3.2 Adaptation of the varying time of concentration concept in flood modelling and development of the dynamic SUH

The empirical synthetic unit hydrograph (SUH) that was implemented for this thesis consisted of a linear rising and an exponentially decreasing recession limb. The choice of the exponential recession limb was based on historical events, in which it was evident that the flood recession can be frequently approached satisfactorily by a relationship similar to that of a linear reservoir recession equation. The proposed hydrograph's peak and base time of the SUH are expressed respectively as:

$$t_p = \frac{DT}{2} + \beta t_c \tag{3.5}$$

$$t_b = DT + \gamma t_c \tag{3.6}$$

where β and γ are parameters with $0<\beta<1$ and $\gamma \geq 1$; base time less than t_c has no physical substance. The parameter β was introduced to regulate the steepness of the rising limb. Analogously, γ was introduced in order to account for the slow response of the basin that sometimes indicates the existence of subsurface storm flow, and the hydrograph shape in general.

In the numerical simulations, the times t_b and t_p are rounded in order to be expressed as integer multiples of the rainfall sampling interval DT. For given t_p and t_b values (or β and γ values) the ordinates of the SUH are calculated as follows. For $t \leq t_p$ (rising limb) the discharge values are calculated by a linear equation as:

$$q(t) = q_p t / t_p \tag{3.7}$$

where q_p is the peak time of the SUH. For $t>t_p$ (recession limb) the discharge values are calculated by a negative exponential function as:

$$q(t) = q_p \exp\left(-k\left(t - t_p\right)\right) \tag{3.8}$$

where k is such, so that for $t=t_b$ the discharge is equal with a minimum value q_0 or $q(t_b)=q_0$. So, from Eq. (3.8) the attenuation/damping factor is:

$$k = -\ln\left(\frac{q_0}{q_p}\right) / \left(t_b - t_p\right) \tag{3.9}$$

The discharge at the passing of the base time is considered analogous to the basin's area A in km^2 as $q_0=0.0001A$ m^3/s. This value was chosen very small, so that for basins of about 100 km^2 (which is close to the mean area of the study basins), the discharge of the SUH at the end of the base time, becomes practically zero (0.01 m^3/s/km^2).

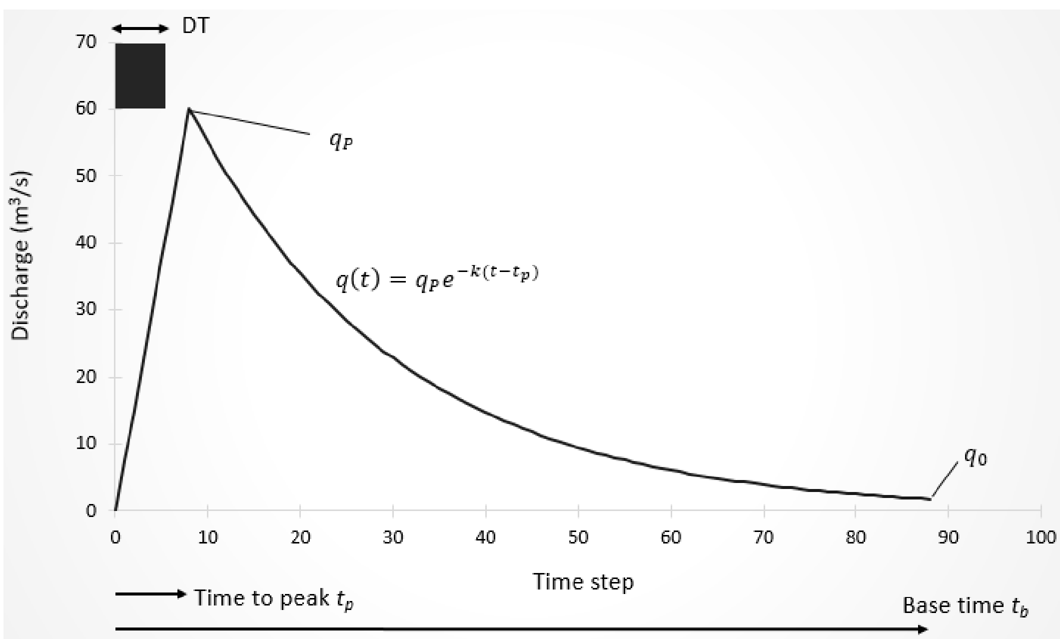

Figure 3.3: The developed *dynamic SUH*.

The discharge peak is calculated numerically from the equation of continuity, that is the equation of the SUH volume with unit rainfall volume $V_0=h_0A$, where $h_0=10$ mm the rainfall height of the unit rainfall and A the basin's area.

The SUH parameters β and γ were later calibrated for each basin. Additionally, for the extraction of the excess rainfall the SCS-CN method was used with a fixed abstraction ratio, λ, in each basin.

The base and peak time of the SUH are functions of the time of concentration, estimated from the formulas of chapter 3.1. Therefore, the model proposed is a parametrised simple SUH, taking into account the geomorphological basin diversities and the effect of excess rainfall intensity in each time step in a dynamic manner, thus, creating a sort of *dynamic synthetic unit hydrograph* (Figure 3.3). So, for a given net rainfall, the output hydrograph is the result of the convolution process, stemming from a SUH whose shape changes dynamically according to the excess rainfall intensity of the studied storm event. The above *dynamic SUH* was first introduced in the PhD thesis of Michailidi (2018) and here it was further developed.

4. APPLICATION

4.1 Data collection

The study basins are small-to-medium size and mostly mountainous, located in Greece, Italy and Cyprus (Table 2). The selection of the study basins was carried out based on the following criteria:

1. Non-urbanised basin, unaffected by technical interventions at least at the largest percentage of the total cover area.

2. Absence of a reservoir controlled by a dam upstream of the hydrometric station; the existence of a dam causes alteration the flood peak and the form of the hydrograph, depending, also, from the operational rules of the gate.

3. Availability of both discharge or stage and rainfall data in a fine temporal scale (≤1 *h*) in the same time period. More preference was also given towards basins with reliable rainfall data from different meteorological stations inside the basin or in the vicinity.

The majority of the study basins were located in Emilia Romagna, Italy due to the abundance and accessibility of the data. In specific, the platform DEXT3R (http://www.smr.arpa.emr.it/dext3r/) developed by the Regional Agency for Environmental protection (Agenzia Regionale per la Protezione Ambientale – ARPA) of Emilia Romagna, permits the user to download with easiness hydrometeorological data of a large number of stations in the region. The temporal availability of the data is case-specific and here was 10 years on average.

The basins of Nedontas and Sarantapotamos in Greece and Peristerona and Xeros in Cyprus were part of the “DEUCALION research project – Assessment of flood flows in Greece under conditions of hydroclimatic variability: Development of physically established conceptual-probabilistic framework and computational tools” conducted by the National Technical University of Athens (http://deucalionproject.itia.ntua.gr/). For the Greek basins the hydrometeorological stations were installed and maintained and the data transmitted for the full duration of the research project (March 2011–March 2014). The discharge and rainfall series of these are available in http://openmeteo.org/ and http://hoa.ntua.gr/.

The two basins located in Cyprus had an older hydrometeorological network with 15-minute time step events dating from 1977 to 2007 for Peristerona and from 1989 to 2000 for Xeros. The location of the basins can be seen in Figure 4.1. The name of the stations, their nature and their coordinates (in WGS84 EPSG: 4326) are presented in Table 3.

Table 2. Study basins and their geomorphological characteristics (A: area; L: length of longest flow path; J: average slope of main stream; Δz: difference between mean and outlet elevation; t_G, t_K: time of concentration estimated through the Giandotti and Kirpich formulas, respectively).

River basin (outlet)	Country	A (km^2)	L (km)	J (%)	Δz (m)	t_G (h)	t_K (h)
Sarantapotamos (Gyra Stefanis)	GR	143.7	32.1	3.8	369	6.3	3.4
Nedontas (Kalamata)	GR	114.8	21.6	7.5	819	3.3	1.9
Baganza (Marzolara)	IT	125.5	32.7	3.7	538	5.1	3.5
Scoltenna (Pievepelago)	IT	129.7	14.9	11.7	583	3.5	1.2
Ceno (Ponte Lamberti)	IT	328.7	38.2	3.8	517	7.1	3.9
Nure (Ferriere)	IT	48.3	12.1	7.9	489	2.6	1.2
Leo (Fanano)	IT	36.9	10.6	18.7	752	1.8	0.8
Montone (Castrocaro)	IT	235.7	47.4	4.2	455	7.8	4.4
Enza (Vetto)	IT	293.5	31.5	5.5	551	6.2	2.9
Nure (Farini)	IT	200.6	24.4	5.0	513	5.1	2.5
Xeros (Lazarides)	CY	67.5	12.9	12.4	436	3.1	1.1
Peristerona (Panagia Bridge)	CY	77.8	23.6	8.4	466	4.1	2.0

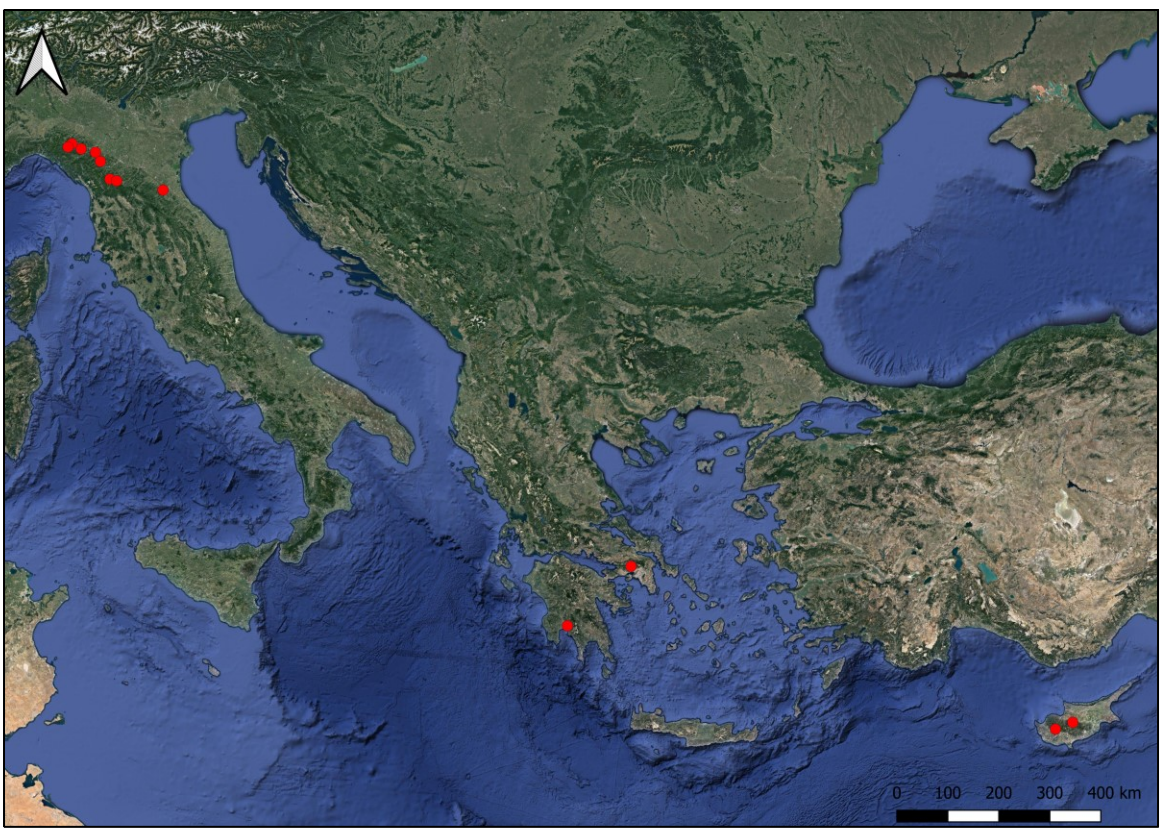

Figure 4.1: Location of the study basins (in red).

Table 3. Location of hydrometeorological stations and sampling time interval of the data (M: Meteorological S-H: Stage-Hydrometric station).

Country	Basin (Outlet)	Station name	Type	Longitude/Latitude	Sampling time interval
Greece	Nedontas (Kalamata)	Kalamata	M, S-H	22.12798, 37.06251	15 min
		Alagonia	M	22.24400, 37.10674	10 min
		Karveliotis	M	22.22361, 37.07348	15 min
	Sarantapotamos (Gyra Stefanis)	Gyra Stefanis	S-H	23.53301, 38.13283	15 min
		Prasino	M	23.51312, 38.18613	10 min
		Vilia	M	23.32774, 38.16471	10 min
		Mandra	M	23.563779, 38.122983	10 min
Italy	Scoltenna (Pievepelago)	Pievepealgo	S-H	10.630172, 44.215298	30 min
		Pievepealgo	M	10.577236, 44.194281	30 min
		Doccia di Fiumalbo	M	10.67311, 44.190126	30 min
	Baganza (Marzolara)	Marzolara	S-H	10.171386, 44.634852	30 min
		Marra	M	10.047463, 44.473424	30 min
		Berceto	M	9.983008, 44.510475	30 min
		Calestano	M	10.124518, 44.605912	30 min
		Casaselvatica	M	10.035641, 44.547812	30 min
	Ceno (Ponte Lamberti)	Ponte Lamberti	S-H	9.8121, 44.650975	30 min
		Varsi	M	9.821058, 44.649419	30 min
		Bardi	M	9.732836, 44.633788	30 min
		Noveglia	M	9.766839, 44.592693	30 min
		Pione	M	9.633999, 44.619463	30 min
		Farfanaro	M	9.67953, 44.56668	30 min
		Nociveglia	M	9.610037, 44.547104	30 min
		Casalporino	M	9.547383, 44.527112	30 min
		Frassineto	M	9.585078, 44.581571	30 min

	Nure (Farini)	Farini	M, S-H	9.56966, 44.7121	30 min
		Cassimoreno	M	9.57935, 44.6362	30 min
		Ferriere Pluvio	M	9.49596, 44.6445	30 min
		Selva Ferriere	M	9.48245, 44.5868	30 min
		Groppalo	M	9.59791, 44.6963	30 min
	Nure (Ferriere)	Ferriere	S-H	9.48964, 44.6437	30 min
		Cassimoreno	M	9.57935, 44.6362	30 min
		Ferriere Pluvio	M	9.49596, 44.6445	30 min
		Selva Ferriere	M	9.48245, 44.5868	30 min
	Leo (Fanano)	Fanano	S-H	10.7991, 44.2039	30 min
		Lago Pratignano	M	10.8178, 44.1774	30 min
		Doccia di Fiumalbo	M	10.6731, 44.1901	30 min
		Sestola	M	10.7687, 44.2321	30 min
	Montone (Castrocaro)	Castrocaro	M, S-H	11.9494, 44.1701	30 min
		Monte Grosso	M	11.8718, 44.0715	30 min
		Prataci	M	11.6652, 44.0018	30 min
		Vallicelle	M	11.8049, 44.0294	30 min
	Enza (Vetto)	Vetto	M, S-H	10.3300, 44.4934	30 min
		Lago Ballano	M	10.1021, 44.3695	30 min
		Lago Paduli	M	10.1385, 44.3458	30 min
		Succiso	M	10.1925, 44.3634	30 min
		Isola Palanzano	M	10.1622, 44.4284	30 min
		Ramiseto	M	10.2756, 44.4114	30 min
		Castelnovo ne' Monti	M	10.3947, 44.4349	30 min
Cyprus	Persiterona (Panagia bridge)	Panagia	S-H	33.081881, 35.019603	15 min
		Panagia	M	-	15 min
		Apliki	M	-	15 min
		Alona	M	-	15 min
	Xeros (Lazarides)	Alonoudi	S-H	32.699669, 34.927281	15 min
		Alonoudi	M	-	15 min
		Pano Vrisi	M	-	15 min
		Mouti	M	-	15 min

4.2 Data processing

After the raw stage data for the basins in Italy were gathered, the equivalent discharges were calculated. The ARPA issues for every year the Annual Hydrological Reports (Annali Idrologici) that include among else, updated stage and discharge information for each hydrometric station. From these values, the rating curve for each station and year was calculated. Since the Italian basins offered an abundance of flood data, at least for the recent years, the events with the largest daily discharge of each month were selected. Following the appropriate rating curve and year, the stage information was transformed into discharge by interpolation or, in some cases, extrapolation of the fitted stage-discharge relationship. A verification was later performed with the daily discharge values published in the reports and in the cases of substantial incongruences between the published and calculated daily discharges, the candidate flood event was excluded.

For Greek basins the available time period was much more limited, so, a different selection criteria was applied; the selection of the episodes was performed by setting a threshold of 0.5 m^3/km^2. In the cases with absence or shortage of such events, smaller flood events were included, as well. The sample of the two basins in Cyprus included major flood events that occurred after 1977 and 1989.

In some cases, the rainfall data needed to be aggregated in order to match the discharge time interval (e.g. Sarantapotamos and Nedontas). After both discharge and point rainfall referred to the same time interval the contribution of the mean areal rainfall of each station to the entire basin was estimated by Thiessen polygons.

4.3 Base flow separation

In order to apply the combined methodology of NRCS-CN for the hydrological losses and the *dynamic SUH*, the direct runoff (runoff produced from the effective rainfall) of each observed event needed to be estimated or in other words, the base flow from the total hydrograph needed to be removed. Base flow, here, denotes the flow that is not caused by the current precipitation event, but it occurs due to previous flood events and/or due to the groundwater recharge.

Hewlett and Hibbert (1967) have quite gloomily stated that separating base flow from surface runoff is “one of the most desperate analysis techniques in use in hydrology” and Appleby (1970) has complemented this notion by referring to this procedure as a “fascinating arena of fancy and speculation”.

Understanding where surface runoff starts is not a cumbersome task; in the majority of the observed hydrographs, especially in relatively small basins, the rising limb is notably abrupt, indicating approximately the start. However, when the basin’s geomorphological and geological features as well as aquifer properties favour the existence of interflow, determining the end of surface runoff contribution is challenging. Additionally, determining the contribution of base flow before the recession is almost impossible.

The separation techniques used during the past years are based on graphical methods, digital filters and algorithms, analytical solutions and natural tracers, with the latter being the most accurate according to Blume *et al.* (2007). Essentially, the majority of these are somewhat arbitrary and are based on some assumptions (Dingman, 2002). Hewlett and

Hibbert (1967) proposed that since the arbitrariness cannot be avoided one should use a common arbitrary rule for all the hydrographs of the small basins. Linsley Jr *et al.* (1982) were in favour towards the idea of defining the surface runoff end based on experience, in a qualitative manner, as “too short...too short...and about right.”

Here, a very simple rule was applied, as proposed by Dingman (2002); the end of surface runoff occurs $N=0.827A^{0.2}$ days after the peak, where A (km^2) is the drainage area. The rate of change of the base flow was considered constant, in the most simplistic manner. For the two-peaked events the reference point was the second peak (regardless of its magnitude in comparison with the peak occurring previously). In a lot of cases, the evolution of the estimated base flow seemed visually pleasing; when this did not occur, the end of surface runoff was shifted forward to a location where the gradient of the discharge was more constant and closer to zero. It is important to mention that in our case studies, the baseflow was a small percentage of the total flow and in many cases even non-existent. For rivers with significant baseflow a more thorough approach is necessary.

4.4 Calibration framework

A global multi-criteria optimisation framework was implemented on 160 episodes from 10 basins, in order to adapt the parameters of the *dynamic SUH* method to the hydrographs of each basin. In specific, the parameters β (time-to-peak parameter) and γ (base time parameter) were optimised. In this thesis, the abstraction ratio, λ, is considered as constant and equal to 0.05, since the study basins are mainly low infiltration and mountainous and are therefore less likely to be characterized by high initial losses.

For a specific λ value and for a given total rainfall height P and for a given runoff discharge Q of every episode the potential maximum retention S was calculated analytically using the following equation obtained by eq. (4.1) when solved for S:

$$S = (2\lambda P + (1-\lambda)Q - (Q[Q(1-\lambda)^2 + 4\lambda P])^{0.5})/(2\lambda^2) \quad (4.1)$$

So, for every group of parameter values of the optimization process, the reproduction of the volume of the observed hydrographs is guaranteed. The adopted objective function to minimise was the following:

$$F(\beta,\gamma) = \sum_{i=1}^{j}(10\sum_{t=1}^{n}\frac{|q_{obs,i,t} - q_{sim,i,t}|}{q_{obs,i,t}} + 3000\frac{|q_{p,obs,i} - q_{p,sim,i}|}{q_{p,obs,i}} + 1000\frac{|t_{start,obs,i} - t_{start,sim,i}|}{t_{start,obs,i}} + 1000\frac{|t_{peak,obs,i} - t_{peak,sim,i}|}{t_{peak,obs,i}}) \quad (4.2)$$

where j is the total number of flood events in a basin, i event of tested basin, $q_{obs,i,t}$ and $q_{sim,i,t}$ the observed and simulated discharge at time t, respectively, $q_{p,obs,i}$ and $q_{p,sim,i}$ observed and simulated peak, $t_{start,obs,i}$ and $t_{start,sim,i}$ the observed and simulated runoff start, $t_{peak,obs,i}$ and $t_{peak,sim,i}$ the observed and simulated peak time. Main objective of the minimisation was to reduce the error between the simulated and observed: discharge values, peaks, start and end of event runoff. The weights before each part establish a satisfactory compromise among the individual parts of the objective function. The calibration framework was applied to each basin, separately, in order to obtain a two-parameter set (β, γ) for each basin.

The Evolutionary Annealing-Simplex (EAS) optimisation algorithm was used, originally developed by Efstratiadis (2008) and written in MATLAB, available freely in https://www.itia.ntua.gr/en/softinfo/29/, permitting to carry out complex optimisation problems in a computationally efficient manner.

5. RESULTS

5.1 Model performance and regionalization of its parameters

After the calibration of the model in ten different basins, its performance in each flood event was evaluated. The simulation of the flood events showed a very good fit in the majority of the events; the Nash-Sutcliffe efficiency exceeded 0.65 for more than 70 % of the events even under very complex rainfall patterns (see APPENDIX A: Event graphs). The mean Nash-Sutcliffe coefficient for each basin ranged from 0.40 in the Baganza basin to 0.81 in the Nure (Farini) basin. The fitness of the model is remarkably high, considering its parsimony (2 parameters) and its computational and conceptual simplicity. In Figure 5.1 it is noticed that the observed and simulated peaks in the totality of events- except from some instances- are impressively close.

Despite its satisfactory fit in the majority of the cases, in some instances the peak seemed to be significantly underestimated (e.g. P_P_6_10, P_P_11_14, BG_M_11_12, N_FA_3_11, etc.; see APPENDIX A: Event graphs), while in others the peak was significantly overestimated (e.g. P_P_2_10, P_P_3_13, P_P_12_13, P_P_3_15, etc.). These deviations from the observed values can occur for various reasons. The mechanisms of infiltration and runoff generation can be quite complex. Therefore, a simple and parsimonious method, such as the NRCS-CN, cannot fully capture the dynamics of these mechanisms. In many cases of peak underestimation, a pronounced discharge peak was present right at the beginning of the event, caused by a very high precipitation height that fell from the start of the event, in a very short time period. In some events where high rainfall values fell progressively, the model found no difficulty in their simulation (e.g. P_P_10_12, BG_M_11_08, C_PL_4_12, L_FN_5_08, L_FN_11_12, N_FA_8_06; N2_2012, etc.). The change in soil moisture before and during an event can be decisive in the production of runoff and in intense events these changes can depend greatly on a soil moisture balance, which is not accounted for in the NRCS-CN method. Additionally, some observed peaks can appear higher than their actual values, since they are a result of an extrapolation of the rating curve way beyond the measurement levels. Nevertheless, the fit of the model is quite impressive, given its conceptual simplicity and parsimony.

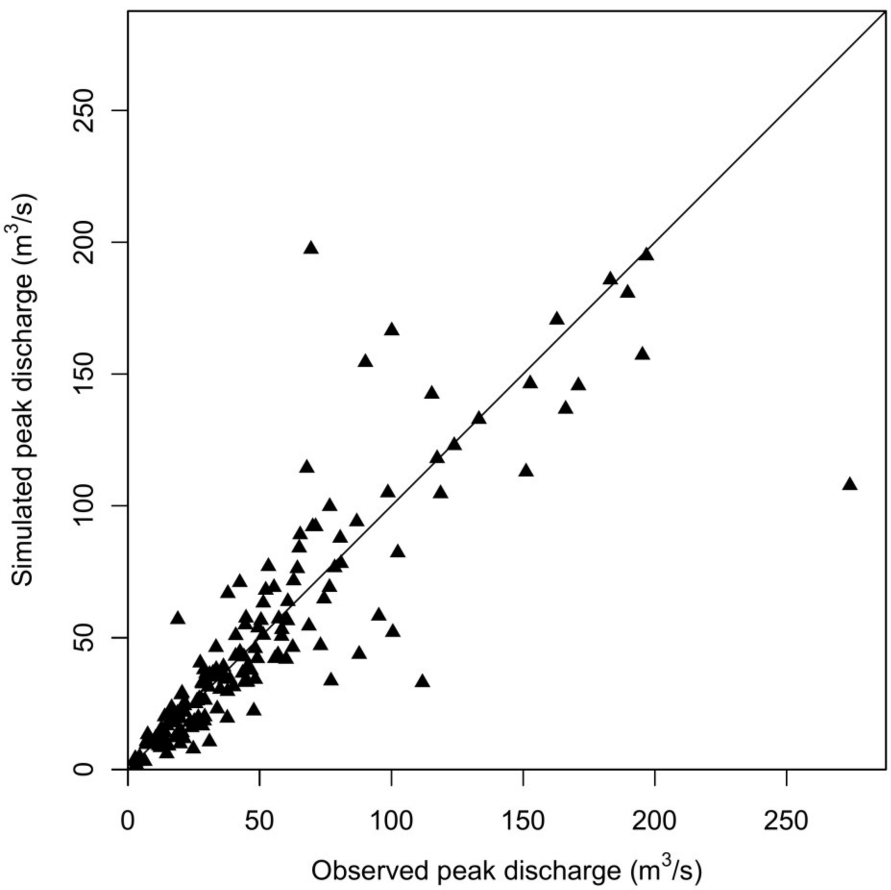

Figure 5.1: The observed and simulated peaks for the 160 flood events.

The resulting set of parameters (peak and base time), after the implementation of the calibration framework on the events of each basin, are given in Table 4, along with the mean Nash-Sutcliffe efficiency for each basin.

Table 4. Calibrated β and γ parameters for each basin and the mean NSE value for each basin.

River basin (outlet)	β	γ	*Mean NSE*
Sarantapotamos (Gyra Stefanis)	0.57	3.61	0.57
Nedontas (Kalamata)	0.55	10.91	0.62
Baganza (Marzolara)	0.59	8.84	0.56
Scoltenna (Pievepelago)	0.51	12.55	0.40
Ceno (Ponte Lamberti)	0.78	6.98	0.73
Leo (Fanano)	0.88	21.26	0.79
Montone (Castrocaro)	0.69	6.06	0.80
Nure (Farini)	0.52	6.12	0.81
Xeros (Lazarides)	0.79	16.01	0.69
Peristerona (Panagia Bridge)	0.88	22.03	0.77

The most defining parameter of the modified SCS and *dynamic SUH* method is γ, which is related to the base time and affects the peak; an increase of γ leads to a decrease of the peak. For the study basins this ranged from 3.61 to 22.03 with a mean value of 11.44 and is characterised by a large variation (standard deviation equals to 6.13). An attempt to correlate γ with the basins' geomorphological characteristics led to fruitful results. The highest linear correlations appeared with the catchment area, A, the mean main stream slope, J, and the length, L equal with -0.72, 0.80 and -0.69, respectively. Therefore, the next step was to provide a regional formula for γ as a function of key basin characteristics. After some attempts to model linearly or exponentially the parameters, a power-law model was chosen for its nice fit. The parameters a_0, a_1, a_2 and a_3 of the power-based model, $\gamma=a_0A^{a}{}_1J^{a}{}_2L^{a}{}_3$ were calibrated by minimizing the error between the γ

optimized for each event and the one provided by the regional formula. First results showed a convergence of a_2 and a_3 to the same value, approximately 1.17, therefore a common parameter was set for both that eventually reduced the total number of parameters. It is noted that the product $J*L$ expresses another geomorphological characteristic of the basin, i.e. the difference in elevation of the basin. The developed regional relationship for γ, the base time parameter, is given by Eq. (5.1).

$$\gamma = 74.1JL/\sqrt{A} \tag{5.1}$$

where A (km^2) is the basin's size, J (m/m), the mean main stream slope, and L (km) the main stream length. As it can be seen from Figure 5.2 the predictive capacity of the regional relationship is very satisfactory.

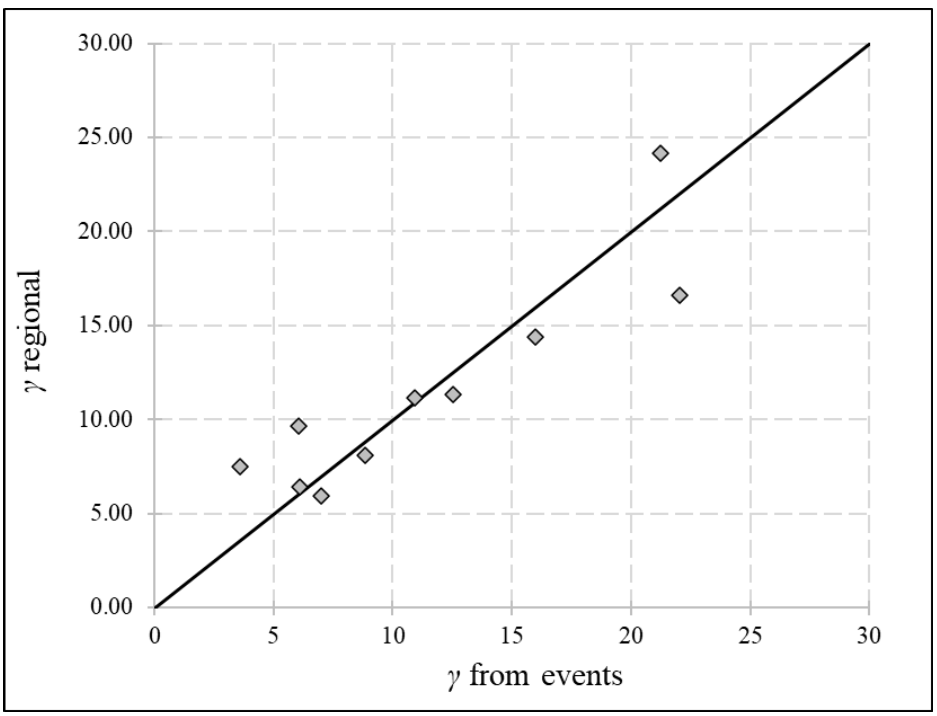

Figure 5.2: Predictive capacity of the regional relationship for γ.

The peak time parameter β ranges from 0.51 to 0.88 with an average value of 0.68, very close to the NRCS value of 0.60, and a standard deviation of 0.15. The highest linear correlations appeared with the mean main stream width, b, and the product $J*L$ equal to -0.48 and 0.60, respectively. A similar regionalisation attempt was carried out for β, as well, as it can be seen in the following equation:

$$\beta = (JL)^{0.43} b^{-0.22} \tag{5.2}$$

Here, b (m) is the mean main stream width, J (m/m), the mean main stream slope, and L (km) the main stream length. The predictive capacity of the above regional relationship, regarding the β parameter can be seen in Figure 5.3. One can note the satisfactory predictive capacity, but for an outlier, which corresponds to the largest-sized basin of the outlet (Ceno at Ponte Lamberti).

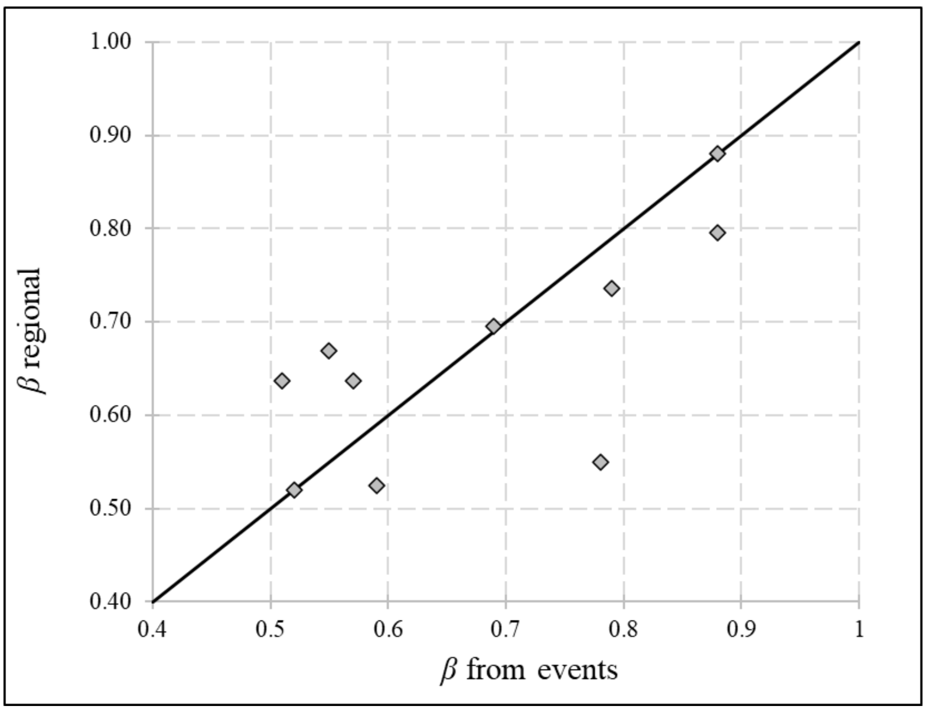

Figure 5.3: Predictive capacity of the regional relationship for *β*.

5.2 Validation

The regional relationships of the peak and base time parameters, β and γ, as a function of the basin's geomorphological characteristics were later validated in 23 events in a subbasin of Nure, with outlet at the Ferriere hydrometric station. The most important flood events in the available series were selected, as described previously, and the same methodological procedure was applied, but in this case β and γ were obtained from the regional relationships (5.1) – (5.2) and therefore equal to 0.55 and 10.2, respectively. The abstraction ratio, λ, was set to a value of 0.05, since the basin is characterised as mountainous with low infiltrations.

As it is confirmed in Figure 5.4 and Figure 5.5, despite the model's parsimony, the simulated events approximate with much precision the observed ones, in terms of peak, time-to-peak, attenuation and overall hydrograph form. The only cases of poor model performance (i.e. peak underestimation) are the peaks caused by a great rainfall height that falls suddenly, combined with low runoff coefficients. In the event N_FE_2_06, right before the discharge peak, there is a period where only 2 mm fell in 7 hours (at a small basin, whose t_c according to Giandotti is 2.6 h), and the discharge values do not exceed 3 m^3/s. After that, a much more elevated rainfall intensity occurs causing an abrupt rising of the discharge to almost 20 m^3/s, while the simulated is about half. This abrupt rise can be explained by the high amount of rainfall that fell before the 7-hour period and reached a total of 56 mm, saturating the upper soil layer. Similarly, in the event N_FE_8_06, a sudden rise of rainfall intensity to 54 mm/h with the antecedent rainfall summing to 23 mm, hurls the discharge from 4 to 38 m^3/s (simulated discharge is underestimated by 58 %). These very sudden and complex changes in soil moisture content might be better approximated by conceptual models that take them explicitly in consideration. Additionally, soil moisture conditions before the start of the flood event can be of extreme importance.

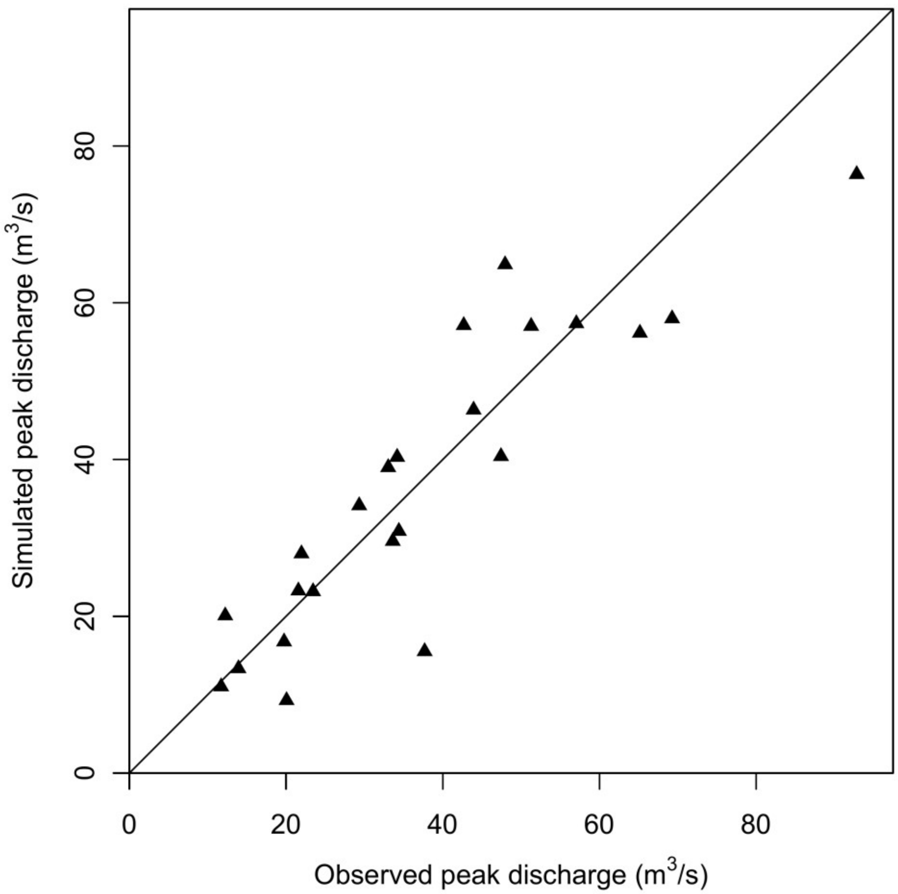

Figure 5.4: The observed and simulated peaks for the Ferriere flood events.

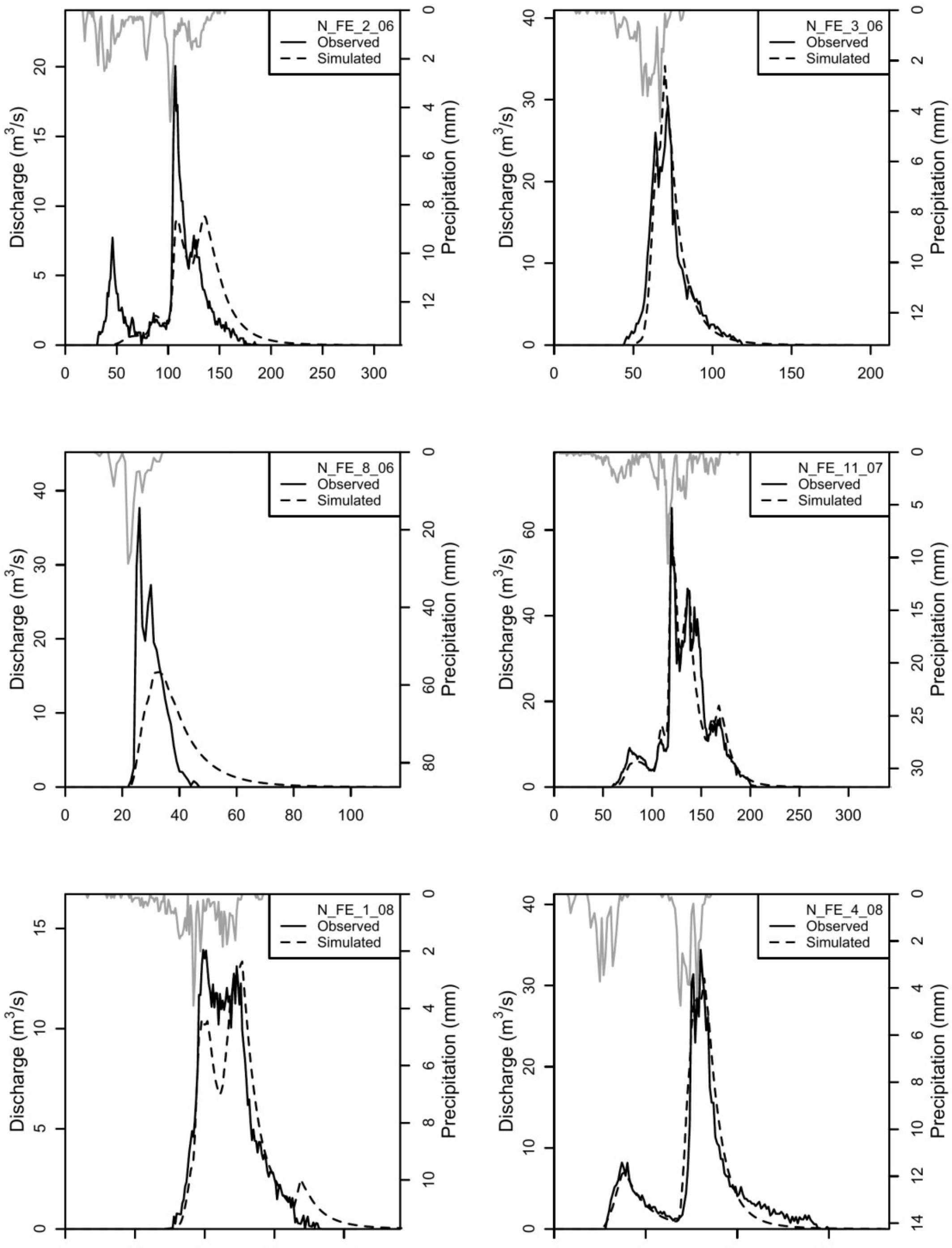
N_FE_2_06
Observed
Simulated
N_FE_3_06
Observed
Simulated
N_FE_8_06
Observed
Simulated
N_FE_11_07
Observed
Simulated
N_FE_1_08
Observed
Simulated
N_FE_4_08
Observed
Simulated
Discharge (m3/s)
Precipitation (mm)

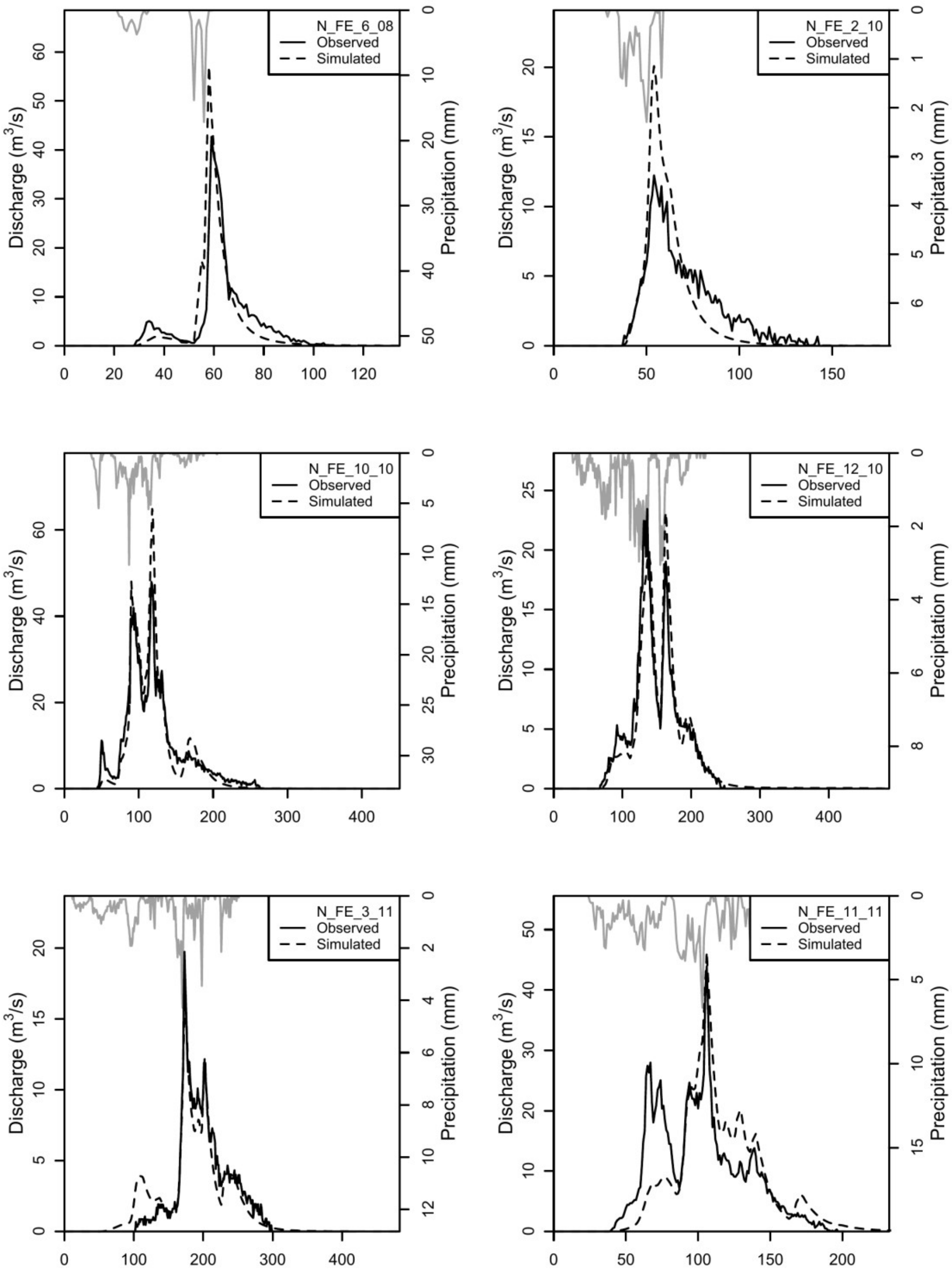
N_FE_6_08
N_FE_2_10
N_FE_10_10
N_FE_12_10
N_FE_3_11
N_FE_11_11
Observed
Simulated
Discharge (m3/s)
Precipitation (mm)

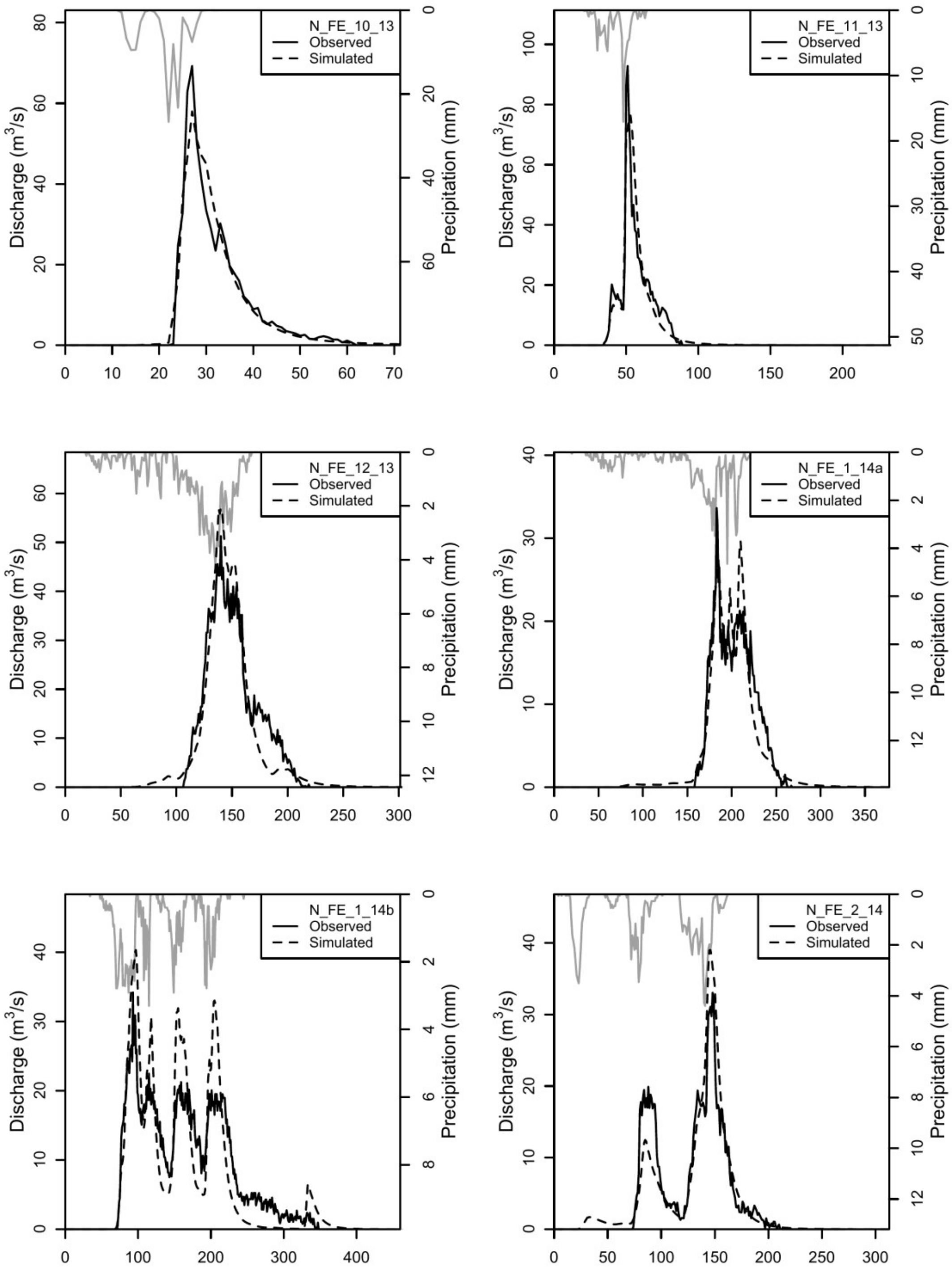
N_FE_10_13
Observed
Simulated
Discharge (m3/s)
Precipitation (mm)
N_FE_11_13
Observed
Simulated
Discharge (m3/s)
Precipitation (mm)
N_FE_12_13
Observed
Simulated
Discharge (m3/s)
Precipitation (mm)
N_FE_1_14a
Observed
Simulated
Discharge (m3/s)
Precipitation (mm)
N_FE_1_14b
Observed
Simulated
Discharge (m3/s)
Precipitation (mm)
N_FE_2_14
Observed
Simulated
Discharge (m3/s)
Precipitation (mm)

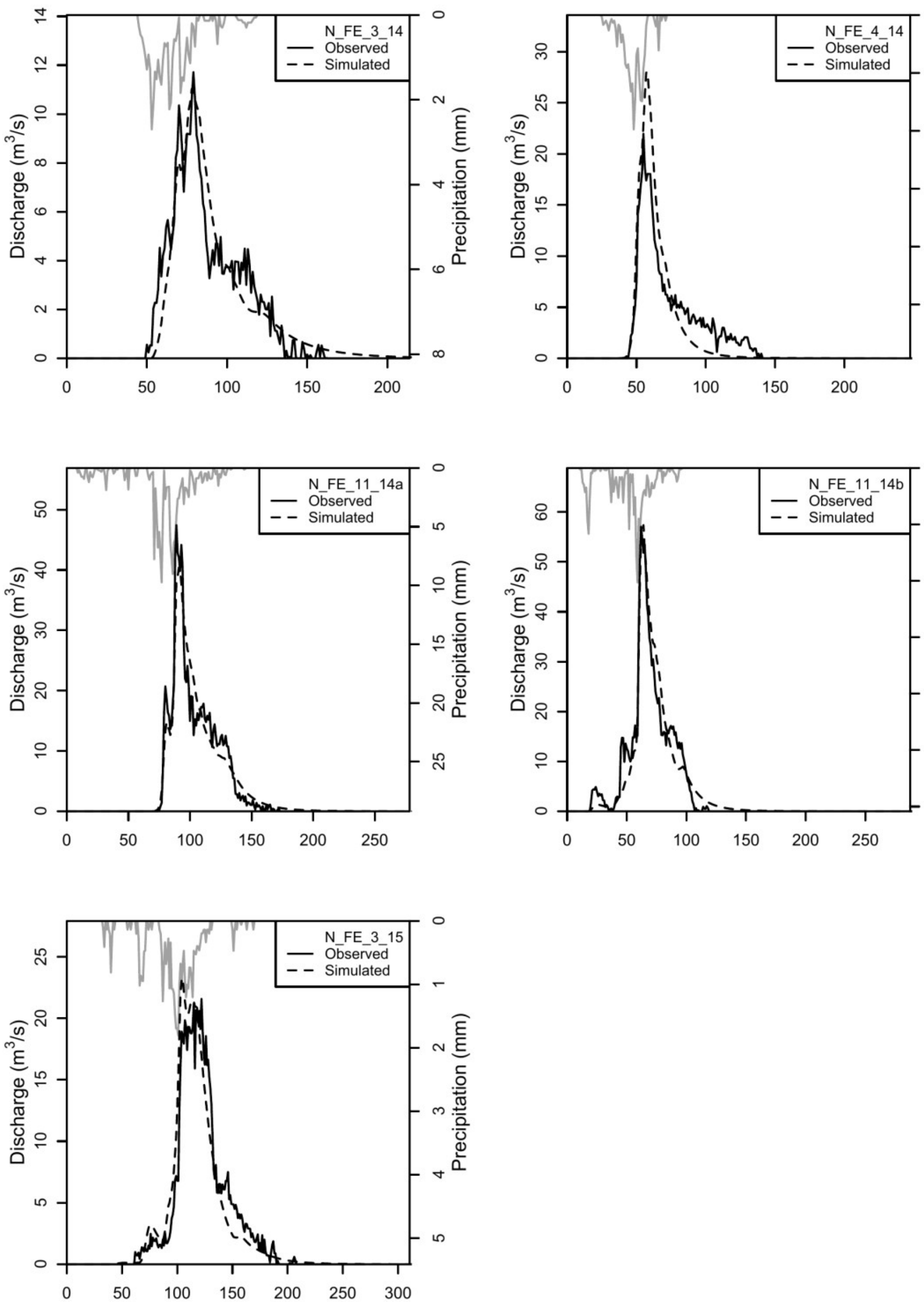

Figure 5.5: Observed and simulated flood events at the Ferriere hydrometric station.

The proposed model performs notably well, especially in the cases of gradual increase of the rainfall height, even under complex temporal rainfall patterns (e.g. N_FE_3_06, 1_08, 4_08, 11_14a, 11_14b). This is also confirmed by the very high Nash-Sutcliffe coefficients as seen in Table 5. In fact, in more than 70 % of the events, the NSE exceeded 0.80 and even reached 0.94, with an average value of 0.81.

Table 5. Total and excess rainfall height (*h* and *he*), runoff coefficient *c*, observed and simulated discharge peak (*Qp* and *Qp,sim*), maximum potential retention *S*, CN and Nash-Sutcliffe coefficient for each event of the Nure (Ferriere) catchment.

Event code	**h (mm)**	**he (mm)**	**c**	**Qp (m^3/s)**	**Qp,sim (m^3/s)**	**S (mm)**	**CN**	**NSE**
N_FE_2_06	113	18	0.16	20	9	394	39	0.45
N_FE_3_06	52	22	0.42	29	34	62	80	0.91
N_FE_8_06	132	10	0.08	38	16	756	25	0.44
N_FE_11_07	203	77	0.38	65	56	276	48	0.92
N_FE_1_08	58	21	0.36	14	13	84	75	0.89
N_FE_4_08	72	26	0.36	34	31	104	71	0.91
N_FE_6_08	64	17	0.27	43	57	134	66	0.63
N_FE_2_10	20	13	0.62	12	20	11	96	0.58
N_FE_10_10	177	85	0.48	48	65	166	60	0.87
N_FE_12_10	122	42	0.34	23	23	190	57	0.92
N_FE_3_11	119	30	0.25	20	17	272	48	0.91
N_FE_11_11	178	60	0.34	44	46	281	47	0.60
N_FE_10_13	114	21	0.19	69	58	343	43	0.94
N_FE_11_13	101	40	0.40	93	76	128	66	0.90
N_FE_12_13	143	76	0.53	51	57	110	70	0.90
N_FE_1_14°	108	46	0.42	34	30	125	67	0.91
N_FE_1_14b	158	109	0.69	34	40	65	80	0.64
N_FE_2_14	126	45	0.36	33	39	185	58	0.83
N_FE_3_14	42	14	0.33	12	11	68	79	0.88
N_FE_4_14	43	19	0.44	22	28	48	84	0.75
N_FE_11_14°	157	41	0.26	47	40	337	43	0.94
N_FE_11_14b	120	48	0.40	57	57	150	63	0.94
N_FE_3_15	42	32	0.76	22	23	12	95	0.91

In order to understand how the model copes in large basins, near the upper area limits of the calibration range, we tested it at 22 observed events of a sub-basin of Enza with outlet at the Vetto hydrometric station (294 km^2). As in the previous case, the β and γ parameter were calculated from the regional relationships (5.1) – (5.2) and were equal to 0.62 and 7.5, respectively, and the initial abstraction losses ratio was set equal to 0.05. In more than 60 % of the events, the NSE exceeded 0.77 and even reached 0.93 (Table 6), with an average value of 0.68, despite the bigger dimension of the basin, proving the model's impressive fitness. Unfortunately, in general, the model performed poorer in respect to Ferriere in terms of NSE, and some of the bigger peaks were overestimated by 38 % in average (Figure 5.6 and Figure 5.7) and thus, raising some doubts about its applicability in bigger basins.

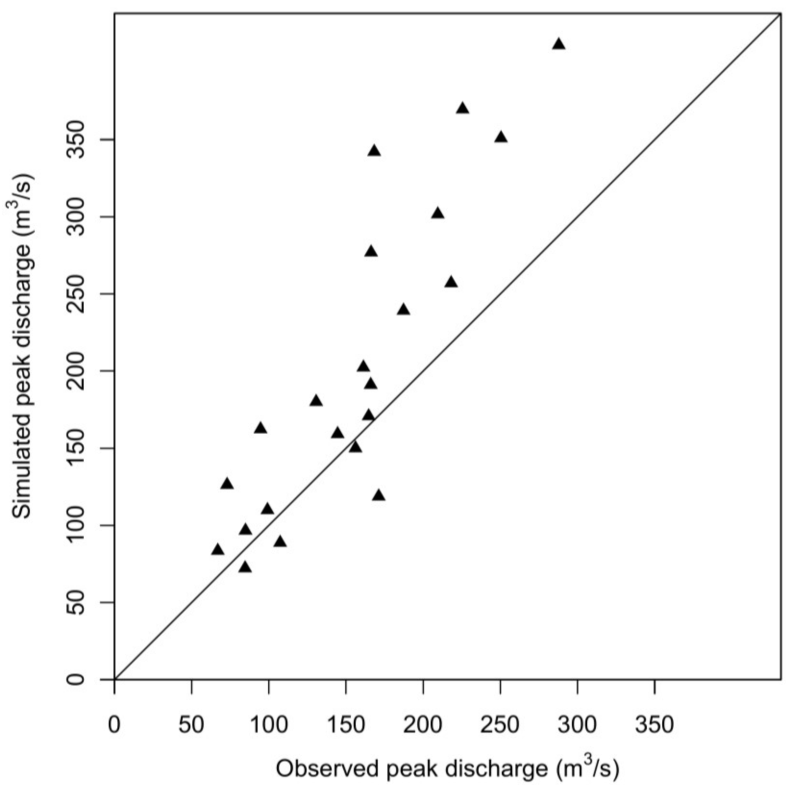

Figure 5.6: The observed and simulated peaks for the Vetto flood events.

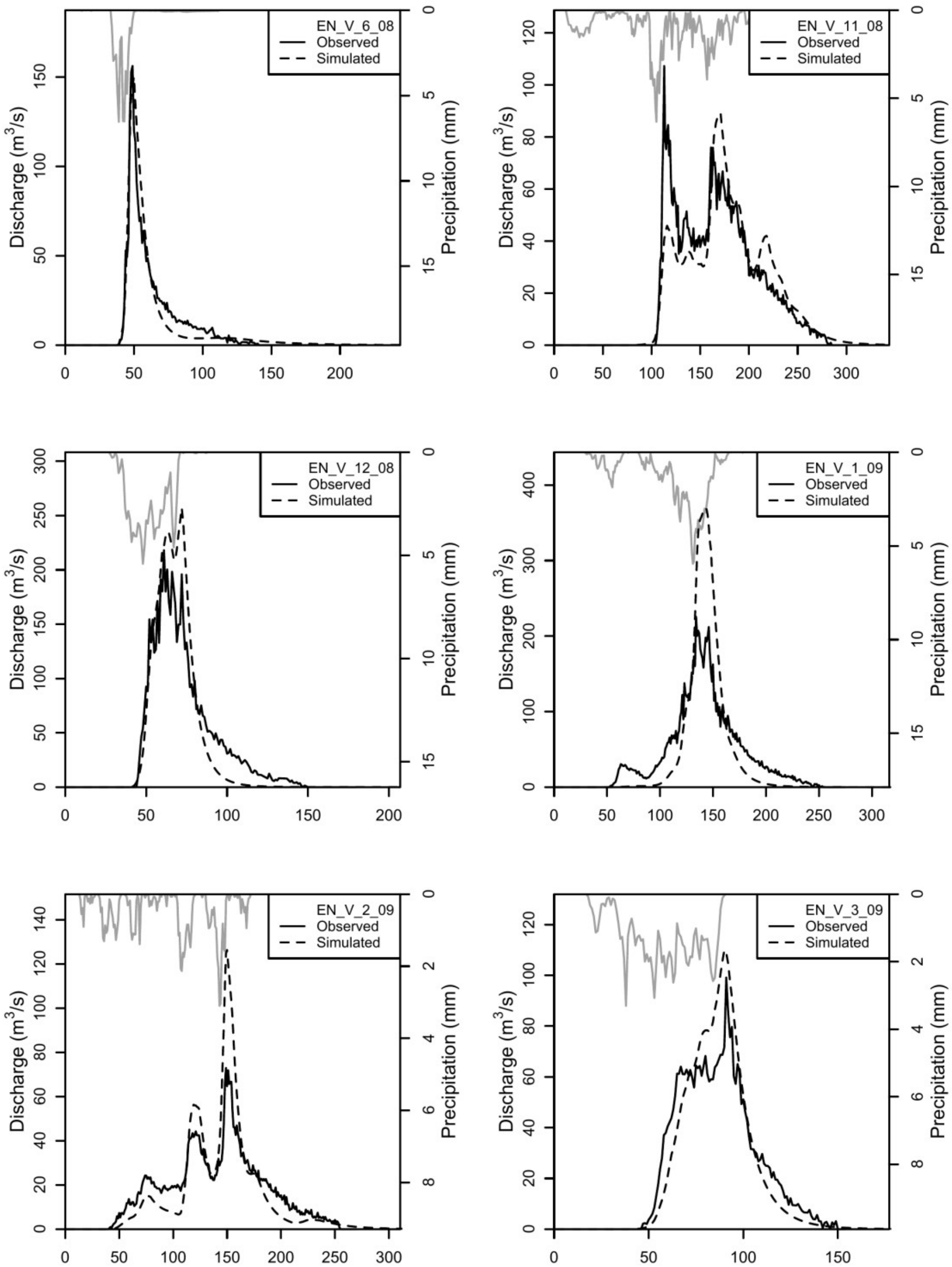
EN_V_6_08
Observed
Simulated
EN_V_11_08
EN_V_12_08
EN_V_1_09
EN_V_2_09
EN_V_3_09
Discharge (m³/s)
Precipitation (mm)

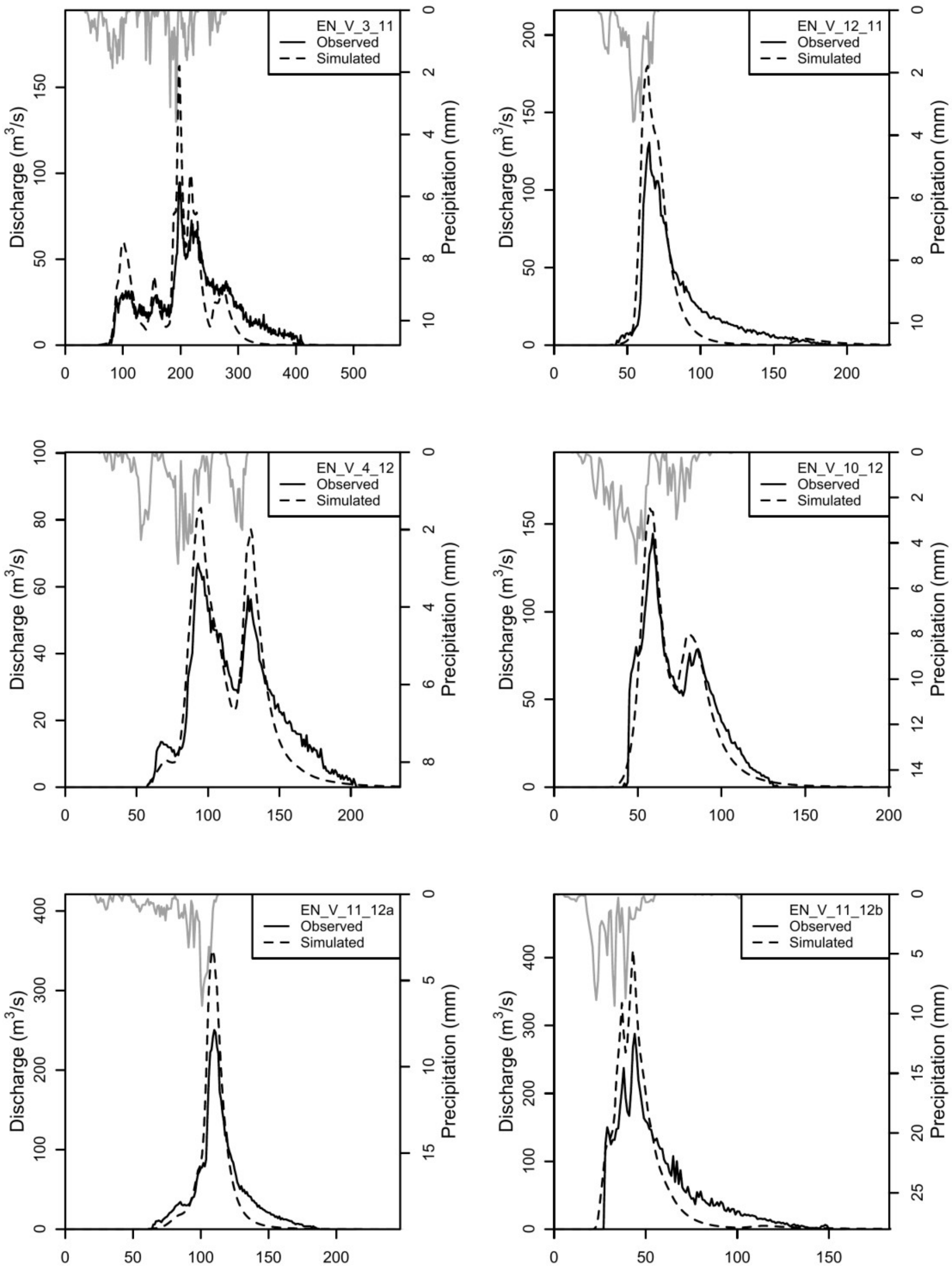
EN_V_3_11
Observed
Simulated
EN_V_12_11
Observed
Simulated
EN_V_4_12
Observed
Simulated
EN_V_10_12
Observed
Simulated
EN_V_11_12a
Observed
Simulated
EN_V_11_12b
Observed
Simulated
Discharge (m3/s)
Precipitation (mm)

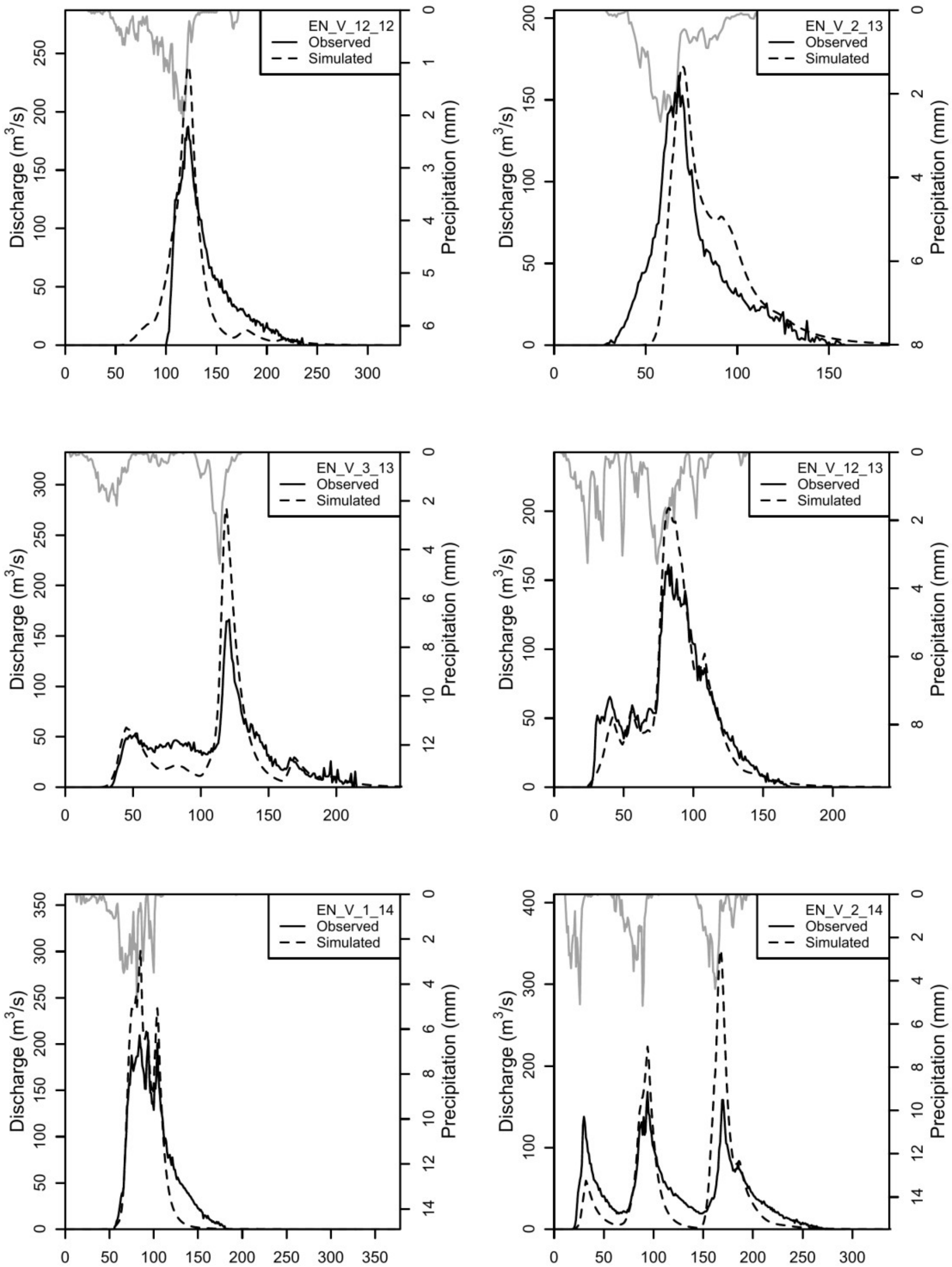
EN_V_12_12
Observed
Simulated
Discharge (m3/s)
Precipitation (mm)
EN_V_2_13
Observed
Simulated
Discharge (m3/s)
Precipitation (mm)
EN_V_3_13
Observed
Simulated
Discharge (m3/s)
Precipitation (mm)
EN_V_12_13
Observed
Simulated
Discharge (m3/s)
Precipitation (mm)
EN_V_1_14
Observed
Simulated
Discharge (m3/s)
Precipitation (mm)
EN_V_2_14
Observed
Simulated
Discharge (m3/s)
Precipitation (mm)

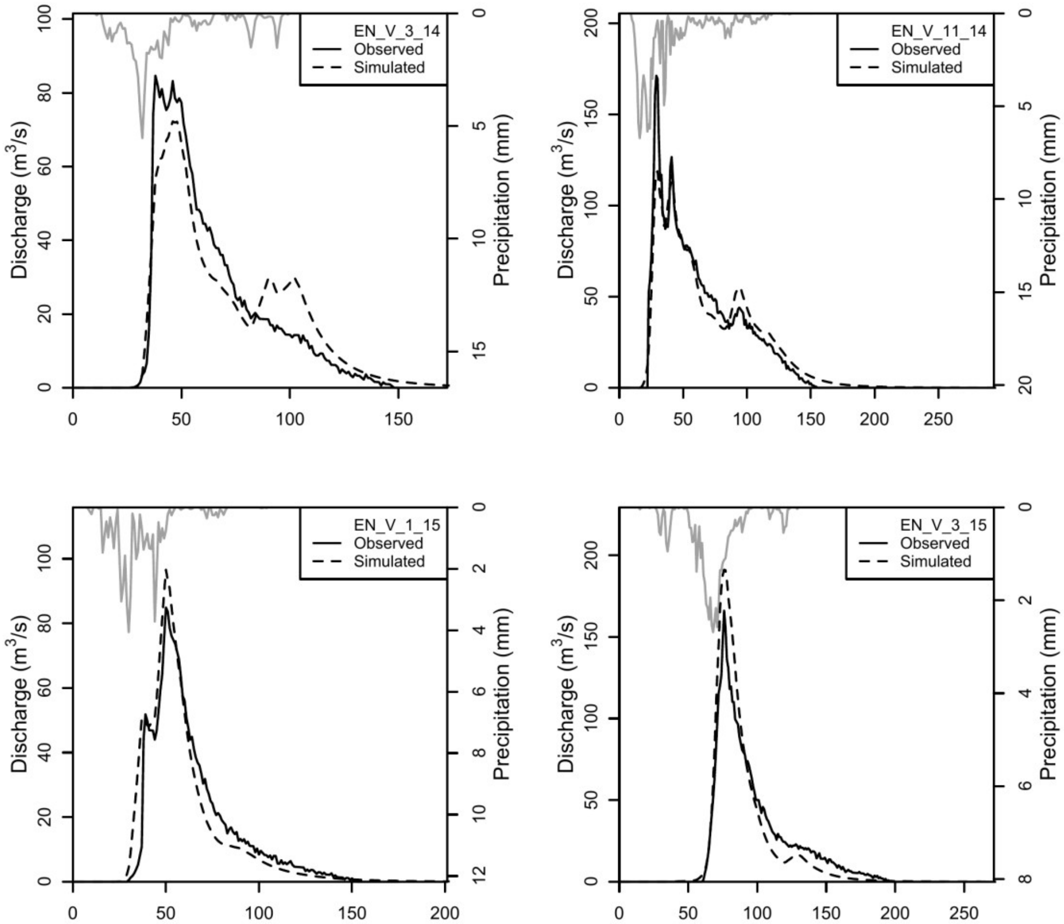

Figure 5.7: Observed and simulated flood events at the Vetto hydrometric station.

Table 6. Total and excess rainfall height (*h* and *he*), runoff coefficient *c*, observed and simulated discharge peak (*Qp* and *Qp,sim*), maximum potential retention *S*, CN and Nash-Sutcliffe coefficient for each event of the Enza (Vetto) catchment.

Event code	h (mm)	he (mm)	c	Qp (m^3/s)	Qp,sim (m^3/s)	S (mm)	CN	NSE
EN_V_6_08	55	14	0.26	156	150	117	68	0.92
EN_V_11_08	213	37	0.17	107	89	688	27	0.80
EN_V_12_08	113	40	0.35	218	257	171	60	0.81
EN_V_1_09	171	66	0.39	226	370	227	53	0.20
EN_V_2_09	75	27	0.36	73	126	109	70	0.41
EN_V_3_09	98	21	0.22	99	110	257	50	0.85
EN_V_3_11	106	53	0.50	95	162	94	73	0.46
EN_V_12_11	45	22	0.48	131	180	42	86	0.65
EN_V_4_12	68	22	0.32	67	84	118	68	0.84
EN_V_10_12	107	29	0.27	145	159	222	53	0.91
EN_V_11_12°	96	37	0.39	250	351	127	67	0.76
EN_V_11_12b	114	49	0.43	288	411	126	67	0.66
EN_V_12_12	60	43	0.72	187	239	21	92	0.78
EN_V_2_13	64	32	0.50	165	171	55	82	0.64
EN_V_3_13	89	43	0.48	166	277	84	75	0.34
EN_V_12_13	108	49	0.45	161	202	113	69	0.87
EN_V_1_14	103	60	0.58	209	302	66	79	0.83
EN_V_2_14	155	72	0.47	168	342	153	62	-0.45
EN_V_3_14	66	19	0.28	85	72	131	66	0.89
EN_V_11_14	129	38	0.30	171	119	241	51	0.93
EN_V_1_15	51	16	0.31	85	97	90	74	0.89
EN_V_3_15	53	29	0.55	166	191	39	87	0.88

5.3 Proposal for hydrological design

The above presented hydrological model can be used in hydrologic design. To this end, given a design hyetograph, the following procedure can be followed in order to obtain a design hydrograph:

1. The abstraction ratio of the NRCS-CN method is set, possibly after obtaining some geomorphological and hydrological data of the studied

basin. As mentioned previously, lower values than the theoretical value of 0.2, e.g. 0.05, seem to be more appropriate for a vast majority of cases. However, when certain peculiarities exist (e.g. higher permeability, low slopes), higher values can also be considered.

2. The CN values for AMCII should be estimated from the tables of the NRCS. These should be adjusted, however, when lower abstraction ratios are used. As mentioned above, for $\lambda=0.05$, adjustment equations are available in the literature. An AMC condition is set, according to the engineer's judgement or regulation and the CN value is adjusted, accordingly.
3. Given the geomorphological characteristics of the basin, the time of concentration parameters are estimated using the regional formulas presented in Chapter 3.1 or alternatively through the procedure developed by Michailidi *et al.* (2018), with the correction of the travel time of the most upstream basin, as presented in Chapter 3.1.
4. For each time step and precipitation values of the design hyetograph, the base and peak time of the *dynamic SUH* can be estimated through the regional formulas of Chapter 5.1 and the time of concentration parameters of the previous step. Through the convolution principle, the design hydrograph is estimated.
5. One might opt to add also a mean baseflow value to the design hydrograph.

5.4 Discussion

Despite existing bibliographical demonstrations that the triangular SUH developed by the NRCS is in a lot of instances inappropriate for flood modelling, its performance was tested here, as well. Assuming typical values for the peak time parameter $\beta=0.6$ and base time parameter $t_b=2.67\ t_p$ (Table 1) for the triangular SUH- thus ignoring the effect that excess rainfall intensity has on the discharge peak- and an initial abstraction ratio $\lambda=0.05$ the model was applied to the 160 flood events. It is noted that the large majority (if not totality) of the empricial SUHs' present in the literature do not take into consideration the varying time of concentration and the form of the triangular SUH- often used in many studies- can produce hydrographs that are atypical, especially for mountainous basins. As it is observed from some characteristic examples in Figure 5.8, the standard triangular SUH constantly overestimates (in a lot of cases exceptionally) the peaks and fails to capture the evolution of the flood events (see also the very low NSE coefficients of Table 7), providing in this manner unrealistic hydrographs. This overestimation occurs due to the very low value of the base time parameter γ and the slow recession limb of the hydrographs observed in most events. More importantly, the lack of integration of the concept of the varying time of concentration in other cases, leads to misestimation of the peak discharge.

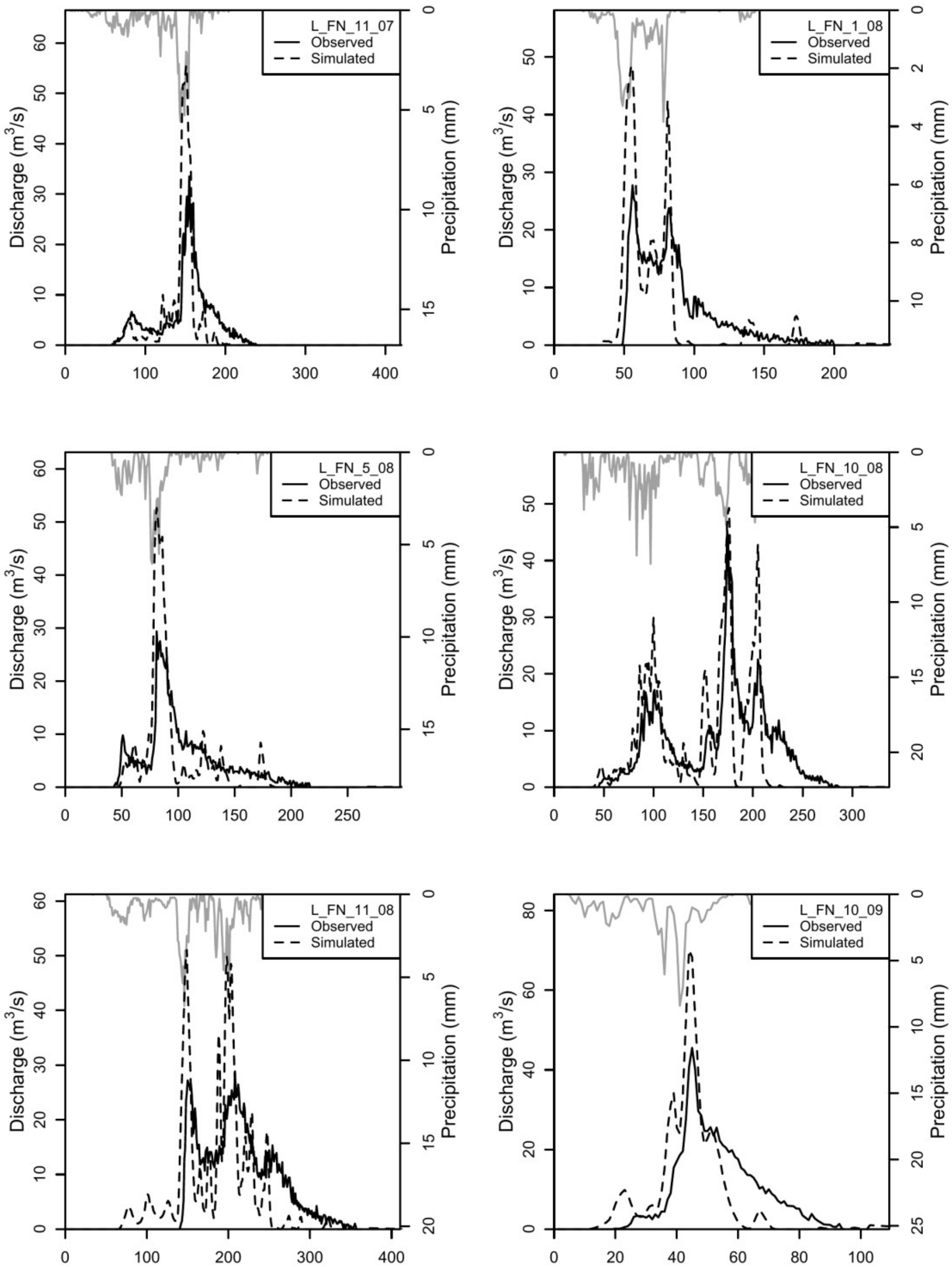

Figure 5.8: Characteristic examples of observed and simulated hydrographs from Fanano using the triangular SUH.

Table 7. The mean NSE value for each basin when applying the standard NRCS-CN method.

River basin (outlet)	*Mean NSE*
Sarantapotamos (Gyra Stefanis)	0.22
Nedontas (Kalamata)	-1.25
Baganza (Marzolara)	-0.21
Scoltenna (Pievepelago)	0.13
Ceno (Ponte Lamberti)	0.60
Leo (Fanano)	0.07
Montone (Castrocaro)	0.35
Nure (Farini)	0.66
Xeros (Lazarides)	-0.20
Peristerona (Panagia Bridge)	-0.72

In fact, the developed *dynamic SUH* overcomes these issues. In fact, as it is evident from Figure 5.9 and the previous chapter, the model performs exceptionally better in terms of peak estimation.

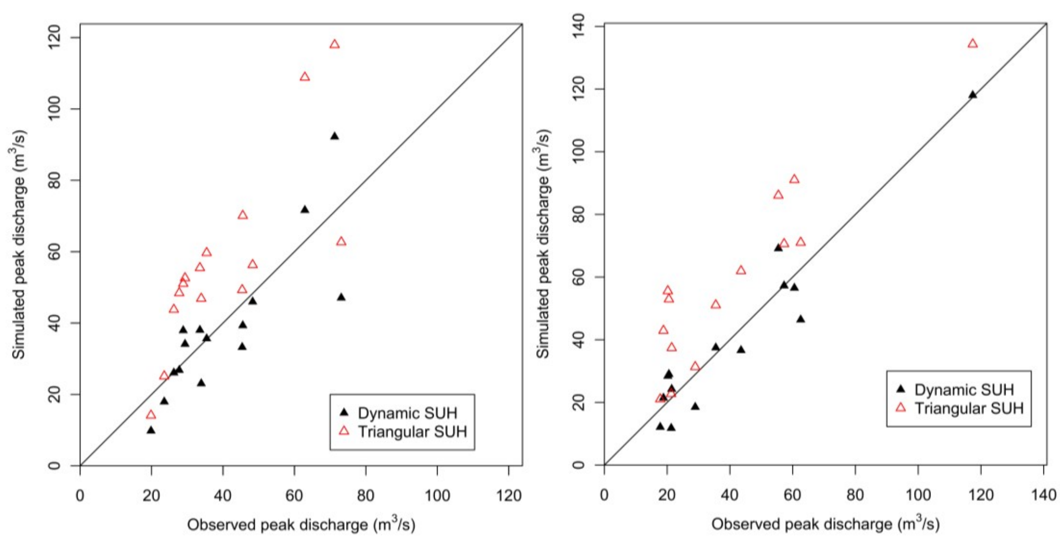

Figure 5.9: Observed and simulated peak discharges using the dynamic SUH and the triangular SUH for Fanano (left) and Peristerona (right).

However, certain considerations should be made prior to its implementation in ungauged basins. Permeable basins with high percolation ratios, whose runoff generation mechanisms can be quite different, and bigger basins (e.g. >200 km^2) could pose a problem. In the latter case, the user is encouraged to discretise the study basin into smaller sub-basins, based on the engineer's judgement, apply the model individually and then implement a routing model to obtain the hydrograph at the outlet.

It should be noted that this thesis does not resolve the problems that arise with the implementation of the NRCS-CN method for runoff production. It is widely accepted that the NRCS-CN method for the estimation of direct runoff height is highly sensitive to the CN parameter (see sudden jumps in runoff when changing the type of Antecedent Soil Moisture conditions), which happens to be highly variable and uncertain. In fact, according to NRCS-CN, the estimation of CN depends on soil and land characteristics and the soil moisture content right before the start of a rainfall event. As mentioned previously, the latter is represented by the Antecedent Soil Moisture (AMC) conditions, which consider the 5-day antecedent precipitation and the season (dormant or growing). However, NRCS-CN has recognised after analysing past events, the variability of CN and its dependence on other factors, as well, such as rainfall intensity and duration, total rainfall, cover density and temperature. More recently, researchers have provided CN models to incorporate other parameters such as slope, soil moisture, and storm duration factors (Mishra et al., 2008; Savvidou et al., 2018; Ajmal et al., 2020, Shi and Wang, 2020). Other researchers have either tried to associate CN with the number of days of antecedent precipitation (Caletka et al., 2020; Kang and Yoo, 2020) or with the rainfall volume (Soulis and Valiantzas, 2012; Tedela et al., 2012; Hawkins et al., 2019).

In this study, attempts to explain the CN's (or the maximum potential retention's) variability using only the cumulative 5-day antecedent precipitation proved somewhat futile. In Figure 5.10 the maximum potential retention, *S*, as a function of the 5- and 10-day antecedent precipitation for the Ferriere catchment is represented. It is evident that although a decreasing relationship between the two can be slightly observed, it fails to explain the variability of *S*. Similar results, were obtained for the Vetto catchment (Figure 5.11). It is worth mentioning that the behaviour observed in these figures are typical for watersheds where surface runoff is prevalent (NRCS, 2004). To the same conclusions regarding the lack of a clear relationship between antecedent precipitation and curve number arrived also Cronshey (1983), Van Mullem (1992) and Hjelmfelt (1991). The latter has even proposed to treat CN as a random variable. In any case, the issue of the estimation of CN is certainly not a simple one to resolve, however important improvements have been made the past years, motivating to conduct further research for its full comprehension.

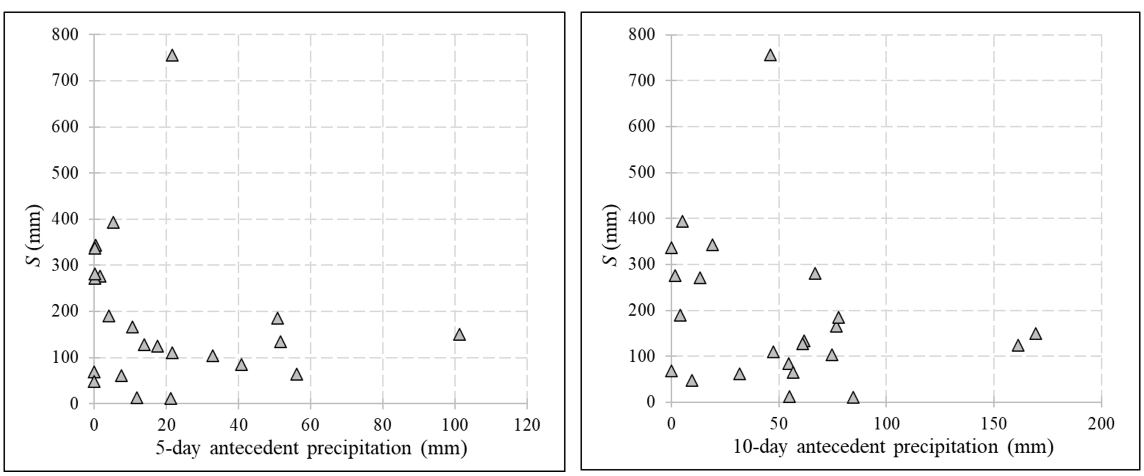

Figure 5.10: The maximum potential retention, *S*, as a function of the 5- (top) and 10-day (bottom) antecedent precipitation for the Ferriere catchment.

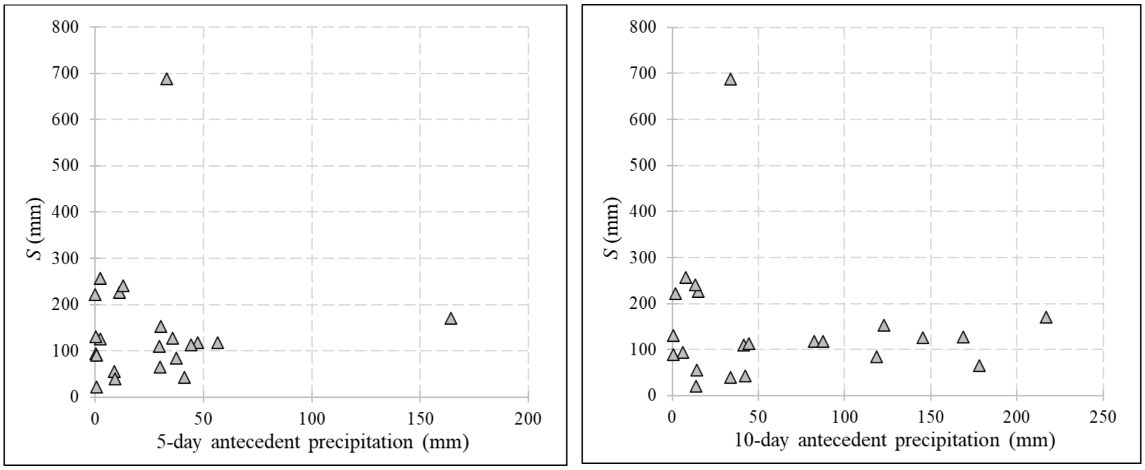

Figure 5.11: The maximum potential retention, *S*, as a function of the 5- (top) and 10-day (bottom) antecedent precipitation for the Vetto catchment.

6. CONCLUSIONS

6.1 Conclusions

In everyday engineering practices, specifically in the context of rainfall-runoff modelling, the time of concentration is considered as constant, despite numerous demonstrations of its variability in different flood events. Even though varying time of concentration relationships do exist, their integration in hydrological tools, such as the SUHs', is still lacking. On the other hand, widely applied SUHs', such as the triangular one developed by the NRCS, lead to significant misestimations that can be attributed to its shape.

The scope of this research is to introduce the concept of variable time of concentration in a simple and parsimonious SUH- whose exponential shape resembles better the observed hydrographs- allowing its implementation under almost any data scarcity and/or lack of resources. In the beginning, the physically-based method for the estimation of the varying time of concentration, developed by Michailidi *et al.* (2018), was improved and the regional relationships were updated. Then, the concept of the varying time of concentration was integrated in the SUH approach, accounting for the change in excess rainfall intensity at each time step, thus obtaining a sort of *dynamic SUH*. In the proposed model, the two integral components of the SUH were parametrised, namely the time to peak through the β parameter and the base time of the event through the γ parameter, in order to account for the rapid increase in discharge and the slow attenuation, present in the hydrographs of many mountainous basins.

The model was calibrated in different basins and various geomorphological contexts and an attempt was made to regionalise these parameters. A total of 160 events in 10 different basins were used and the results showed a remarkable fit of the simulated events to the observed ones. The initial abstraction losses of the NRCS-CN method, was set equal to 0.05 as per literature suggestion for mountainous and low-infiltration basins, which is much lower than the suggested NRCS-CN value of 0.20. Two regional formulas- functions of the basin's geomorphological characteristics- were developed for the β and γ parameters that can be used in absence of rainfall and runoff data. Next, the model and the regional formulas were validated in 23 events of a gauged basin in Northern Italy, producing very high Nash-Sutcliffe coefficients, in spite of their parsimony. A validation of the model in 22 events, however, in a basin with area at the upper limit of the calibration range, showed that despite the overall very satisfactory model fitness, there seems to be an overestimation of the largest flood events, questioning a bit its applicability in bigger basins.

In fact, a more robust implementation of the proposed model in ungauged basins would include their discretization in smaller sub-basins and the application of the model in each sub-basin individually, possibly coupling it with an appropriate routing scheme, thus respecting more the flood generation dynamics that are present in the basin.

In the literature, a plethora of models already exists but are often calibrated in very specific case studies and almost barely validated thoroughly. Much focus is aimed on developing new models, which of course, leads to confusion and uncertainty on their application; instead, improving and thoroughly testing simple models is often wrongfully overlooked. The contribution of this study regarded the latter and provided means for flood designing in small basins in the absence of discharge data.

6.2 Further research

As mentioned previously, simple and easily applied models are attractive to everyday engineering practices. This study focused mainly on the development of a realistically designed empirical SUH that integrates the varying time of concentration concept, and the development of regional relationships that permit its implementation in ungauged basins. To this end, the proposed model should be further tested to other basins, within its calibration range in order to better understand its performance.

More attention should be given on the estimation of the hydrological losses. The NRCS-CN method can cope remarkably well in different hydrological scenarios, despite its parsimony and conceptual simplicity. But, the "correct" estimation of the CN can prove cumbersome and can affect dramatically the runoff. Therefore, further investigations should be carried out regarding its nature and the factors that influence it. Particular focus must be given on various factors such as the soil moisture rainfall intensity and duration, total rainfall, cover density, temperature, growing season and antecedent moisture conditions. The better comprehension of the runoff generation mechanisms can prompt the development of models for the proper estimation of CN, assisting in the updating or the eventual substitution of the tabulated- and sometimes limited- values of the NRCS.

Additionally, another point of research is the regionalisation of the initial abstraction ratio of the NRCS-CN method. Regional formulas or tabulated values can be given for its application to ungauged basins. As a consequence, tabulated values for CN should be updated for different initial abstraction ratios.

Finally, the proposed model should depart from its deterministic implementation and it should be applied in a more stochastic context. Direct runoff estimation is very sensitive to the choice of the CN parameter and, as it has been previously discussed, the choice of the most representative CN is not straightforward. Antecedent precipitation- proxy of the soil moisture content- can have a huge effect on maximum potential retention, and thus CN. Therefore, since antecedent precipitation is a stochastic variable, the CN parameter should be considered as stochastic. In fact, this could entail the development of a relationship that would eventually assign a CN value, for a particular antecedent precipitation based on a probabilistic distribution. This would resolve also the problem of the sudden jumps in runoff for the different AMC conditions and enhance the reliability of the model output.

7. APPENDIX A: EVENT GRAPHS

7.1 ITALY

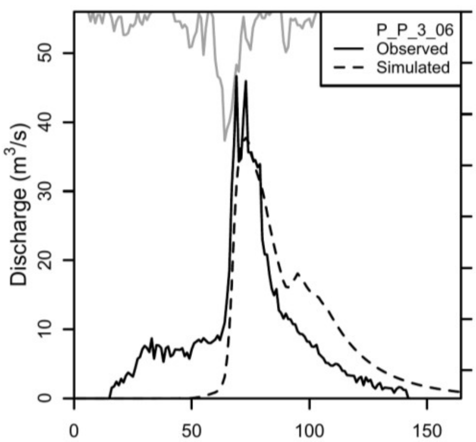

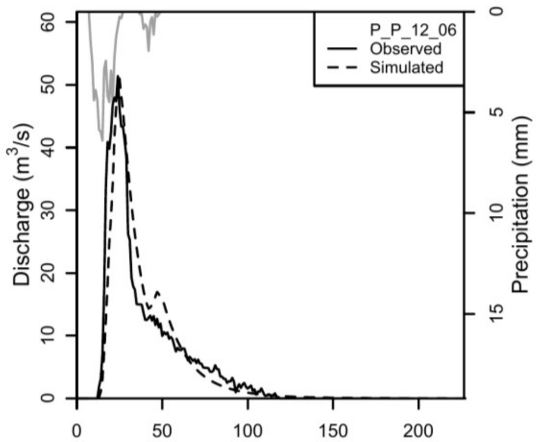

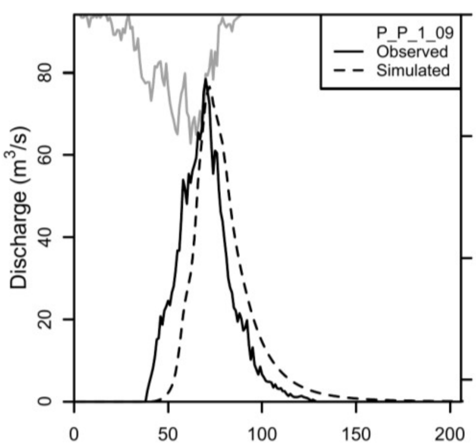

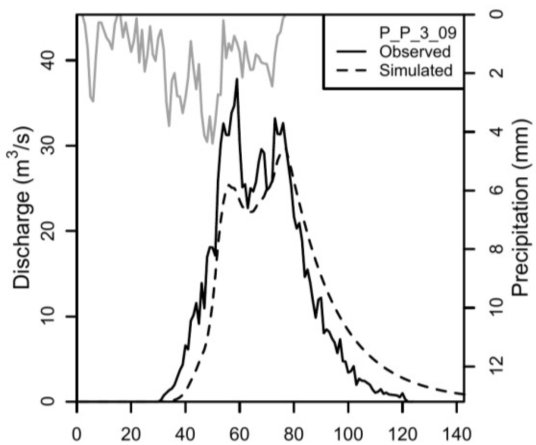

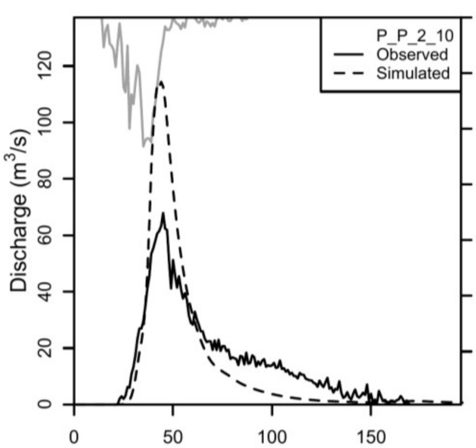

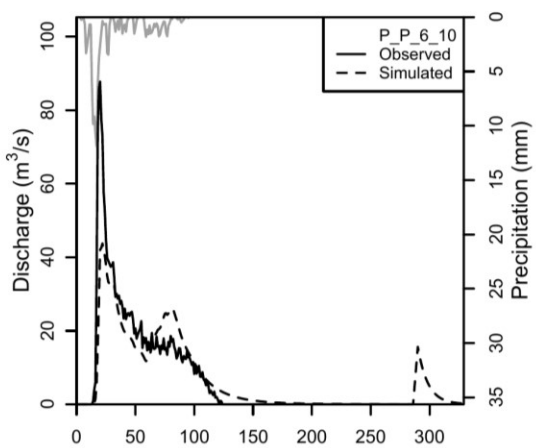

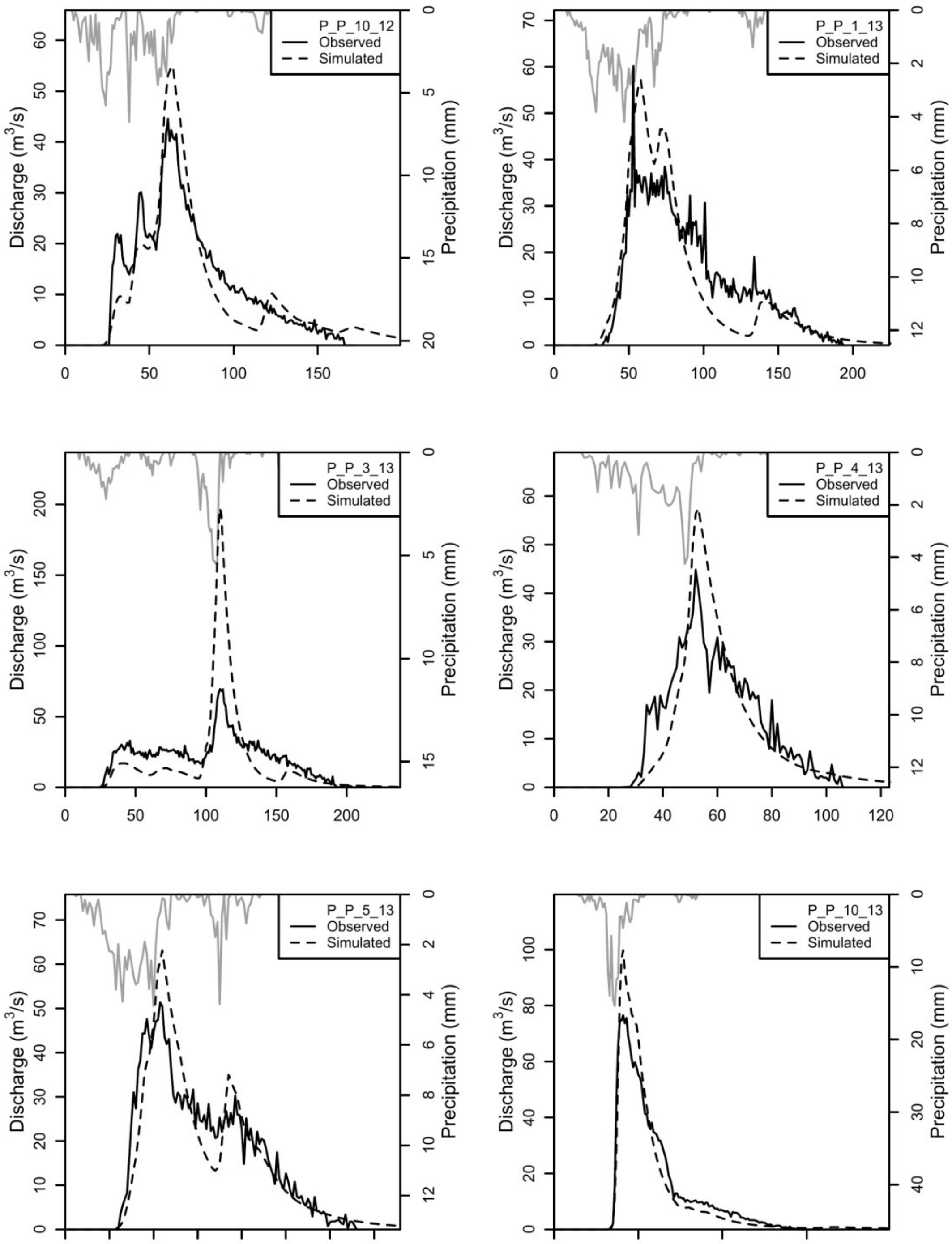
P_P_10_12
Observed
Simulated
P_P_1_13
P_P_3_13
P_P_4_13
P_P_5_13
P_P_10_13
Discharge (m3/s)
Precipitation (mm)

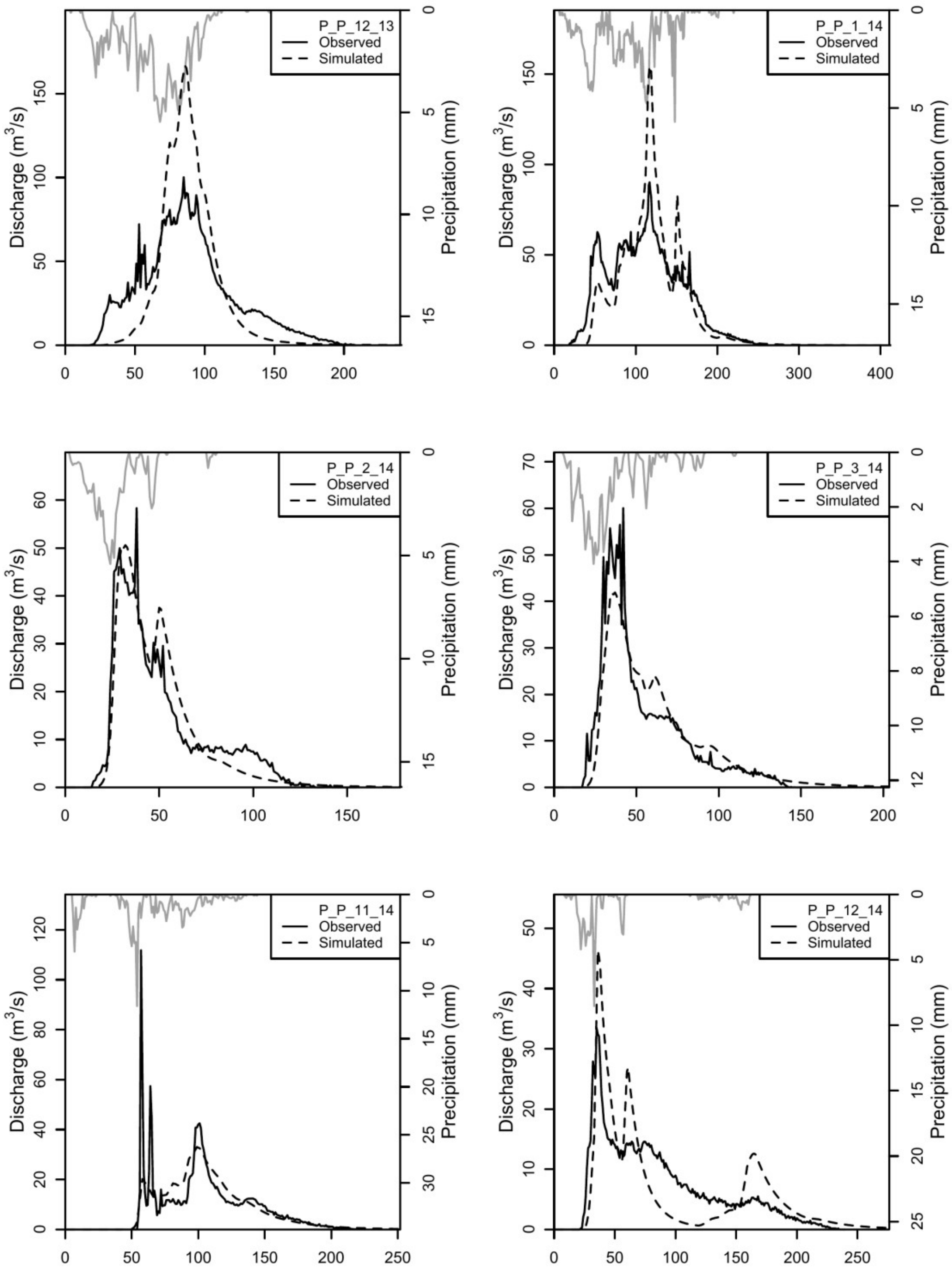
P_P_12_13
Observed
Simulated
Discharge (m^3/s)
Precipitation (mm)
P_P_1_14
Observed
Simulated
Discharge (m^3/s)
Precipitation (mm)
P_P_2_14
Observed
Simulated
Discharge (m^3/s)
Precipitation (mm)
P_P_3_14
Observed
Simulated
Discharge (m^3/s)
Precipitation (mm)
P_P_11_14
Observed
Simulated
Discharge (m^3/s)
Precipitation (mm)
P_P_12_14
Observed
Simulated
Discharge (m^3/s)
Precipitation (mm)

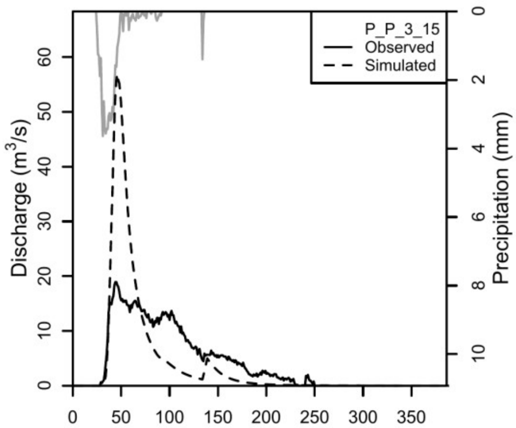

Figure 7.1: Observed and simulated flood events at the Pievepelago hydrometric station.

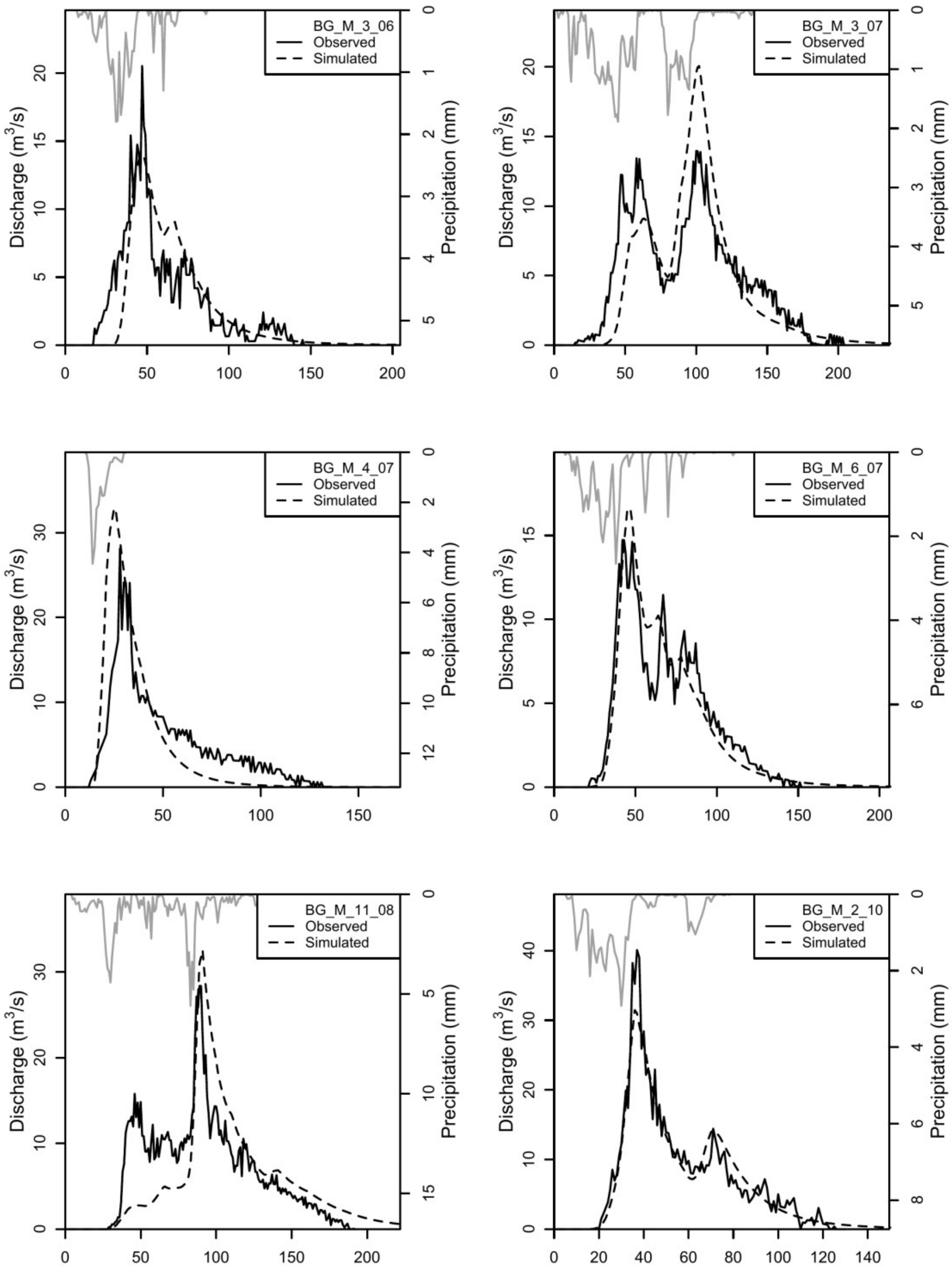
BG_M_3_06
Observed
Simulated
Discharge (m^3/s)
Precipitation (mm)
BG_M_3_07
Observed
Simulated
Discharge (m^3/s)
Precipitation (mm)
BG_M_4_07
Observed
Simulated
Discharge (m^3/s)
Precipitation (mm)
BG_M_6_07
Observed
Simulated
Discharge (m^3/s)
Precipitation (mm)
BG_M_11_08
Observed
Simulated
Discharge (m^3/s)
Precipitation (mm)
BG_M_2_10
Observed
Simulated
Discharge (m^3/s)
Precipitation (mm)

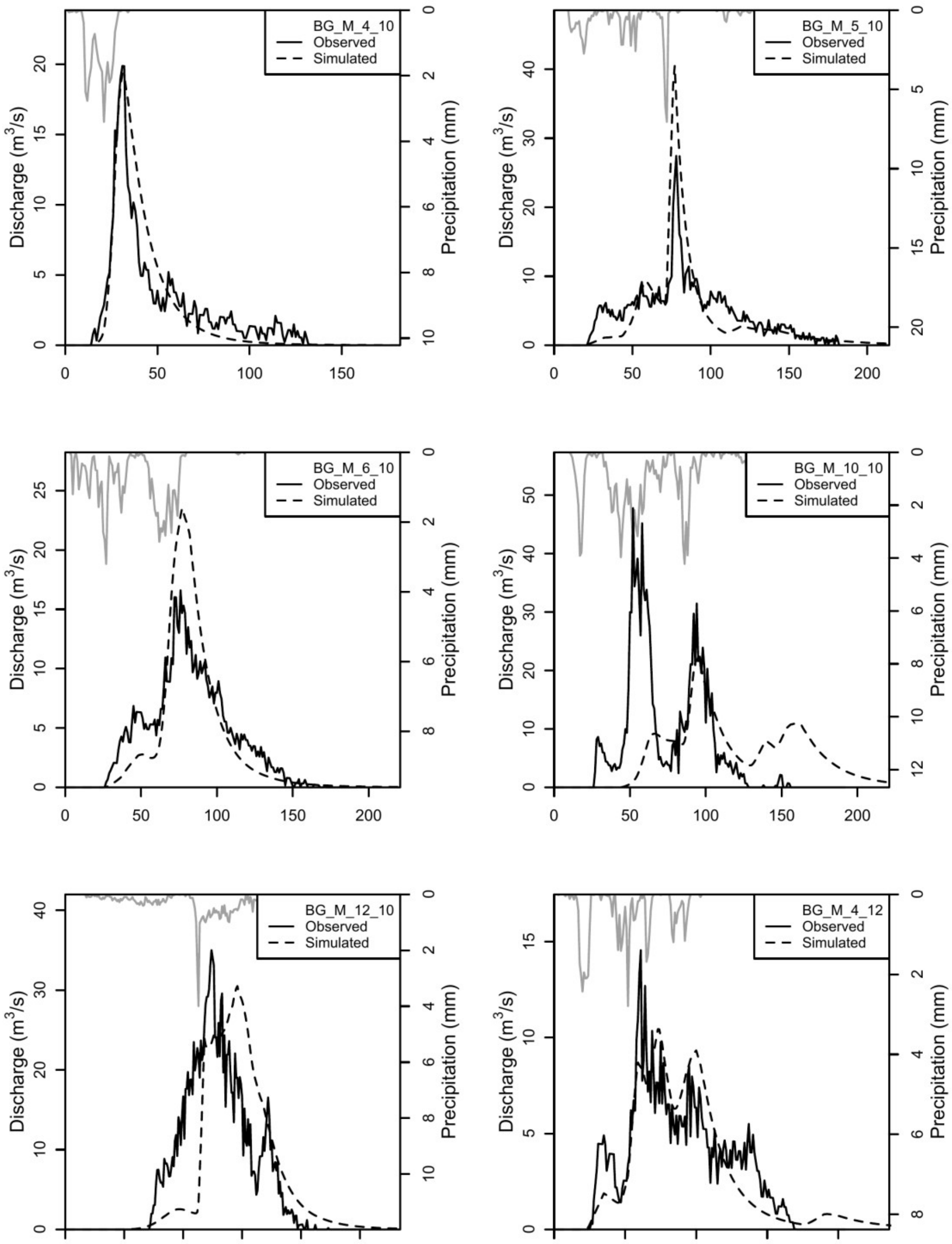
BG_M_4_10
Observed
Simulated
BG_M_5_10
Observed
Simulated
BG_M_6_10
Observed
Simulated
BG_M_10_10
Observed
Simulated
BG_M_12_10
Observed
Simulated
BG_M_4_12
Observed
Simulated
Discharge (m^3/s)
Precipitation (mm)

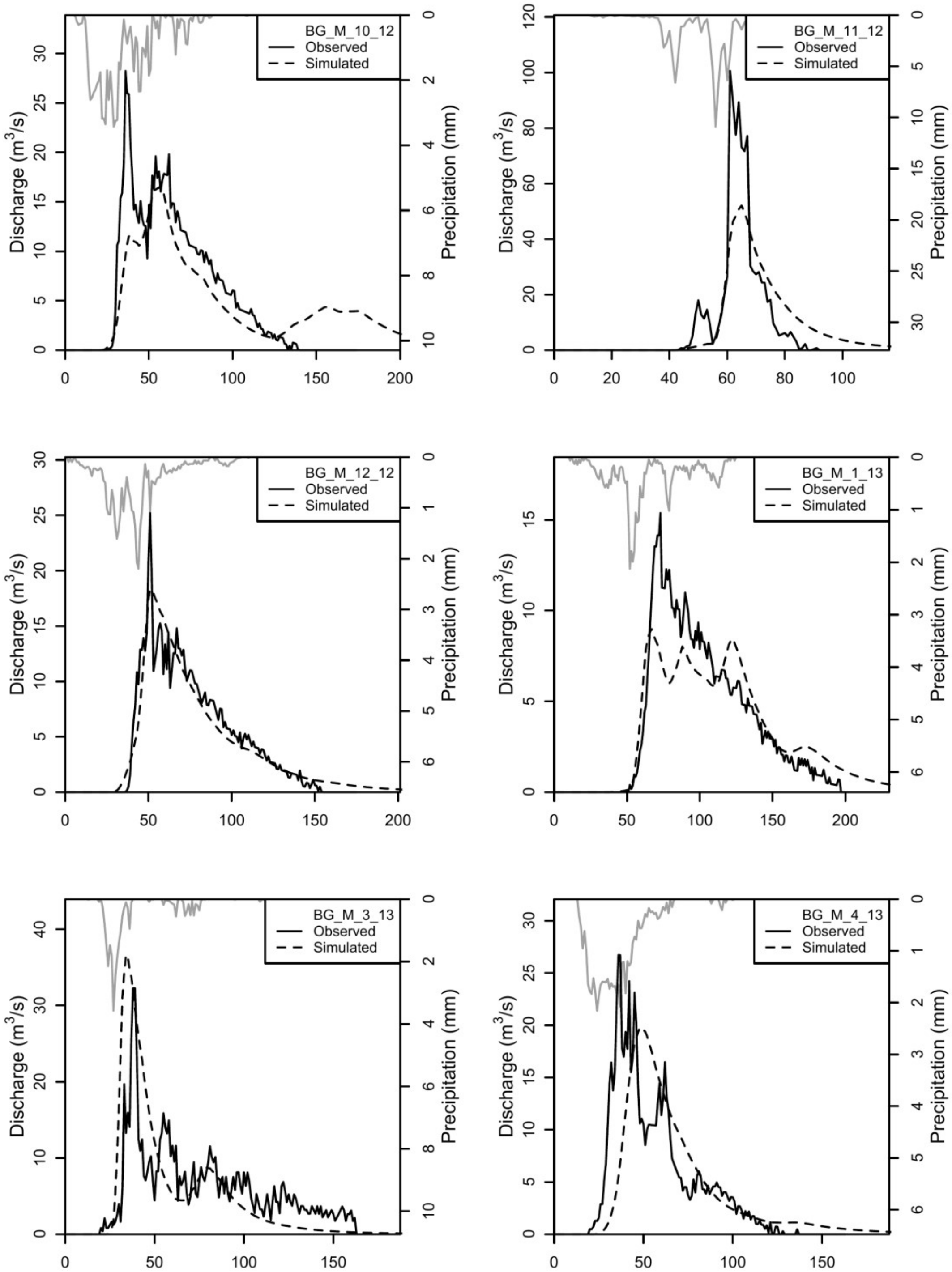
BG_M_10_12
Observed
Simulated
BG_M_11_12
Observed
Simulated
BG_M_12_12
Observed
Simulated
BG_M_1_13
Observed
Simulated
BG_M_3_13
Observed
Simulated
BG_M_4_13
Observed
Simulated
Discharge (m3/s)
Precipitation (mm)

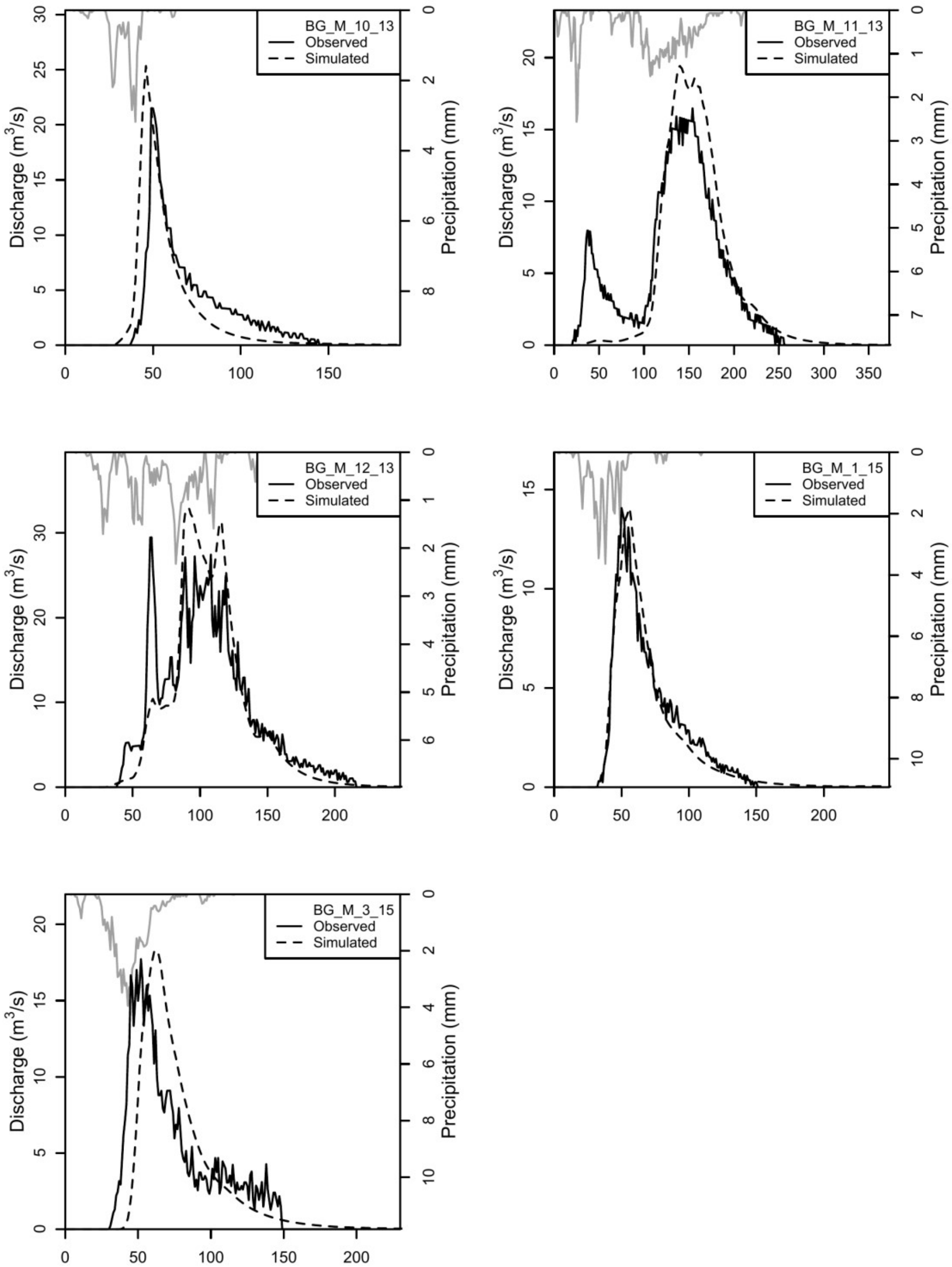

Figure 7.2: Observed and simulated flood events at the Marzolara hydrometric station.

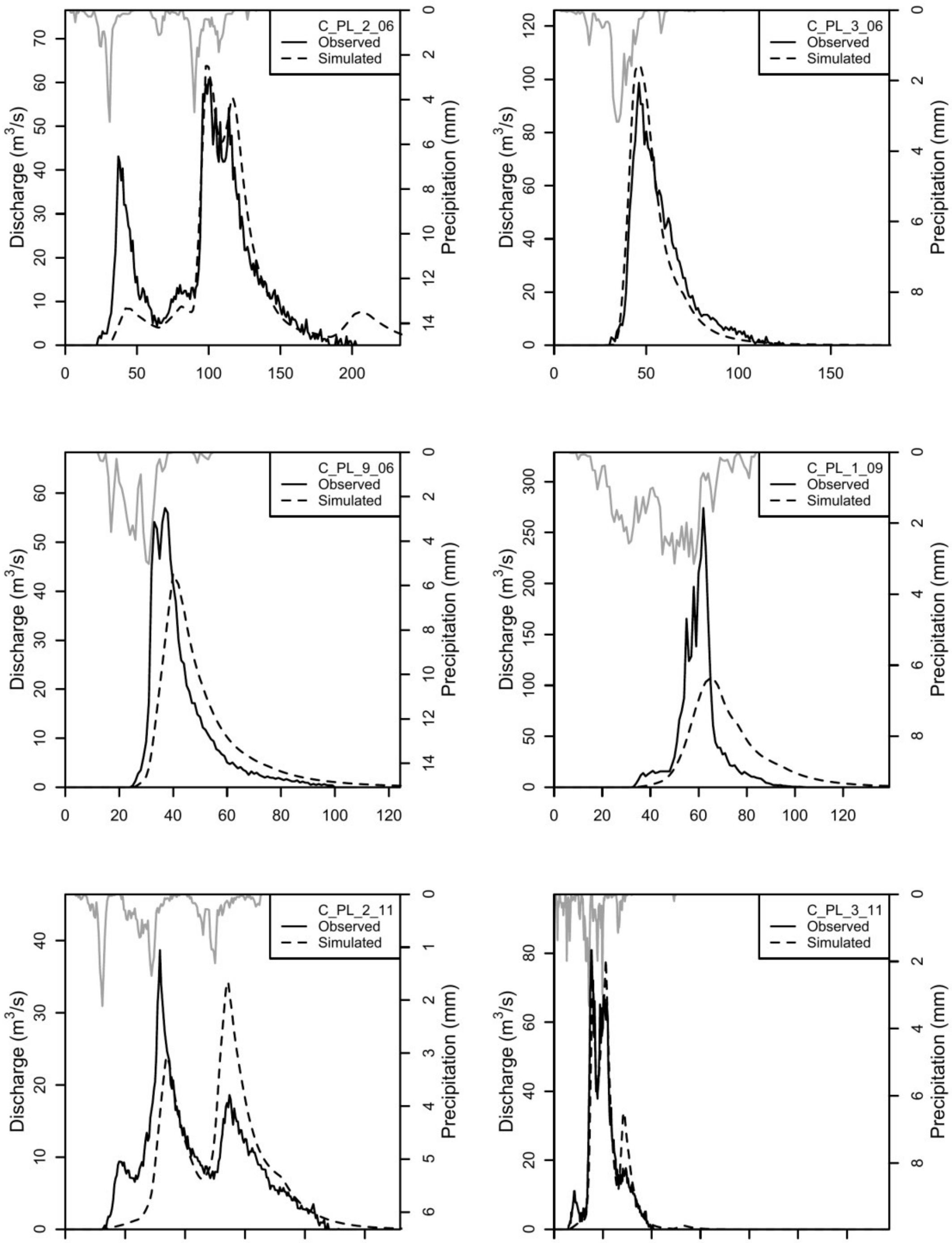
C_PL_2_06
Observed
Simulated
Discharge (m3/s)
Precipitation (mm)
C_PL_3_06
Observed
Simulated
Discharge (m3/s)
Precipitation (mm)
C_PL_9_06
Observed
Simulated
Discharge (m3/s)
Precipitation (mm)
C_PL_1_09
Observed
Simulated
Discharge (m3/s)
Precipitation (mm)
C_PL_2_11
Observed
Simulated
Discharge (m3/s)
Precipitation (mm)
C_PL_3_11
Observed
Simulated
Discharge (m3/s)
Precipitation (mm)

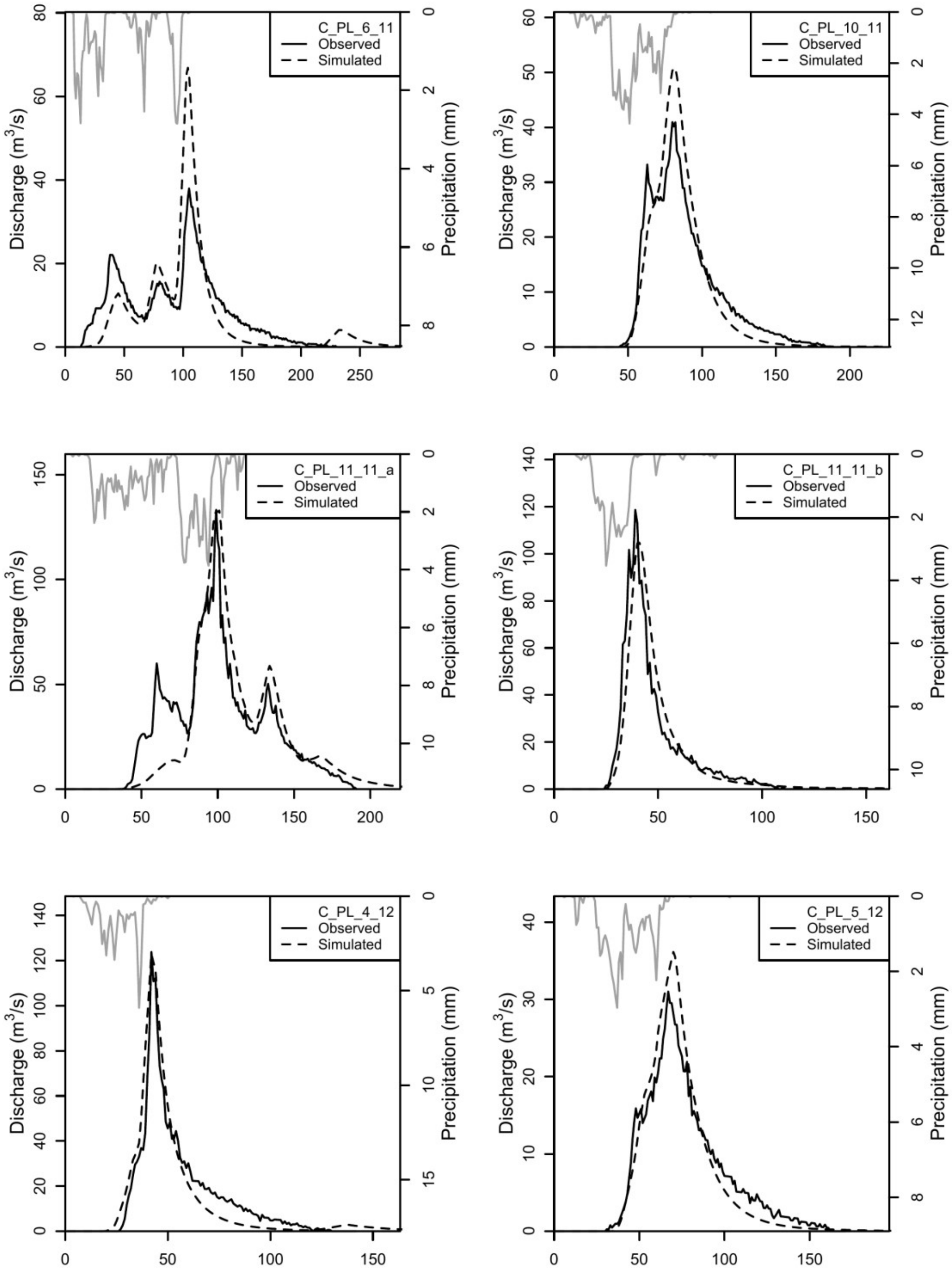
C_PL_6_11
Observed
Simulated
Discharge (m3/s)
Precipitation (mm)
C_PL_10_11
Observed
Simulated
Discharge (m3/s)
Precipitation (mm)
C_PL_11_11_a
Observed
Simulated
Discharge (m3/s)
Precipitation (mm)
C_PL_11_11_b
Observed
Simulated
Discharge (m3/s)
Precipitation (mm)
C_PL_4_12
Observed
Simulated
Discharge (m3/s)
Precipitation (mm)
C_PL_5_12
Observed
Simulated
Discharge (m3/s)
Precipitation (mm)

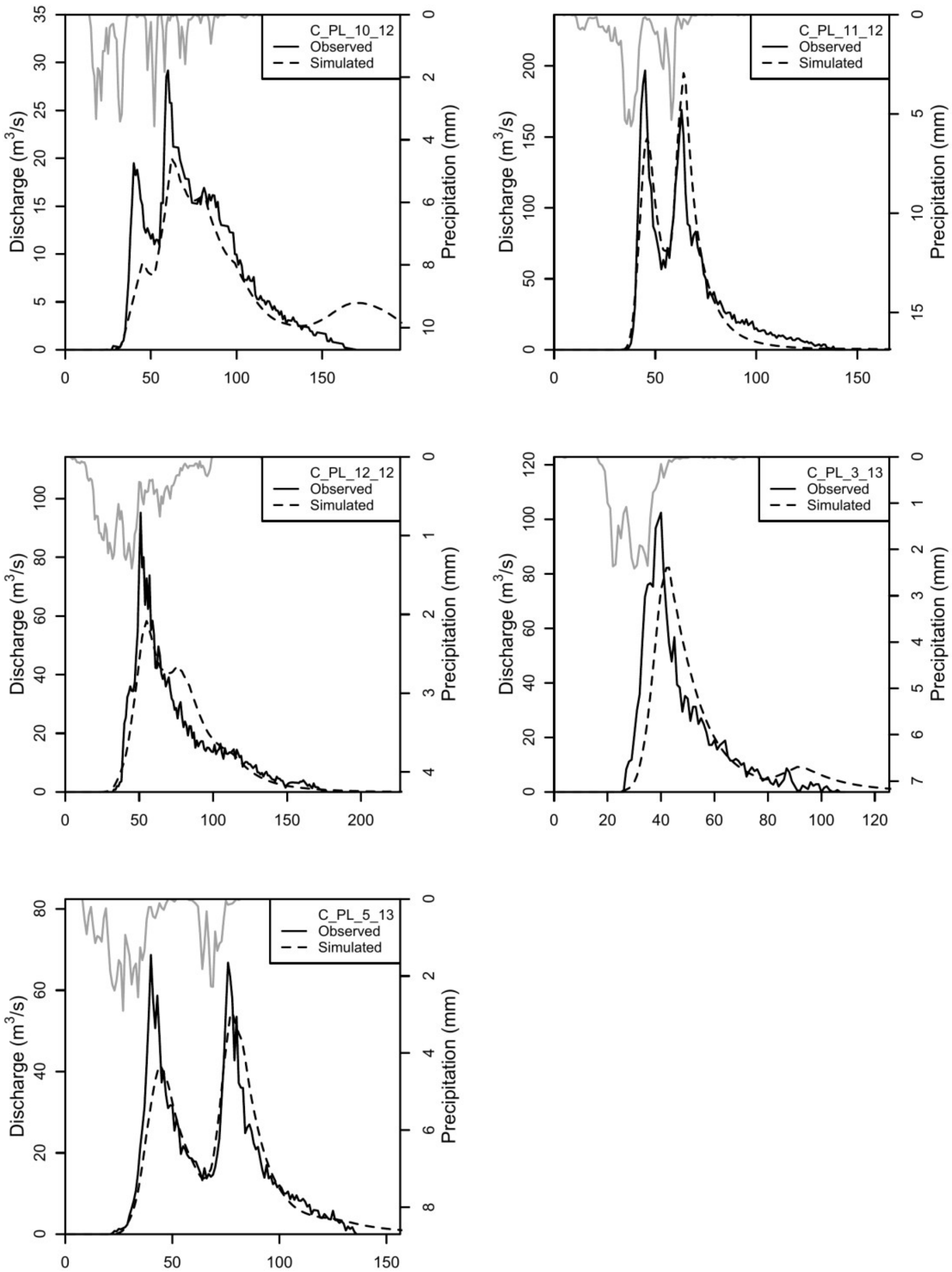

Figure 7.3: Observed and simulated flood events at the Ponte Lamberti hydrometric station.

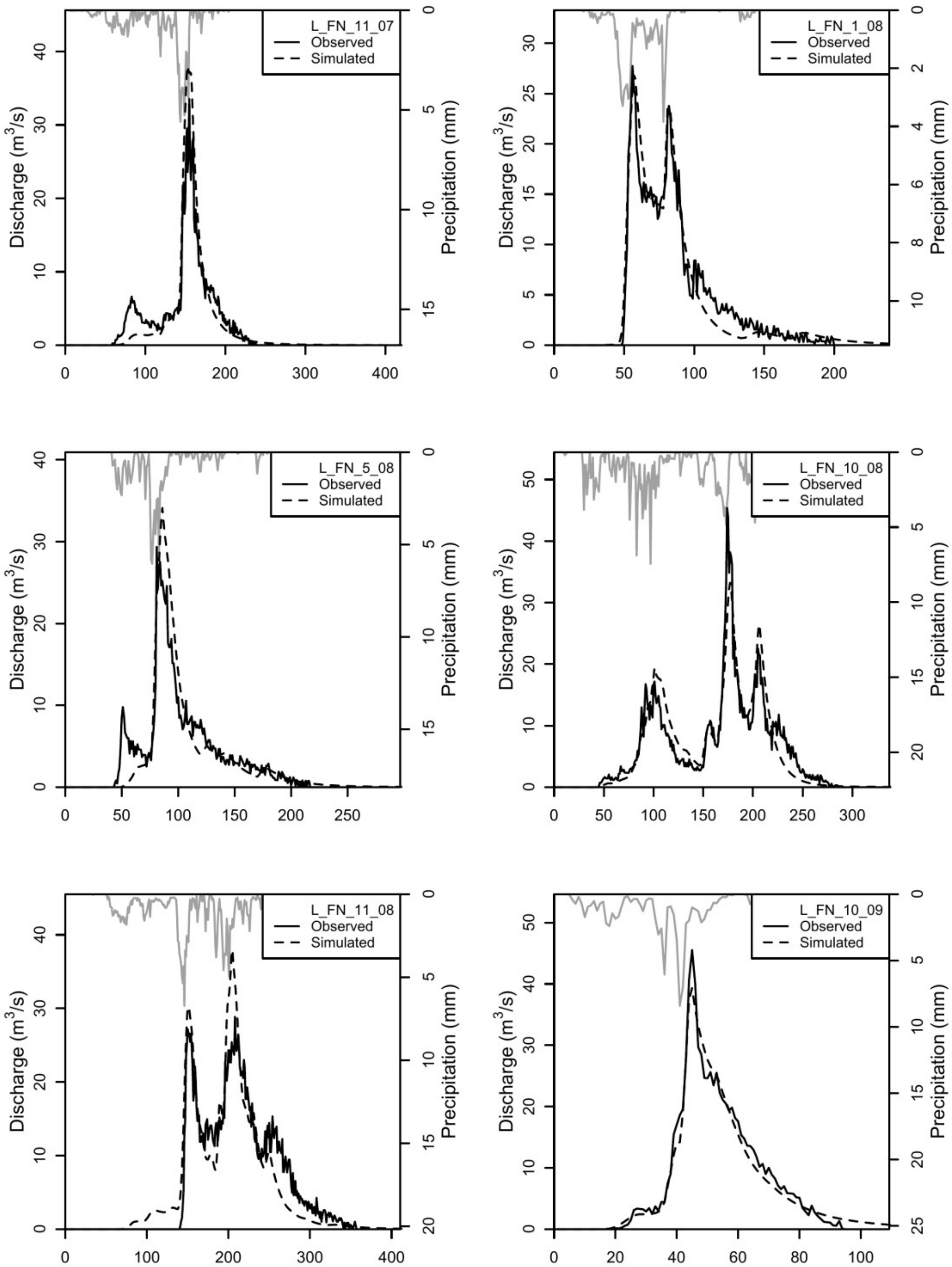
L_FN_11_07
Observed
Simulated
Discharge (m³/s)
Precipitation (mm)
L_FN_1_08
Observed
Simulated
Discharge (m³/s)
Precipitation (mm)
L_FN_5_08
Observed
Simulated
Discharge (m³/s)
Precipitation (mm)
L_FN_10_08
Observed
Simulated
Discharge (m³/s)
Precipitation (mm)
L_FN_11_08
Observed
Simulated
Discharge (m³/s)
Precipitation (mm)
L_FN_10_09
Observed
Simulated
Discharge (m³/s)
Precipitation (mm)

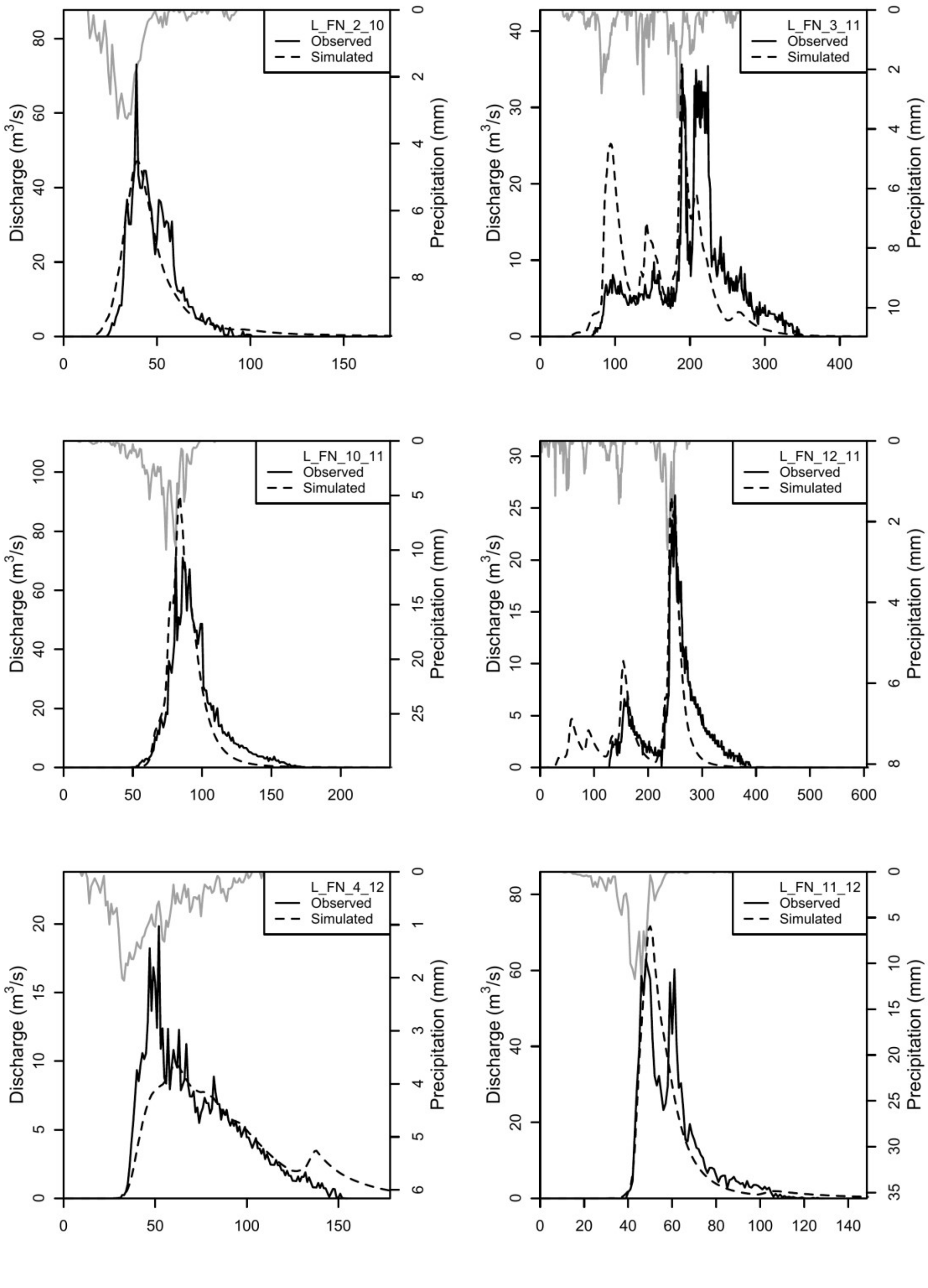
L_FN_2_10
Observed
Simulated
Discharge (m3/s)
Precipitation (mm)
L_FN_3_11
Observed
Simulated
Discharge (m3/s)
Precipitation (mm)
L_FN_10_11
Observed
Simulated
Discharge (m3/s)
Precipitation (mm)
L_FN_12_11
Observed
Simulated
Discharge (m3/s)
Precipitation (mm)
L_FN_4_12
Observed
Simulated
Discharge (m3/s)
Precipitation (mm)
L_FN_11_12
Observed
Simulated
Discharge (m3/s)
Precipitation (mm)

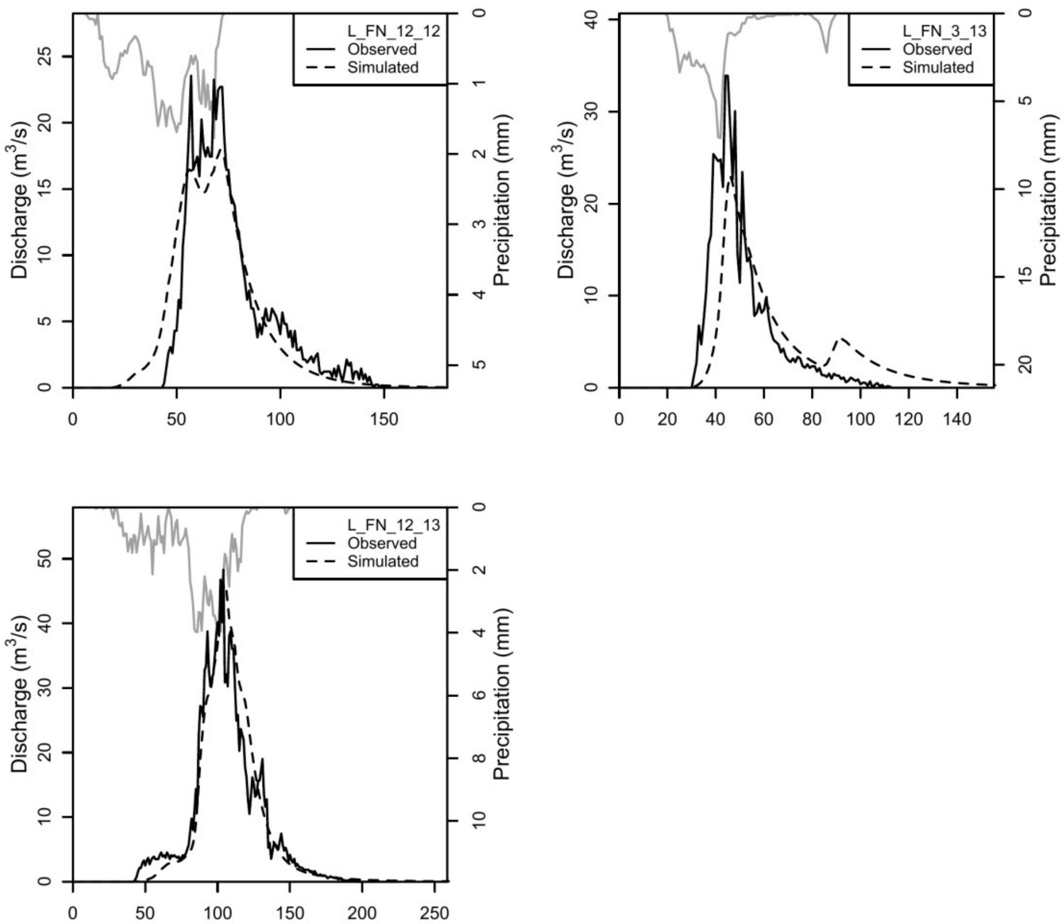

Figure 7.4: Observed and simulated flood events at the Fanano hydrometric station.

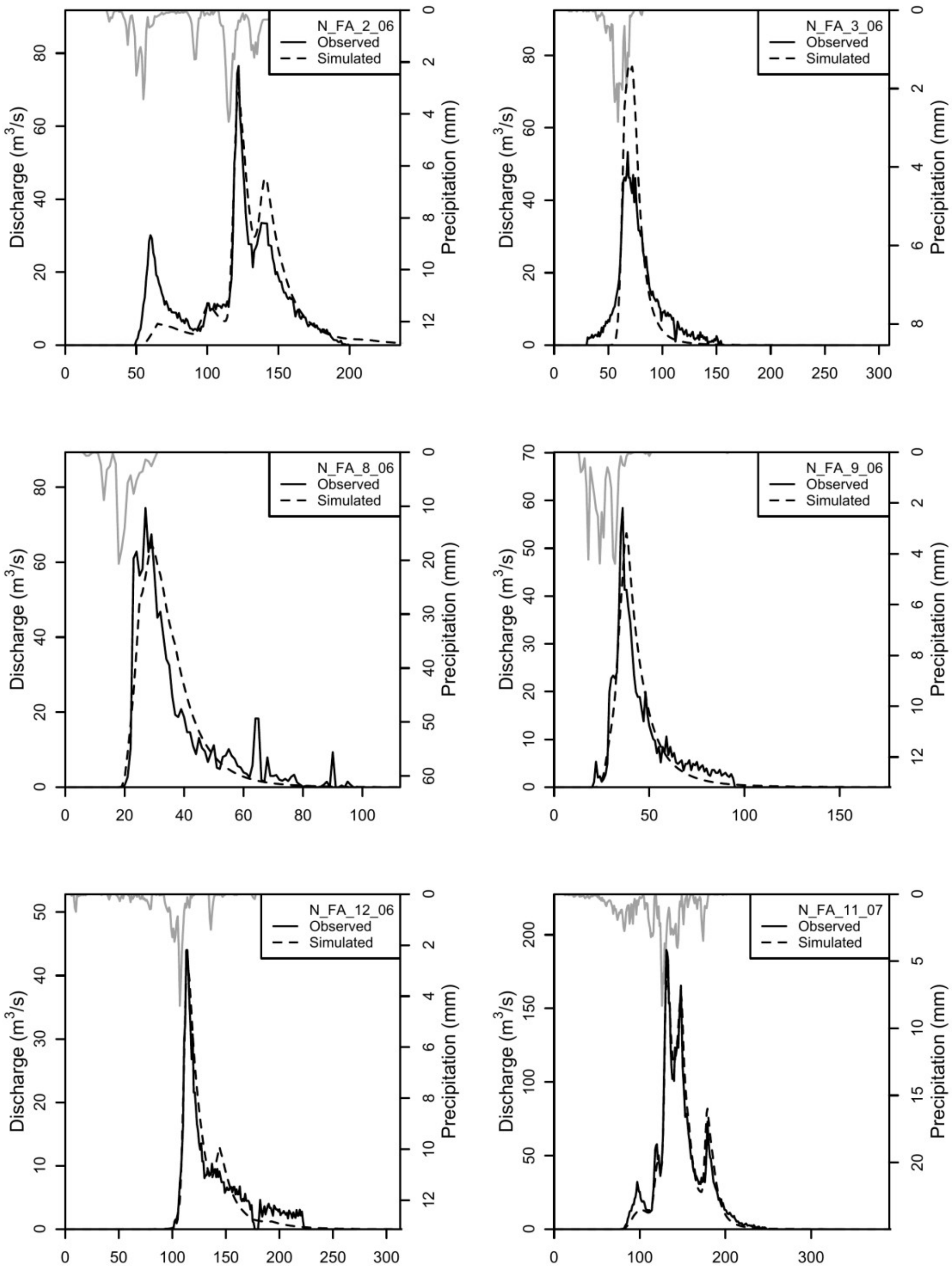
N_FA_2_06
Observed
Simulated
N_FA_3_06
Observed
Simulated
N_FA_8_06
Observed
Simulated
N_FA_9_06
Observed
Simulated
N_FA_12_06
Observed
Simulated
N_FA_11_07
Observed
Simulated
Discharge (m3/s)
Precipitation (mm)

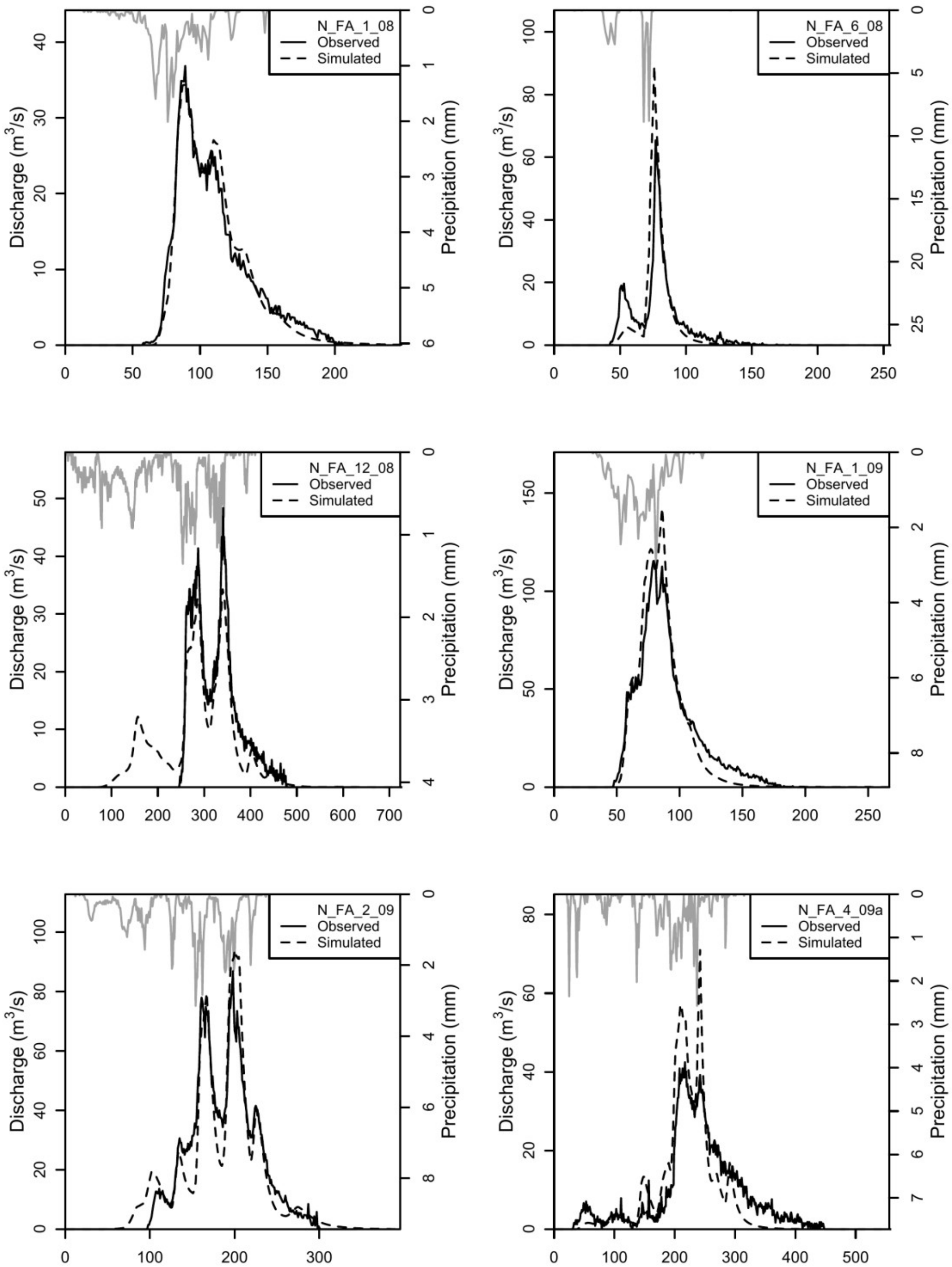

N_FA_1_08
N_FA_6_08
N_FA_12_08
N_FA_1_09
N_FA_2_09
N_FA_4_09a
Observed
Simulated
Discharge (m3/s)
Precipitation (mm)

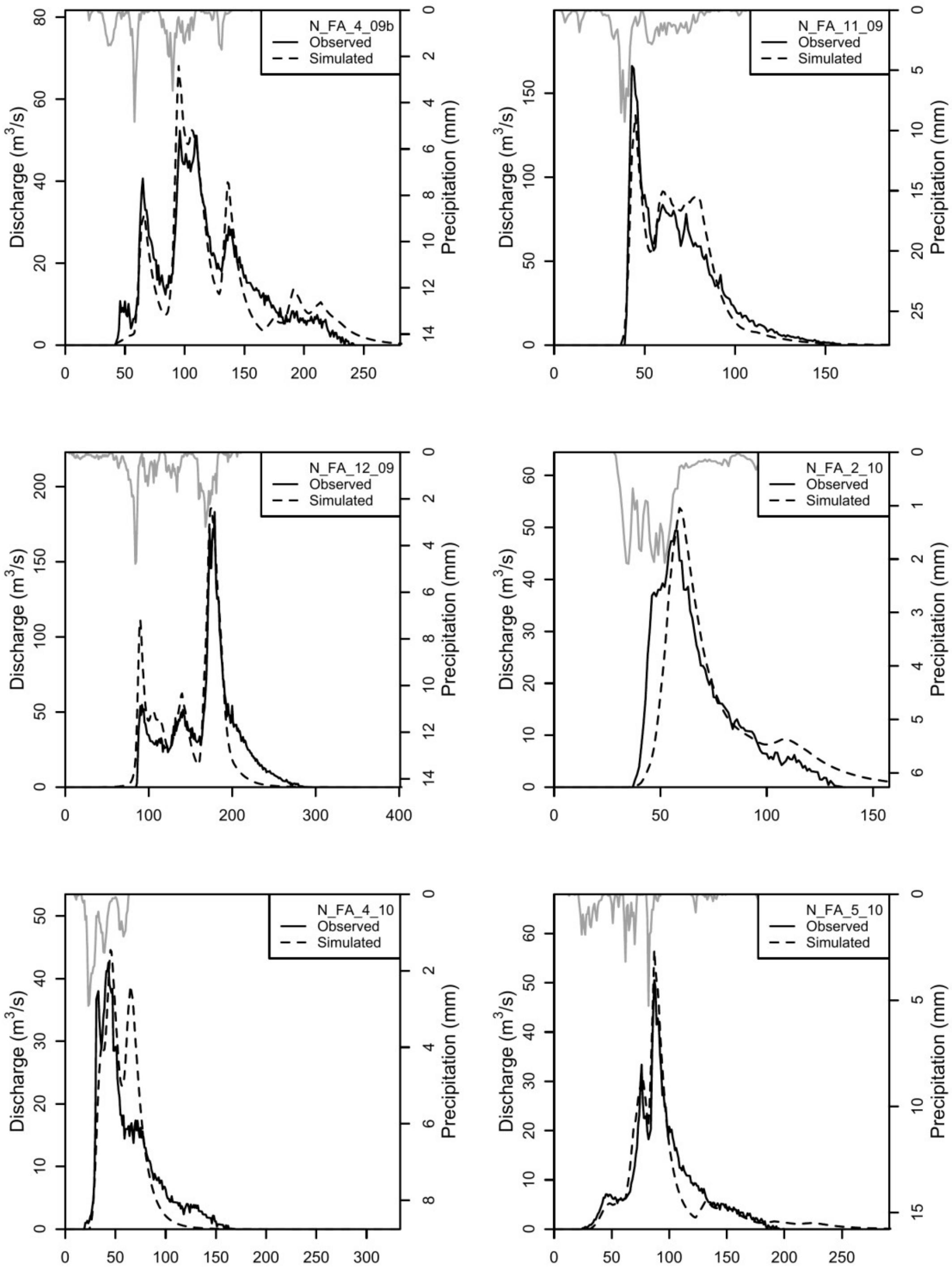
N_FA_4_09b
Observed
Simulated
Discharge (m^3/s)
Precipitation (mm)
N_FA_11_09
Observed
Simulated
Discharge (m^3/s)
Precipitation (mm)
N_FA_12_09
Observed
Simulated
Discharge (m^3/s)
Precipitation (mm)
N_FA_2_10
Observed
Simulated
Discharge (m^3/s)
Precipitation (mm)
N_FA_4_10
Observed
Simulated
Discharge (m^3/s)
Precipitation (mm)
N_FA_5_10
Observed
Simulated
Discharge (m^3/s)
Precipitation (mm)

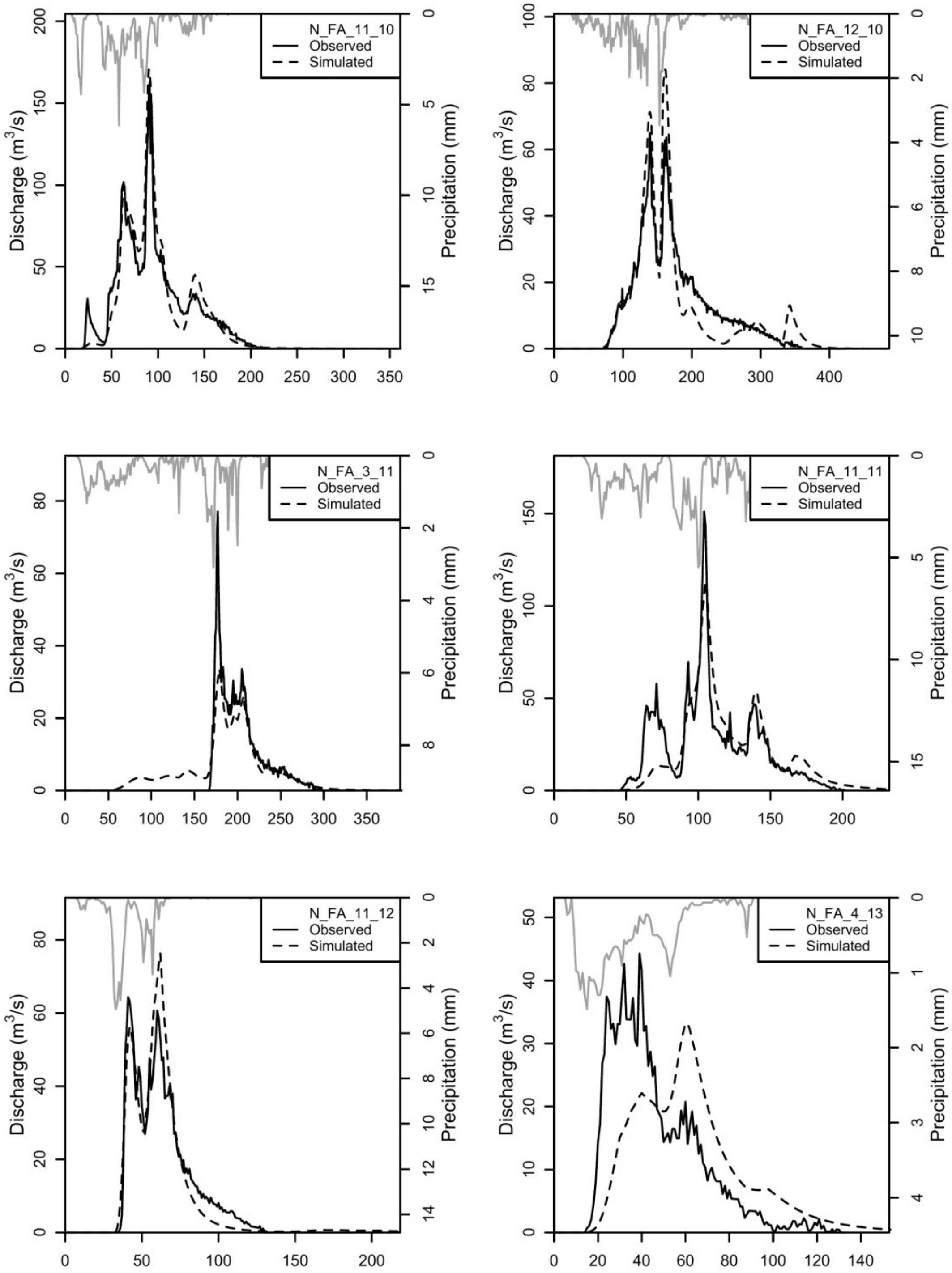
N_FA_11_10
Observed
Simulated
Discharge (m3/s)
Precipitation (mm)
N_FA_12_10
Observed
Simulated
Discharge (m3/s)
Precipitation (mm)
N_FA_3_11
Observed
Simulated
Discharge (m3/s)
Precipitation (mm)
N_FA_11_11
Observed
Simulated
Discharge (m3/s)
Precipitation (mm)
N_FA_11_12
Observed
Simulated
Discharge (m3/s)
Precipitation (mm)
N_FA_4_13
Observed
Simulated
Discharge (m3/s)
Precipitation (mm)

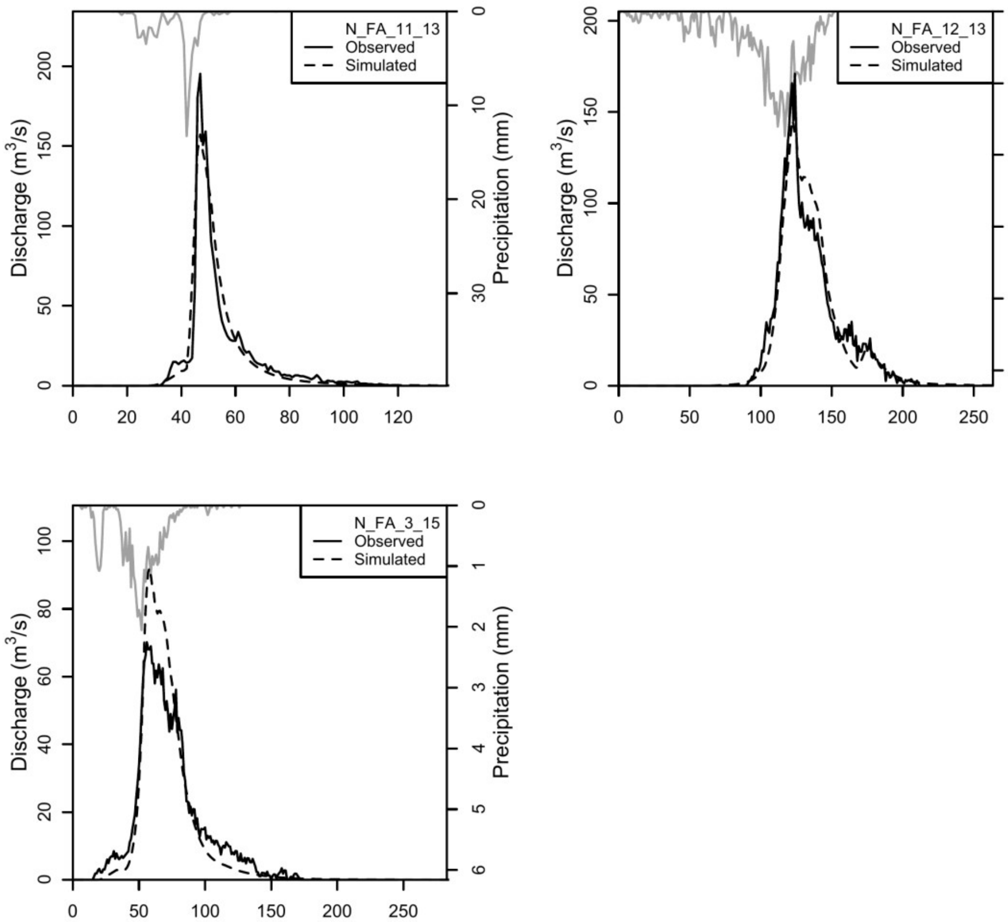

Figure 7.5: Observed and simulated flood events at the Farini hydrometric station.

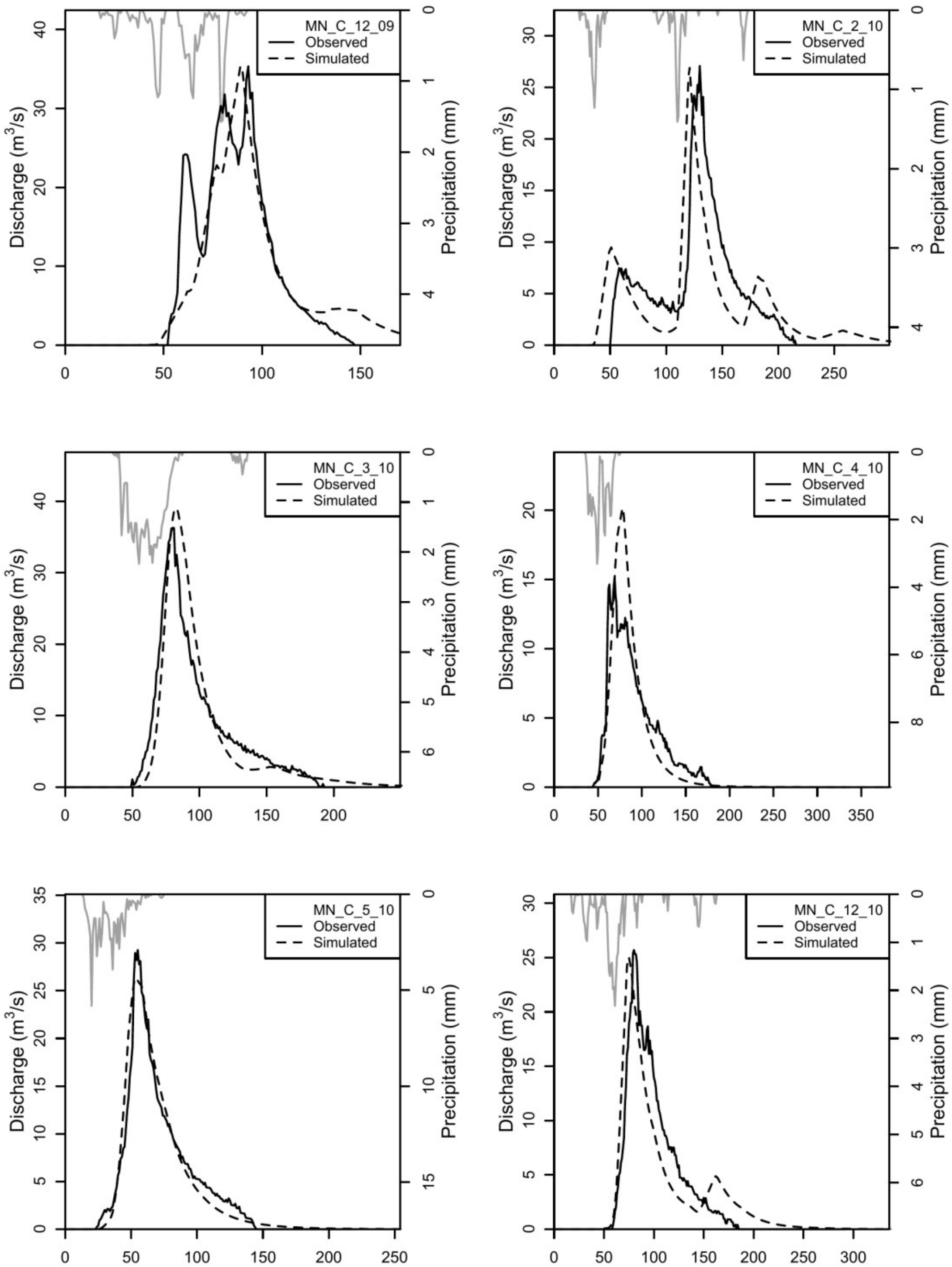
MN_C_12_09
Observed
Simulated
MN_C_2_10
Observed
Simulated
MN_C_3_10
Observed
Simulated
MN_C_4_10
Observed
Simulated
MN_C_5_10
Observed
Simulated
MN_C_12_10
Observed
Simulated
Discharge (m3/s)
Precipitation (mm)

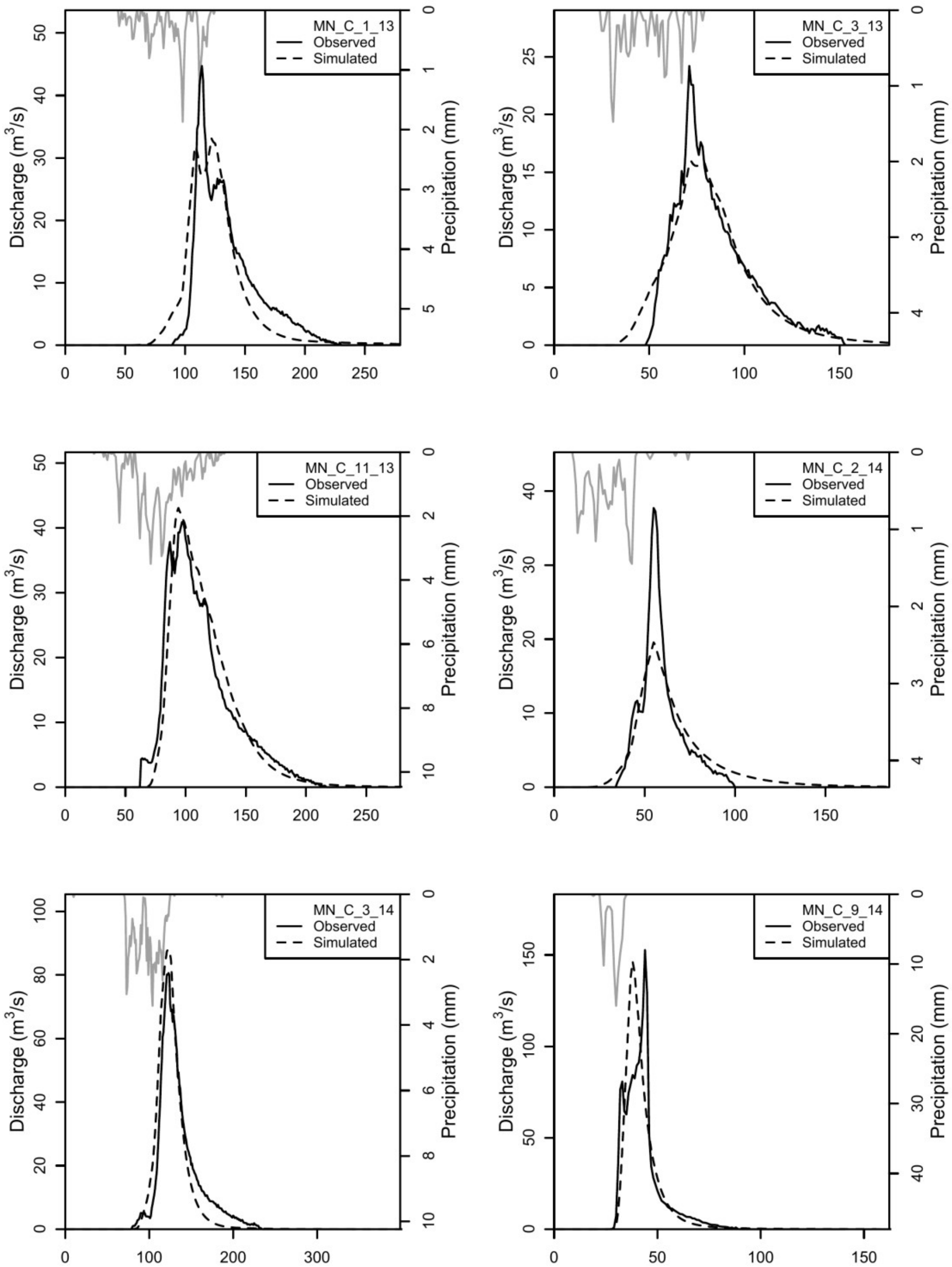

MN_C_1_13
Observed
Simulated
Discharge (m^3/s)
Precipitation (mm)
MN_C_3_13
Observed
Simulated
Discharge (m^3/s)
Precipitation (mm)
MN_C_11_13
Observed
Simulated
Discharge (m^3/s)
Precipitation (mm)
MN_C_2_14
Observed
Simulated
Discharge (m^3/s)
Precipitation (mm)
MN_C_3_14
Observed
Simulated
Discharge (m^3/s)
Precipitation (mm)
MN_C_9_14
Observed
Simulated
Discharge (m^3/s)
Precipitation (mm)

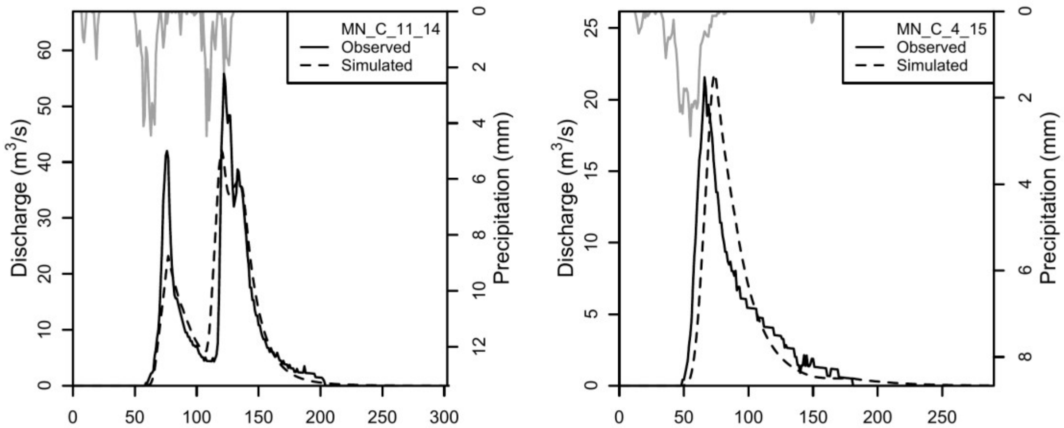

Figure 7.6: Observed and simulated flood events at the Castrocaro hydrometric station.

7.2 GREECE

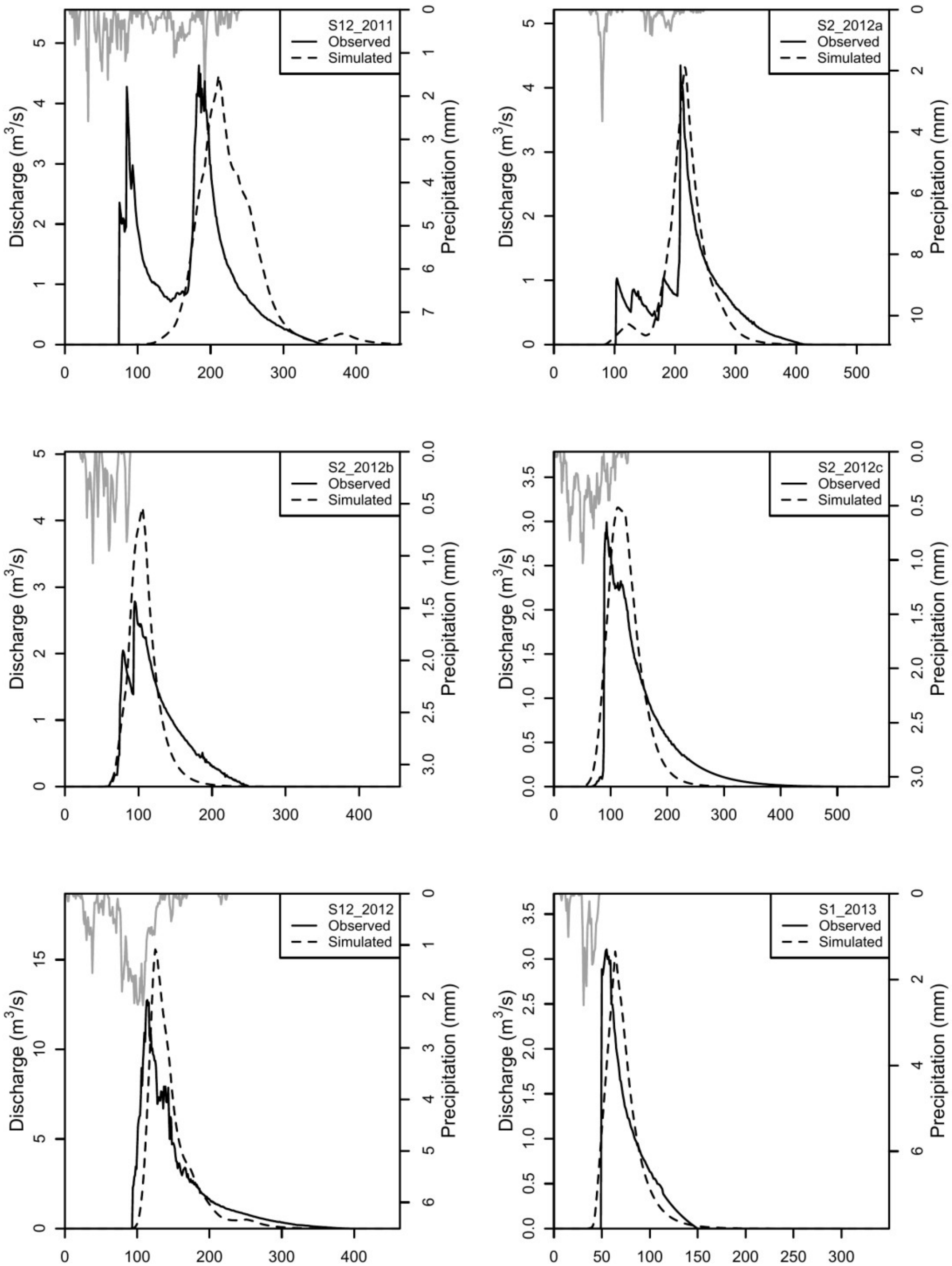
S12_2011
Observed
Simulated
Discharge (m^3/s)
Precipitation (mm)
S2_2012a
Observed
Simulated
Discharge (m^3/s)
Precipitation (mm)
S2_2012b
Observed
Simulated
Discharge (m^3/s)
Precipitation (mm)
S2_2012c
Observed
Simulated
Discharge (m^3/s)
Precipitation (mm)
S12_2012
Observed
Simulated
Discharge (m^3/s)
Precipitation (mm)
S1_2013
Observed
Simulated
Discharge (m^3/s)
Precipitation (mm)

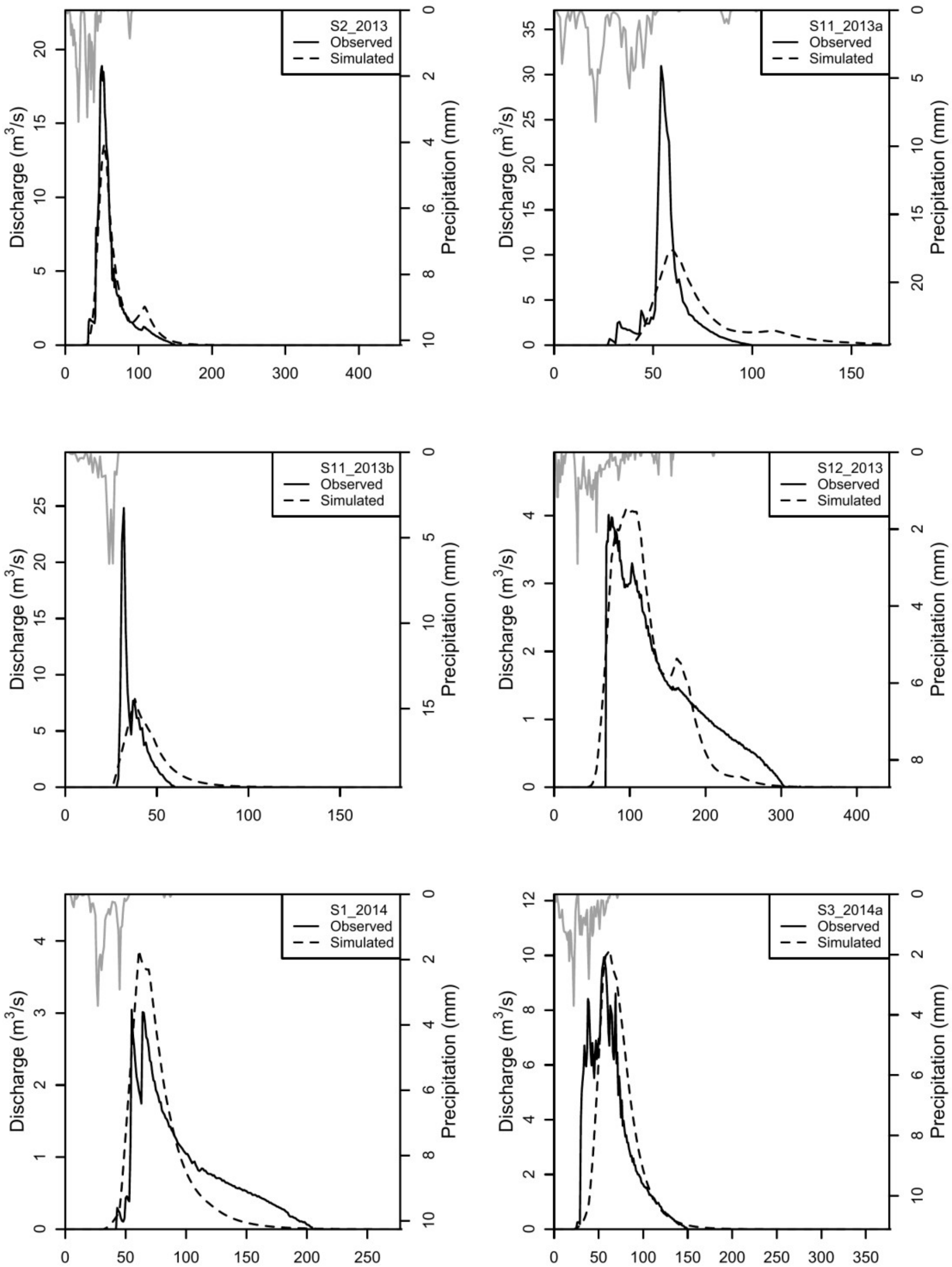

Figure 7.7: Observed and simulated flood events at the Gyra Stefanis (Sarantapotamos) hydrometric station.

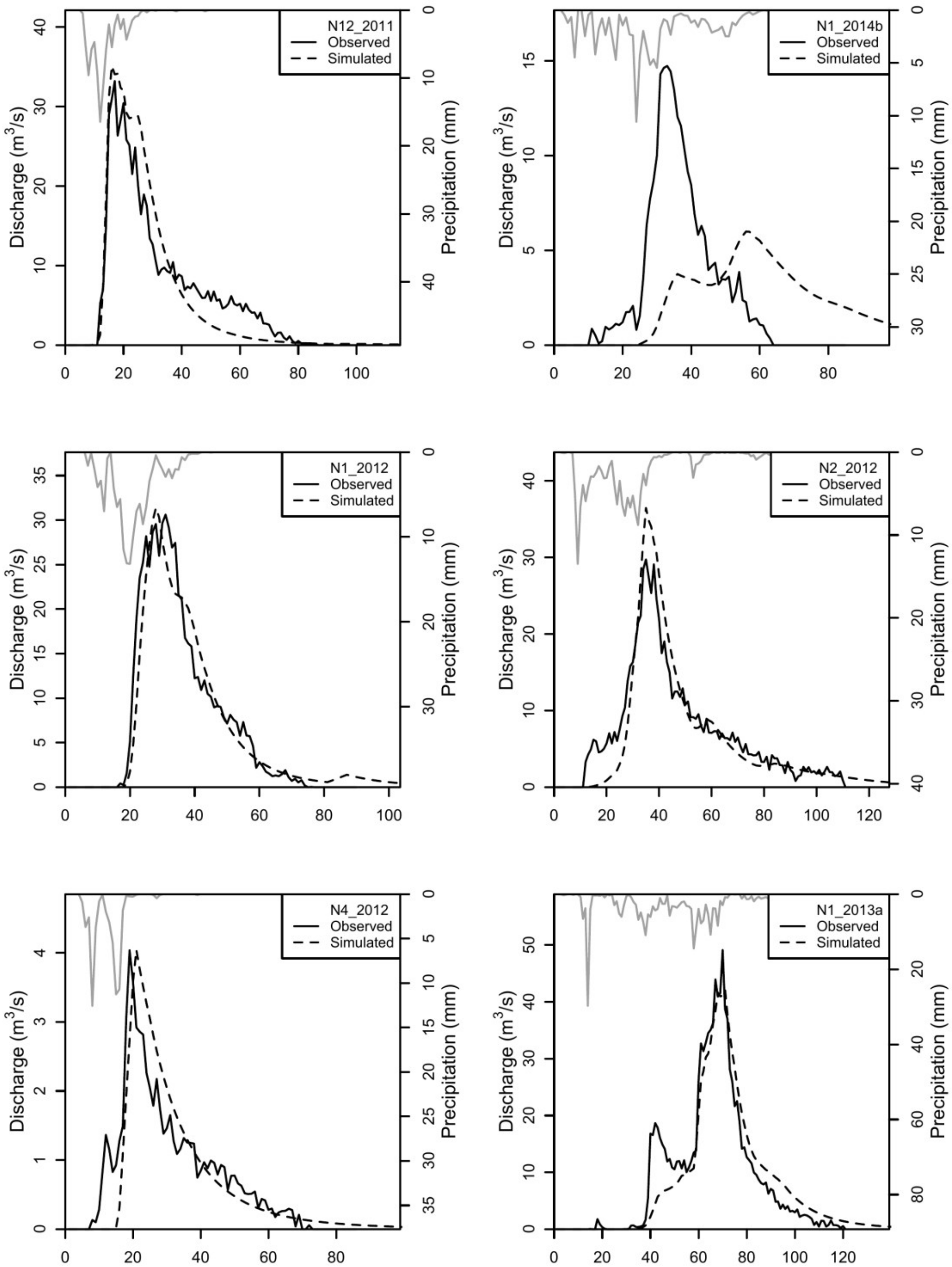
N12_2011
Observed
Simulated
Discharge (m3/s)
Precipitation (mm)
N1_2014b
N1_2012
N2_2012
N4_2012
N1_2013a

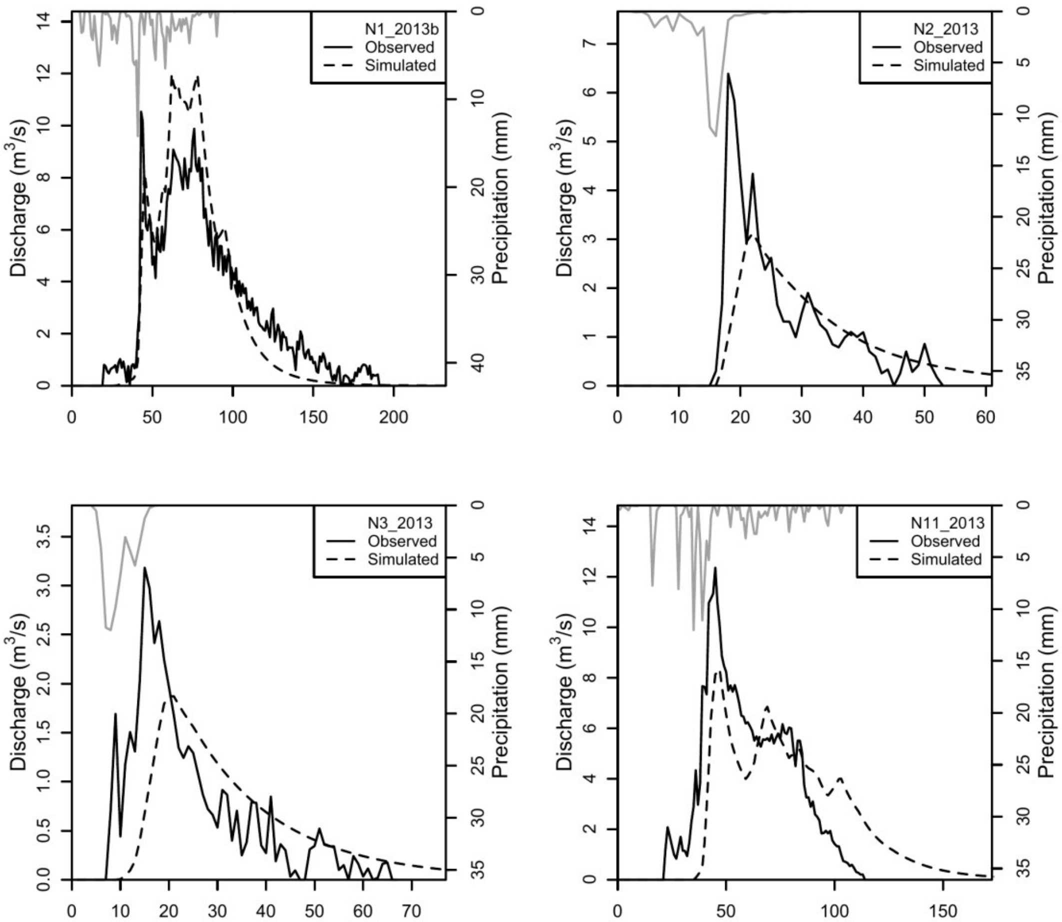

Figure 7.8: Observed and simulated flood events at the Kalamata (Nedontas) hydrometric station.

7.3 CYPRUS

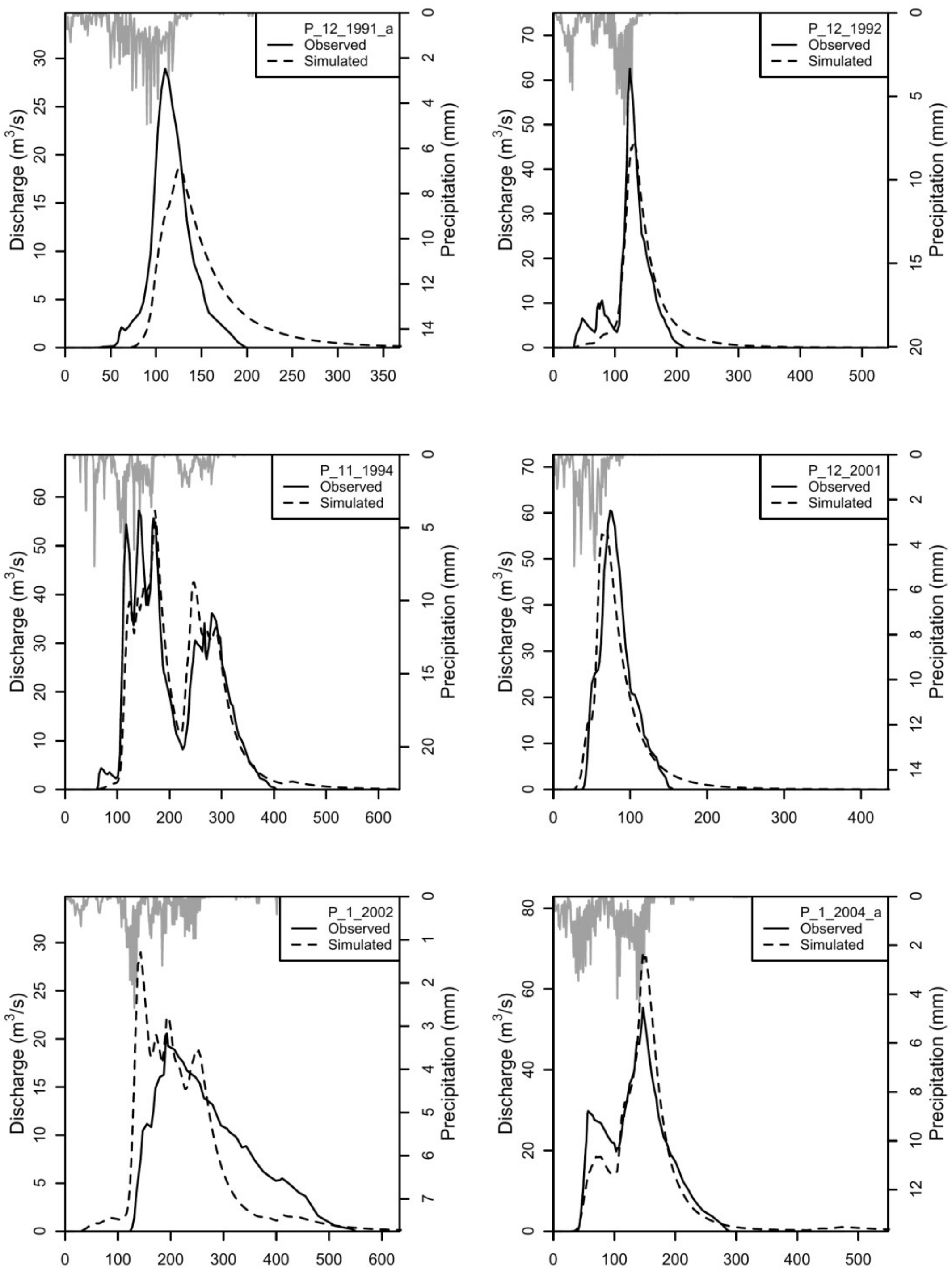
P_12_1991_a
Observed
Simulated
Discharge (m^3/s)
Precipitation (mm)
P_12_1992
Observed
Simulated
Discharge (m^3/s)
Precipitation (mm)
P_11_1994
Observed
Simulated
Discharge (m^3/s)
Precipitation (mm)
P_12_2001
Observed
Simulated
Discharge (m^3/s)
Precipitation (mm)
P_1_2002
Observed
Simulated
Discharge (m^3/s)
Precipitation (mm)
P_1_2004_a
Observed
Simulated
Discharge (m^3/s)
Precipitation (mm)

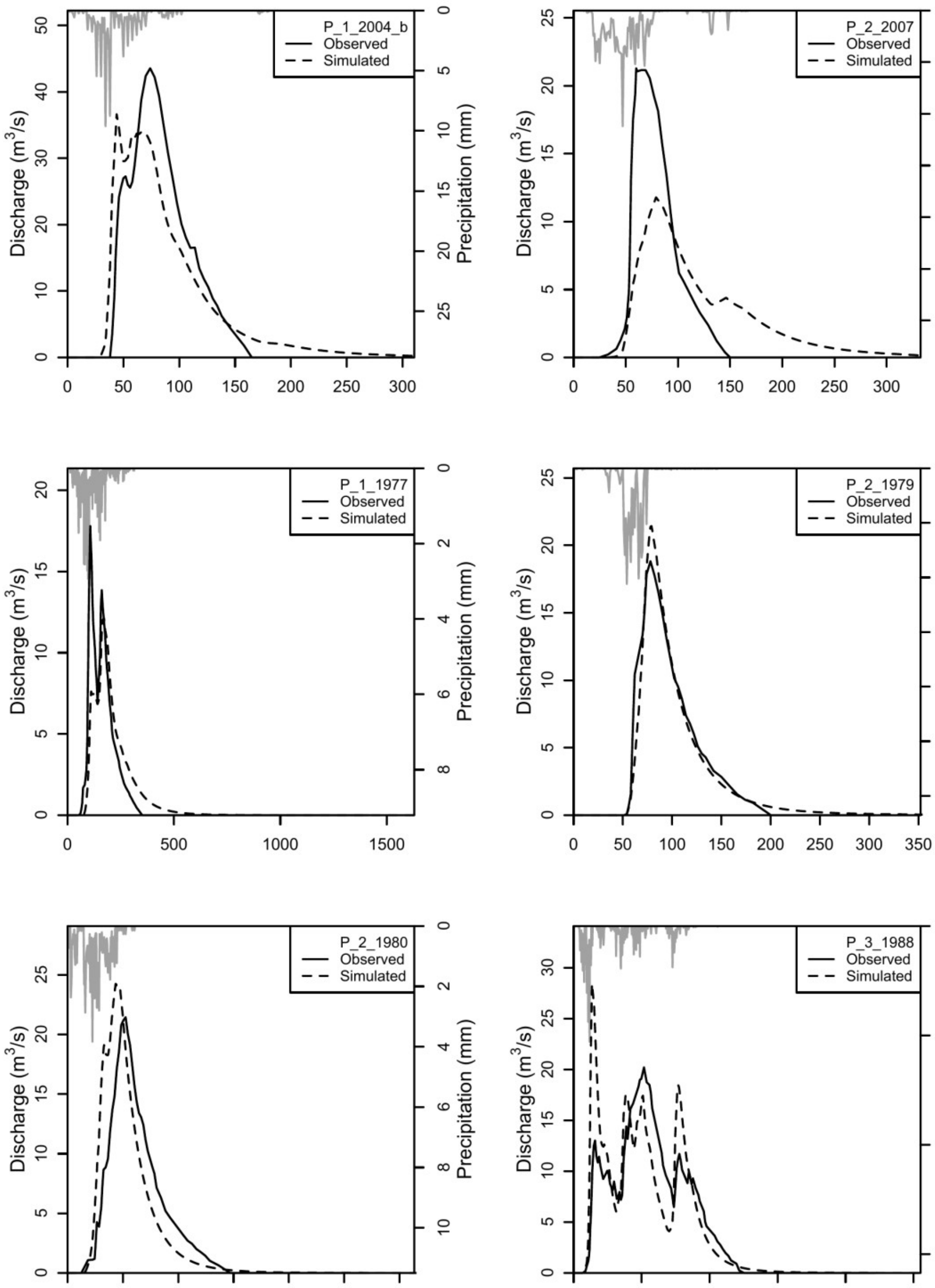
P_1_2004_b
Observed
Simulated
P_2_2007
Observed
Simulated
P_1_1977
Observed
Simulated
P_2_1979
Observed
Simulated
P_2_1980
Observed
Simulated
P_3_1988
Observed
Simulated
Discharge (m3/s)
Precipitation (mm)

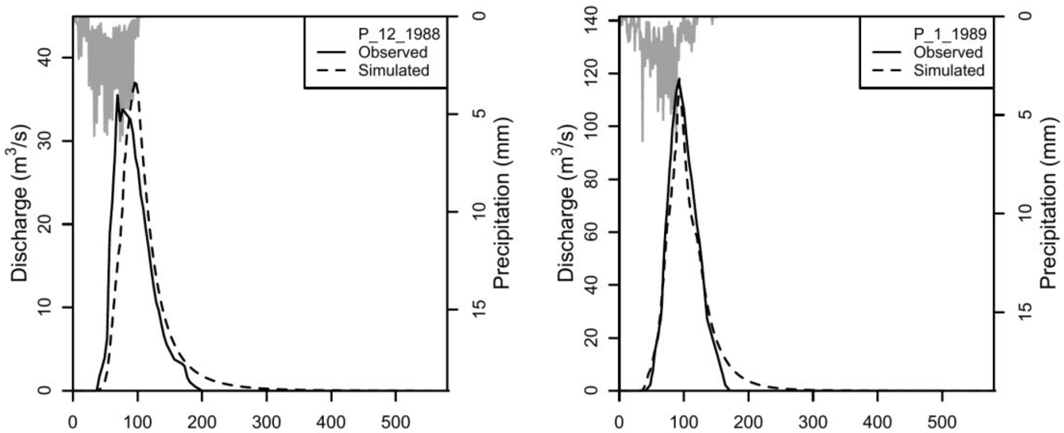

Figure 7.9: Observed and simulated flood events at the Panagia bridge (Peristerona) hydrometric station.

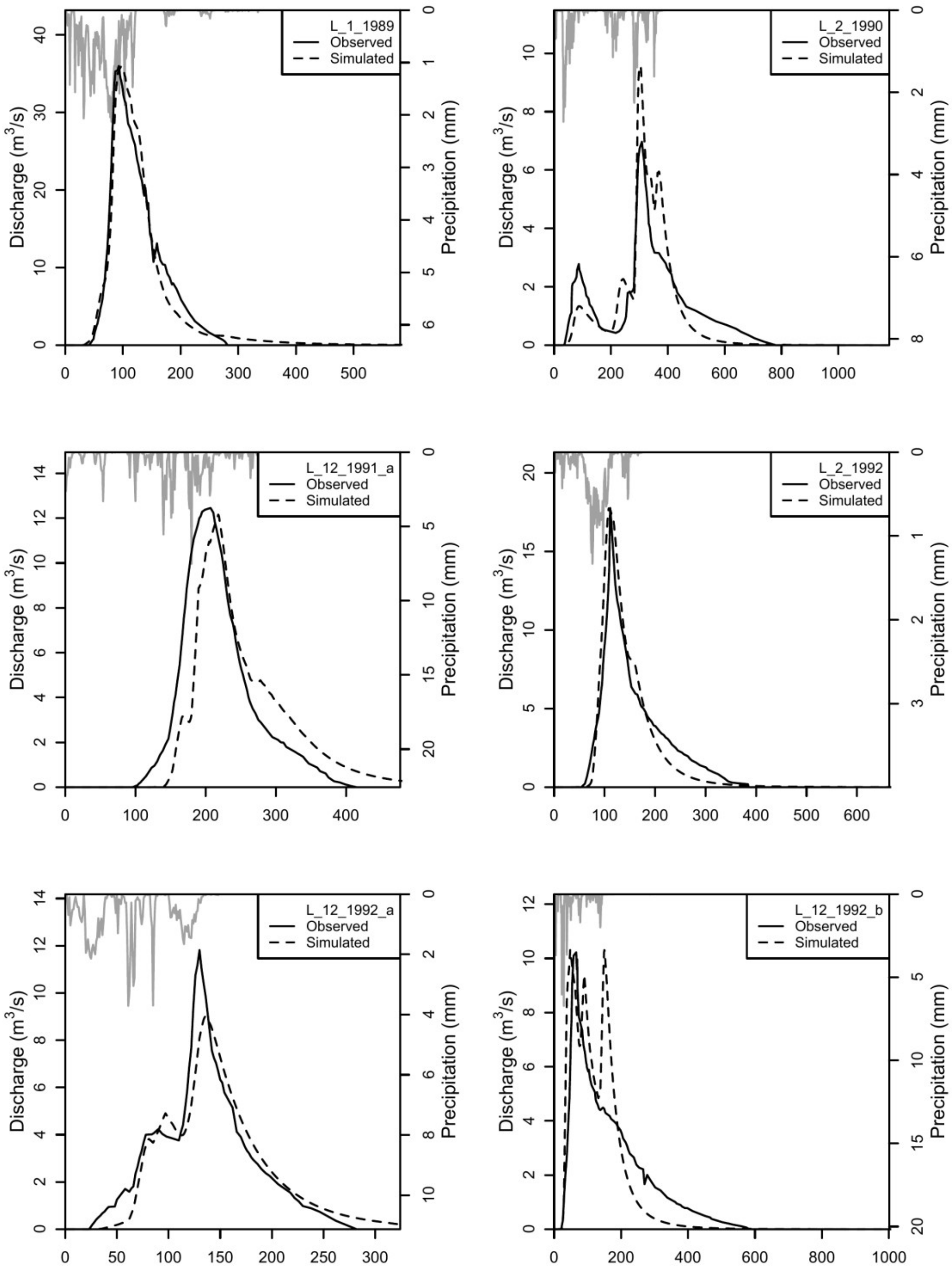
L_1_1989
L_2_1990
L_12_1991_a
L_2_1992
L_12_1992_a
L_12_1992_b
Observed
Simulated
Discharge (m^3/s)
Precipitation (mm)

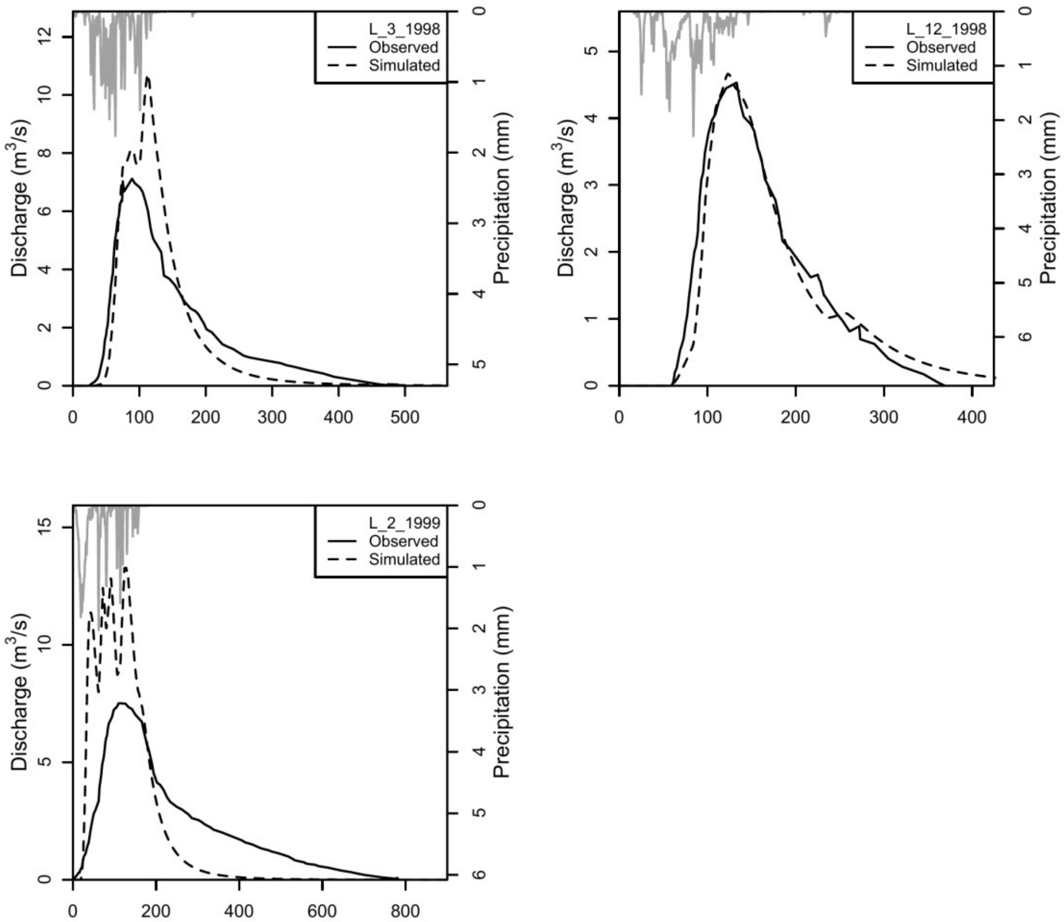

Figure 7.10: Observed and simulated flood events at the Lazarides hydrometric station.

8. APPENDIX B: EVENT TABLES

8.1 ITALY

Table 8. Total and excess rainfall height (*h* and *he*), runoff coefficient *c*, observed and simulated discharge peak (*Qp* and *Qp,sim*), maximum potential retention *S*, CN and Nash-Sutcliffe coefficient for each event of the Scoltenna (Pievepelago) catchment.

Event code	**h (mm)**	**he (mm)**	**c**	**Qp (m^3/s)**	**Qp,sim (m^3/s)**	**S (mm)**	**CN**	**NSE**
P_P_3_06	70	17	0.25	47	38	159	61	0.67
P_P_12_06	68	16	0.24	51	51	158	62	0.88
P_P_1_09	151	30	0.20	78	77	427	37	0.73
P_P_3_09	120	17	0.14	38	30	450	36	0.87
P_P_2_10	76	35	0.46	68	114	78	77	0.33
P_P_6_10	125	31	0.25	88	44	287	47	0.70
P_P_10_12	127	28	0.22	45	55	323	44	0.79
P_P_1_13	116	35	0.30	60	57	214	54	0.65
P_P_3_13	90	55	0.61	70	197	52	83	-1.98
P_P_4_13	53	17	0.32	45	58	88	74	0.67
P_P_5_13	96	30	0.31	51	63	170	60	0.83
P_P_10_13	134	28	0.21	77	100	363	41	0.92
P_P_12_13	201	79	0.39	100	166	260	49	0.27
P_P_1_14	234	99	0.42	90	154	270	49	0.51
P_P_2_14	85	22	0.26	58	51	183	58	0.87
P_P_3_14	83	24	0.28	60	42	162	61	0.86
P_P_11_14	143	26	0.18	112	33	442	36	0.52
P_P_12_14	74	22	0.30	33	46	138	65	0.31
P_P_3_15	62	21	0.34	19	57	96	73	-1.80

Table 9. Total and excess rainfall height (*h* and *he*), runoff coefficient *c*, observed and simulated discharge peak (*Qp* and *Qp,sim*), maximum potential retention *S*, CN and Nash-Sutcliffe coefficient for each event of the Baganza (Marzolara) catchment.

Event code	**h (mm)**	**he (mm)**	**c**	**Qp (m^3/s)**	**Qp,sim (m^3/s)**	**S (mm)**	**CN**	**NSE**
BG_M_3_06	24	7	0.30	21	14	44	85	0.70
BG_M_3_07	63	13	0.21	14	20	170	60	0.55
BG_M_4_07	25	10	0.40	28	33	31	89	0.23
BG_M_6_07	41	9	0.22	15	17	108	70	0.87
BG_M_11_08	106	18	0.17	28	33	351	42	0.42
BG_M_2_10	44	14	0.31	40	31	77	77	0.93
BG_M_4_10	32	6	0.18	20	19	97	72	0.80
BG_M_5_10	57	12	0.21	27	40	156	62	0.19
BG_M_6_10	66	10	0.16	17	24	232	52	0.52
BG_M_10_10	129	18	0.14	48	22	505	33	0.03
BG_M_12_10	50	24	0.48	35	31	48	84	0.45
BG_M_4_12	44	9	0.21	15	10	120	68	0.65
BG_M_10_12	89	14	0.16	28	17	305	45	0.73
BG_M_11_12	82	14	0.17	101	52	262	49	0.72
BG_M_12_12	41	11	0.28	25	18	82	75	0.90
BG_M_1_13	42	11	0.25	15	9	93	73	0.78
BG_M_3_13	25	13	0.53	32	37	20	93	-0.10
BG_M_4_13	54	11	0.20	27	20	151	63	0.44
BG_M_10_13	25	7	0.28	22	25	50	84	0.38
BG_M_11_13	85	20	0.24	16	19	204	55	0.73
BG_M_12_13	64	25	0.39	29	33	85	75	0.69
BG_M_1_15	46	7	0.15	14	14	170	60	0.95
BG_M_3_15	81	10	0.12	18	18	345	42	0.36

Table 10. Total and excess rainfall height (*h* and *he*), runoff coefficient *c*, observed and simulated discharge peak (*Qp* and *Qp,sim*), maximum potential retention *S*, CN and Nash-Sutcliffe coefficient for each event of the Ceno (Ponte Lamberti) catchment.

Event code	**h (mm)**	**he (mm)**	**c**	**Qp (m^3/s)**	**Qp,sim (m^3/s)**	**S (mm)**	**CN**	**NSE**
C_PL_2_06	75	16	0.21	61	64	203	56	0.73
C_PL_3_06	36	12	0.34	99	105	56	82	0.92
C_PL_9_06	53	5	0.09	57	44	277	48	0.58
C_PL_1_09	94	16	0.17	274	108	304	46	0.46
C_PL_2_11	48	10	0.21	39	34	130	66	0.34
C_PL_3_11	70	21	0.29	81	78	133	66	0.92
C_PL_6_11	64	11	0.17	38	67	208	55	0.20
C_PL_10_11	94	9	0.09	41	51	489	34	0.87
C_PL_11_11_a	136	28	0.21	133	133	370	41	0.72
C_PL_11_11_b	41	10	0.25	119	105	92	73	0.89
C_PL_4_12	49	12	0.24	124	123	116	69	0.89
C_PL_5_12	50	6	0.13	31	36	206	55	0.91
C_PL_10_12	58	7	0.12	29	20	257	50	0.79
C_PL_11_12	84	24	0.29	197	195	159	61	0.86
C_PL_12_12	47	15	0.32	95	58	81	76	0.83
C_PL_3_13	36	10	0.27	102	82	77	77	0.68
C_PL_5_13	60	12	0.20	69	54	169	60	0.84

Table 11. Total and excess rainfall height (*h* and *he*), runoff coefficient *c*, observed and simulated discharge peak (*Qp* and *Qp,sim*), maximum potential retention *S*, CN and Nash-Sutcliffe coefficient for each event of the Leo (Fanano) catchment.

Event code	**h (mm)**	**he (mm)**	**c**	**Qp (m^3/s)**	**Qp,sim (m^3/s)**	**S (mm)**	**CN**	**NSE**
L_FN_11_07	113	51	0.46	34	38	116	69	0.79
L_FN_1_08	58	47	0.81	28	27	12	95	0.95
L_FN_5_08	91	48	0.52	29	34	73	78	0.79
L_FN_10_08	229	94	0.41	45	33	277	48	0.86
L_FN_11_08	225	111	0.49	29	38	203	56	0.84
L_FN_10_09	77	40	0.51	46	39	64	80	0.98
L_FN_2_10	58	58	0.99	73	47	0	100	0.86
L_FN_3_11	110	107	0.97	35	36	3	99	0.31
L_FN_10_11	163	97	0.59	71	92	100	72	0.79
L_FN_12_11	66	60	0.91	26	26	6	98	0.75
L_FN_4_12	63	31	0.49	20	10	57	82	0.71
L_FN_11_12	130	58	0.45	63	72	139	65	0.78
L_FN_12_12	54	35	0.65	24	18	27	90	0.87
L_FN_3_13	97	29	0.30	34	23	180	58	0.63
L_FN_12_13	144	78	0.54	48	46	107	70	0.91

Table 12. Total and excess rainfall height (*h* and *he*), runoff coefficient *c*, observed and simulated discharge peak (*Qp* and *Qp,sim*), maximum potential retention *S*, CN and Nash-Sutcliffe coefficient for each event of the Nure (Farini) catchment.

Event code	**h (mm)**	**he (mm)**	**c**	**Qp (m^3/s)**	**Qp,sim (m^3/s)**	**S (mm)**	**CN**	**NSE**
N_FA_2_06	80	20	0.25	77	69	181	58	0.79
N_FA_3_06	31	14	0.43	53	77	35	88	0.64
N_FA_8_06	111	10	0.09	74	65	595	30	0.83
N_FA_9_06	43	8	0.18	58	53	137	65	0.85
N_FA_12_06	41	9	0.21	44	43	114	69	0.94
N_FA_11_07	189	58	0.31	190	181	337	43	0.97
N_FA_1_08	37	14	0.37	37	34	53	83	0.98
N_FA_6_08	45	9	0.20	65	89	127	67	0.54
N_FA_12_08	119	32	0.26	48	34	253	50	0.84
N_FA_1_09	64	40	0.63	115	142	34	88	0.92
N_FA_2_09	120	51	0.42	87	94	140	64	0.89
N_FA_4_09°	83	36	0.43	42	71	93	73	0.65
N_FA_4_09b	78	30	0.38	52	68	106	70	0.84
N_FA_11_09	115	40	0.35	166	137	174	59	0.91
N_FA_12_09	122	67	0.55	183	186	89	74	0.83
N_FA_2_10	48	14	0.29	49	54	92	73	0.75
N_FA_4_10	42	14	0.34	43	45	64	80	0.72
N_FA_5_10	54	15	0.27	51	57	112	69	0.89
N_FA_11_10	148	57	0.39	163	171	194	57	0.89
N_FA_12_10	95	41	0.43	65	84	107	70	0.78
N_FA_3_11	95	16	0.16	77	34	324	44	0.79
N_FA_11_11	159	34	0.22	151	113	418	38	0.76
N_FA_11_12	62	18	0.29	64	76	122	68	0.90
N_FA_4_13	40	13	0.32	44	33	67	79	0.35
N_FA_11_13	68	17	0.25	195	157	154	62	0.92
N_FA_12_13	112	45	0.40	171	146	142	64	0.95
N_FA_3_15	44	25	0.58	70	92	29	90	0.87

Table 13. Total and excess rainfall height (*h* and *he*), runoff coefficient *c*, observed and simulated discharge peak (*Qp* and *Qp,sim*), maximum potential retention *S*, CN and Nash-Sutcliffe coefficient for each event of the Montone (Castrocaro) catchment.

Event code	**h (mm)**	**he (mm)**	**c**	**Qp (m^3/s)**	**Qp,sim (m^3/s)**	**S (mm)**	**CN**	**NSE**
MN_C_12_09	20	10	0.47	35	35	19	93	0.81
MN_C_2_10	16	9	0.54	27	27	12	95	0.48
MN_C_3_10	60	10	0.17	36	39	196	56	0.86
MN_C_4_10	45	5	0.11	15	20	205	55	0.72
MN_C_5_10	65	7	0.11	29	26	291	47	0.95
MN_C_12_10	36	7	0.20	26	25	99	72	0.81
MN_C_1_13	24	11	0.47	45	33	24	91	0.81
MN_C_3_13	15	5	0.37	24	16	21	93	0.92
MN_C_11_13	85	15	0.18	41	43	261	49	0.93
MN_C_2_14	20	4	0.22	38	20	53	83	0.80
MN_C_3_14	83	21	0.25	81	88	185	58	0.90
MN_C_9_14	77	13	0.17	153	146	251	50	0.69
MN_C_11_14	85	15	0.17	56	42	272	48	0.81
MN_C_4_15	52	5	0.10	22	22	249	51	0.67

8.2 GREECE

Table 14. Total and excess rainfall height (*h* and *he*), runoff coefficient *c*, observed and simulated discharge peak (*Qp* and *Qp,sim*), maximum potential retention *S*, CN and Nash-Sutcliffe coefficient for each event of the Sarantapotamos (Gyra Stefanis) catchment.

Event code	**h (mm)**	**he (mm)**	**c**	**Qp (m^3/s)**	**Qp,sim (m^3/s)**	**S (mm)**	**CN**	**NSE**
S12_2011	74	2	0.03	5	4	694	27	-0.08
S2_2012°	37	2	0.04	4	4	302	46	0.61
S2_2012b	19	1	0.05	3	4	134	66	0.53
S2_2012c	35	1	0.04	3	3	297	46	0.79
S12_2012	95	4	0.04	13	16	738	26	0.54
S1_2013	21	1	0.03	3	3	202	56	0.75
S2_2013	47	3	0.06	19	14	324	44	0.91
S11_2013°	101	2	0.02	31	11	1069	19	0.48
S11_2013b	34	1	0.03	25	8	320	44	0.37
S12_2013	49	2	0.04	4	4	385	40	0.82
S1_2014	32	1	0.03	3	4	303	46	0.58
S3_2014°	55	3	0.05	10	10	413	38	0.60

Table 15. Total and excess rainfall height (*h* and *he*), runoff coefficient *c*, observed and simulated discharge peak (*Qp* and *Qp,sim*), maximum potential retention *S*, CN and Nash-Sutcliffe coefficient for each event of the Nedontas (Kalamata) catchment.

Event code	**h (mm)**	**he (mm)**	**c**	**Qp (m^3/s)**	**Qp,sim (m^3/s)**	**S (mm)**	**CN**	**NSE**
N12_2011	95	21	0.22	33	35	246	51	0.86
N1_2014b	106	8	0.07	15	6	639	28	-0.11
N1_2012	136	20	0.15	31	31	502	34	0.93
N2_2012	155	25	0.16	30	36	531	32	0.84
N4_2012	60	2	0.04	4	4	519	33	0.69
N1_2013°	263	34	0.13	49	42	1081	19	0.89
N1_2013b	142	17	0.12	11	12	613	29	0.77
N2_2013	43	2	0.04	6	3	349	42	0.46
N3_2013	63	1	0.02	3	2	641	28	0.29
N11_2013	109	13	0.12	12	8	485	34	0.60

8.3 CYPRUS

Table 16. Total and excess rainfall height (*h* and *he*), runoff coefficient *c*, observed and simulated discharge peak (*Qp* and *Qp,sim*), maximum potential retention *S*, CN and Nash-Sutcliffe coefficient for each event of the Peristerona catchment.

Event code	**h (mm)**	**he (mm)**	**c**	**Qp (m^3/s)**	**Qp,sim (m^3/s)**	**S (mm)**	**CN**	**NSE**
P_12_1991_a	109	15	0.13	29	19	436	37	0.65
P_12_1992	144	28	0.20	63	46	416	38	0.90
P_11_1994	246	84	0.34	57	57	390	39	0.87
P_12_2001	84	31	0.37	61	57	119	68	0.89
P_1_2002	66	41	0.63	21	29	35	88	0.34
P_1_2004_a	152	60	0.39	55	69	197	56	0.84
P_1_2004_b	84	28	0.34	44	37	134	65	0.81
P_2_2007	66	11	0.17	21	12	221	53	0.60
P_1_1977	86	18	0.21	18	12	236	52	0.78
P_2_1979	25	11	0.44	19	21	27	90	0.96
P_2_1980	75	21	0.28	21	24	150	63	0.71
P_3_1988	95	48	0.51	20	28	80	76	0.59
P_12_1988	145	26	0.18	35	37	460	36	0.80
P_1_1989	143	72	0.51	117	118	122	68	0.97

Table 17. Total and excess rainfall height (*h* and *he*), runoff coefficient *c*, observed and simulated discharge peak (*Qp* and *Qp,sim*), maximum potential retention *S*, CN and Nash-Sutcliffe coefficient for each event of the Lazarides catchment.

Event code	**h (mm)**	**he (mm)**	**c**	**Qp (m^3/s)**	**Qp,sim (m^3/s)**	**S (mm)**	**CN**	**NSE**
L_1_1989	98	37	0.38	36	36	132	66	0.96
L_2_1990	83	15	0.18	7	10	262	49	0.64
L_12_1991_a	152	16	0.11	12	12	715	26	0.79
L_2_1992	38	17	0.45	18	18	40	86	0.88
L_12_1992_a	97	11	0.11	12	9	449	36	0.88
L_12_1992_b	78	18	0.23	10	10	194	57	0.62
L_3_1998	36	12	0.32	7	11	62	80	0.71
L_12_1998	47	7	0.15	5	5	170	60	0.95
L_2_1999	52	24	0.45	8	13	55	82	-0.21

Venezia, 30.09.2021

9. BIBLIOGRAPHY

Ajmal, M., Waseem, M., Kim, D., & Kim, T. W., 2020. A pragmatic slope-adjusted curve number model to reduce uncertainty in predicting flood runoff from steep watersheds. Water, 12(5), 1469.

Aron, G., Ball, J.E., and Smith, T.A., 1991. Fractal concept used in time-of-concentration estimates. Journal of Irrigation and Drainage Engineering, 117 (5), 635-641. doi:10.1061/(ASCE)0733-9437(1991)117:5(635).

ASCE-ASABE (American Society of Agricultural and Biological Engineers)-NRCS (Natural Resources Conservation Service) Task Group on Curve Number Hydrology, 2017. Report of Task Group on Curve Number Hydrology, Chapters 8 (Land Use and Land Treatment Classes), 9 (Hydrologic Soil Cover Complexes), 10 (Estimation of Direct Runoff from Storm Rainfall), 12 (Hydrologic Effects of Land Use and Treatment), edited by R. H. Hawkins, T. J. Ward, and D. E. Woodward, 115. Reston, VA.

Askew, A.J., 1970. Derivation of formulae for variable lag time. *Journal of Hydrology*, 10 (3), 225–242. doi:10.1016/ 0022-1694(70)90251-9

Bacchi, B., Brath, A., and Kottegoda, N. T., 1992. Analysis of the relationships between flood peaks and flood volumes based on crossing properties of river flow processes. *Water Resources Research*, 28(10), 2773-2782.

Baltas, E. A., Dervos, N. A., and Mimikou, M. A., 2007. Technical Note: Determination of the SCS initial abstraction ratio in an experimental watershed in Greece, *Hydrol. Earth Syst. Sci.*, 11 (6), 1825–1829, doi: 10.5194/hess-11-1825-2007.

Caletka, M., Šulc Michalková, M., Karásek, P., & Fučík, P., 2020. Improvement of SCS-CN initial abstraction coefficient in the Czech Republic: a study of five catchments. *Water*, 12(7), 1964.

Corps of Engineers, 1954. *Airfield drainage investigation*. Washington, DC: U.S. Army, Los Angeles District for the Office of the Chief of Engineers, Airfield Branch Engineering Division, Military Construction, Data Report.

Bocchiola, D., De Michele, C., Pecora, S., Rosso, R., 2003. On response time of Italian watersheds. *L'Acqua*, 1, 45-55.

Caroni, E., Rosso, R., and Siccardi, F., 1986. Nonlinearity and time-variance of the hydrologic response of a small mountain creek. *In: Scale Problems in Hydrology*. The Netherlands, Dordrecht: Springer, 19-37.

Cho, Y., Engel, B. A., & Merwade, V. M., 2018. A spatially distributed Clark's unit hydrograph based hybrid hydrologic model (Distributed-Clark). *Hydrological Sciences* Journal, 63(10), 1519-1539.

Chow, V.T., Maidment, D.R., and Mays, L.W., 1988. Applied Hydrology. McGraw-Hill Inc., New York, New York.

Dingman, S. L., 2002. *Physical hydrology*, Upper Sadle River, New Jersey, USA: Prentice Hall, ISBN: 1478628073.

Cronshey, R.G., 1983. Discussion—Antecedent moisture condition probabilities. D.D. Gray, et al., *Journal of Irrigation and Drainage Engineering*, 109(2), 296–298

Efstratiadis, A., 2008. *Non-linear methods in multiobjective water resource optimization problems, with emphasis on the calibration of hydrological models*, PhD Thesis, 391 pages, Department of Water Resources and Environmental Engineering, National

Technical University of Athens, full text and extended English abstract are Available from: https://www.itia.ntua.gr/en/docinfo/838/.

Franchini, M., and Galeati, G., 2000. Comparative analysis of some methods for deriving the expected flood reduction curve in the frequency domain. *Hydrology and Earth System Sciences*, 4(1), 155-172.

Freeze, R. A., 1972. Role of subsurface flow in generating surface runoff: 2. Upstream source areas, *Water Resources Research*, 8 (5), 1272–1283, doi: 10.1029/WR008i005p01272.

Gericke, O. J. and Smithers, J. C., 2014. Review of methods used to estimate catchment response time for the purpose of peak discharge estimation, *Hydrological Sciences Journal*, 59(11), 1935–1971, DOI: 10.1080/02626667.2013.866712.

Giandotti, M., 1934. Previsione delle piene e delle magre dei corsi d'acqua. Istituto Poligrafico dello Stato, 8.

Grimaldi, S, Petroselli, A, and Romano, N., 2013a. Curve-Number/Green–Ampt mixed procedure for streamflow predictions in ungauged basins: Parameter sensitivity analysis, *Hydrological processes*, 27 (8), 1265–1275.

Grimaldi, S, Petroselli, A, and Romano, N., 2013b. Green-Ampt Curve-Number mixed procedure as an empirical tool for rainfall–runoff modelling in small and ungauged basins, *Hydrological processes*, 27 (8), 1253–1264.

Hawkins, R. H. and Khojeini, A. V., 2000. *Initial Abstraction and Loss in the Curve Number Method*, Arizona-Nevada Academy of Science, ISSN: 0272-6106.

Hewlett, J. D., 1974. Comments on letters relating to Role of subsurface flow in generating surface runoff: 2. Upstream source areas by R. Allan Freeze, *Water Resources Research*, 10 (3), 605–607, doi: 10.1029/WR010i003p00605.

Hewlett, J. D., 1961. *Soil moisture as a source of base flow from steep mountain watersheds*, Southeastern Forest Experiment Station, US Department of Agriculture, Forest Service.

Hewlett, J. D. and Hibbert, A. R., 1967. Factors affecting the response of small watersheds to precipitation in humid areas, *Forest hydrology*, 1, 275–290.

Izzard, C.F. and Hicks, W.I., 1946. Hydraulics of runoff from developed surfaces. *In: 26th Annual Meetings of the Highway Research Board*, 5–8 December, Washington, DC, 129–150.

Hjelmfelt, A.T., 1991. Investigation of curve number procedure. *Journal of Hydraulic Engineering*, 117 (6), 725–737.

Kang, M., and Yoo, C., 2020. Application of the SCS–CN Method to the Hancheon Basin on the Volcanic Jeju Island, Korea, *Water*, 12, 3350.

Krajewski, A., Sikorska-Senoner, A.E., Hejduk, A., and Hejduk, L., 2020. Variability of the initial abstraction ratio in an urban and an agroforested catchment, *Water*, 12, 415.

Loukas, A. and Quick, M.C., 1996. Physically-based estimation of lag time for forested mountainous watersheds. *Hydrological Sciences Journal*, 41 (1), 1–19. doi:10.1080/02626669609491475.

McCuen, R.H., 2009. Uncertainty analyses of watershed time parameters. *Journal of Hydrologic Engineering*, 14 (5), 490– 498. doi:10.1061/(ASCE)HE.1943-5584.0000011

Michailidi, E.M., Antoniadi, S., Koukouvinos, A., Bacchi, B. and Efstratiadis, A., 2018. Timing the time of concentration: shedding light on a paradox, *Hydrological Sciences Journal*, 63(5), 721-740, DOI: 10.1080/02626667.2018.1450985.

Michailidi, E.M., 2018. Flood risk assessment in gauged and ungauged basins in a multidimensional context, PhD thesis, Università Degli Studi di Brescia, March 2018, Italy.

Mishra, S. K., Pandey, R. P., Jain, M. K., and Singh, V. P., 2008. A rain duration and modified AMC-dependent SCS-CN procedure for long duration rainfall-runoff events. *Water Resources Management*, 22(7), 861-876.

Morgali, J.R. and Linsley, R.K., 1965. Computer simulation of overland flow. *Journal of Hydraulics Division ASCE*, 91 (HY3), 81–100.

Nash, J.E., 1957. The form of the instantaneous unit hydrograph. *Int. Assoc. Sci. Hydrol.*, 45, 114-121.

NRCS (National Research Conservation Service), 2004. *National engineering handbook, Part 630 hydrology*, Washington, DC: US Department of Agriculture.

Papadakis, K.N. and Kazan, M.N., 1987. Time of concentration in small rural watersheds. *In: Proceedings of the ASCE Engineering Hydrology Symposium*. Williamsburg, VA: ASCE, 633–638.

Pasini F., 1914. Relazione sul progetto della bonifica renana, Bologna (in Italian).

Ranzi, R., Galeati, G., and Bacchi, B., 2006. Idrogrammi di piena di progetto dedotti dalla trasformazione afflussi-deflussi. *Proc. of the XXX Convegno di Idraulica e Costruzioni Idrauliche Rome*.

Reed, D. W., Johnson, P., and Firth, J. M., 1975. A non-linear rainfall-runoff model, providing for variable lag time, *Journal of Hydrology*, 25 (3), 295–305, doi: https://doi.org/10.1016/0022-1694(75)90027-X.

Risva, K., 2018. Development of a distributed hydrological software application employing novel velocity-based techniques. Postgraduate thesis. Department of Water Resources and Environmental Engineering, National Technical University of Athens full text and extended English abstract are Available from: https://www.itia.ntua.gr/en/docinfo/1915/.

Rodríguez-Iturbe, I. and Valdés, J. B., 1979. The geomorphologic structure of hydrologic response, *Water Resources Research*, 15 (6), 1409–1420.

Rodríguez-Iturbe, I., González-Sanabria, M., and Bras, R. L., 1982, A geomorphoclimatic theory of the instantaneous unit hydrograph, *Water Resources Research*, 18 (4), 877–886.

Savvidou, E., Efstratiadis, A., Koussis, A. D., Koukouvinos, A., & Skarlatos, D., 2018. The curve number concept as a driver for delineating hydrological response units. *Water*, 10(2), 194.

Shi, Z.-H., *et al.*, 2009. Research on the SCS-CN initial abstraction ratio using rainfall-runoff event analysis in the Three Gorges Area, China, *CATENA*, 77 (1), 1–7, doi: http://dx.doi.org/10.1016/j.catena.2008.11.006.

Shi, W., and Wang, N., 2020. An improved SCS-CN method incorporating slope, soil moisture, and storm duration factors for runoff prediction, *Water*, 12, 1335.

Singh, P. K., Mishra, S. K., & Jain, M. K. (2014). A review of the synthetic unit hydrograph: from the empirical UH to advanced geomorphological methods. *Hydrological Sciences Journal*, 59(2), 239-261.

Snyder, F. F., 1938, Synthetic unit-graphs, *Eos, Transactions American Geophysical Union*, 19 (1), 447–454, doi: 10.1029/TR019i001p00447.

Sutcliffe, J. V., 1978. *Methods of flood estimation: a guide to the Flood Studies Report*, Report, Institute of Hydrology, UK.

Soulis, K. X., & Valiantzas, J. D., 2012. SCS-CN parameter determination using rainfall-runoff data in heterogeneous watersheds–the two-CN system approach. *Hydrology and Earth System Sciences*, 16(3), 1001-1015.

Tedela, N. H., McCutcheon, S. C., Rasmussen, T. C., Hawkins, R. H., Swank, W. T., Campbell, J. L., Adams, M.B, Jackson, C.R., and Tollner, E. W., 2012. Runoff curve numbers for 10 small forested watersheds in the mountains of the eastern United States. *Journal of Hydrologic Engineering*, 17(11), 1188-1198.

Van Mullem, J., 1992. Soil moisture and runoff-another look. *In: Irrigation and Drainage, Proc. Water Forum*, E.T. Engman, ed, ASCE, NY, 372–377.

Ventura G., 1905. Sulla bonifica della bassa pianura bolognese, Giornale del Genio Civile (in Italian).

Verma, S., *et al*., 2017. A revisit of NRCS-CN inspired models coupled with RS and GIS for runoff estimation. *Hydrological Sciences Journal*, 62(12), 1891-1930.

Viparelli, C., 1961. Ricostruzione dell'idrogramma di piena. Napoli: Istituto di Idraulica dell'Università di Palermo, Stab. Tip. Genovese (in Italian).

Viparelli, C., 1963. Ricostruzione dell'idrogramma di piena. L'Energia Elettrica, 6, 421–428 (in Italian).

Woodward, D. E., *et al.*, 2003. Runoff Curve Number Method: Examination of the Initial Abstraction Ratio, *In: World Water Environmental Resources Congress 2003*, 1–10, DOI: doi:10.1061/40685(2003)308.

Woodward, D. E., *et al.*, 2010. Discussion of Modifications to SCS-CN method for long-term hydrologic simulation by K. Geetha, SK Mishra, TI Eldho, AK Rastogi, and RP Pandey, *Journal of Irrigation and Drainage Engineering*, 136 (6), 444–446.

Yuan, Y., *et al.*, 2014. Initial abstraction and curve numbers for semiarid watersheds in Southeastern Arizona, *Hydrological Processes*, 28 (3), 774–783, doi: 10.1002/hyp.9592.